

ISTANBUL TECHNICAL UNIVERSITY ★ GRADUATE SCHOOL OF SCIENCE
ENGINEERING AND TECHNOLOGY

**PRODUCTION AND PROPERTIES OF BIOPOLYMER BASED FIBERS AND
FILMS**



M.Sc. THESIS

Tuğçe KÖROĞLU

Department of Nano Science and Nano Engineering

Nano Science and Nano Engineering Programme

MARCH 2018

ISTANBUL TECHNICAL UNIVERSITY ★ GRADUATE SCHOOL OF SCIENCE
ENGINEERING AND TECHNOLOGY

**PRODUCTION AND PROPERTIES OF BIOPOLYMER BASED FIBER AND
FILMS**

M.Sc. THESIS

Tuğçe KÖROĞLU
(513141023)

Department of Nano Science and Nano Engineering

Nano Science and Nano Engineering Programme

Thesis Advisor: Prof. Dr. Esra ÖZKAN ZAYİM

MARCH 2018

ISTANBUL TEKNİK ÜNİVERSİTESİ ★ FEN BİLİMLERİ ENSTİTÜSÜ

**BİYOPOLİMER TABANLI FİBER VE FİLMLEİN ÜRETİMİ VE
ÖZELLİKLERİ**

YÜKSEK LİSANS TEZİ

**Tuğçe KÖROĞLU
(513141023)**

Nano Bilim ve Nano Mühendislik Anabilim Dalı

Nano Bilim ve Nano Mühendislik Programı

Tez Danışmanı: Prof. Dr. Esra ÖZKAN ZAYİM

MAYIS 2018

Tuğçe Köroğlu, a M.Sc. student of ITU Graduate School of Science Engineering and Technology student ID 513141023, successfully defended the thesis entitled “PRODUCTION AND PROPERTIES OF BIOPOLYMER BASED FIBER AND FILMS”, which she prepared after fulfilling the requirements specified in the associated legislations, before the jury whose signatures are below.

Thesis Advisor : **Prof. Dr. Esra ÖZKAN ZAYİM**
İstanbul Technical University

Jury Members : **Prof. Dr. Nilgün YAVUZ**
İstanbul Technical University

Prof. Dr. Hüseyin DELİGÖZ
İstanbul University

Date of Submission : 12 March 2018
Date of Defense : 14 March 2018





To my family and friends,



FOREWORD

I would like to express my gratitude to my director of studies, Prof. Dr. Esra Özkan Zayim, whose expertise, understanding and patience, supported my work in this thesis.

I must also acknowledge helpfulness of Prof. Dr. Hüceste Giz (Department of Chemistry, ITU) her suggestions for this study and ideas presented here.

I also specially thank to Prof. Dr. Hüseyin Deligöz, Prof. Dr. Murat Baydoğan, Assoc. Prof. Dr. Neşe Şahin Yeşilçubuk, Assoc. Prof. Dr. Cüneyt H. Ünlü, Dr. Ayşe Saygün and R.A. Osman Ürper for their help both theoretically and practically during my study.

Lastly, I would like to thank all my friends for their friendships and supports. I am deeply grateful to my mother Yıldız Çalışkan and my brother Kaan Köroğlu for their endless love and trust, and Aykut Yatıkçı for his presence, care and great encouragement.

March 2018

Tuğçe KÖROĞLU

TABLE OF CONTENTS

	<u>Page</u>
SYMBOLS	xv
LIST OF TABLES	xvii
LIST OF FIGURES	xix
SUMMARY	xxi
ÖZET	xxiii
1. INTRODUCTION	1
1.1 Nanofibers.....	2
1.1.1 Nanofiber production techniques	3
1.1.1.1 Drawing.....	3
1.1.1.2 Phase separation	4
1.1.1.3 Self-assembly	4
1.1.1.4 Electrospinning.....	5
1.1.2 Factors affecting electrospinning process and nanofiber properties	6
1.1.2.1 Solution properties.....	6
1.1.2.2 Concentration	6
1.1.2.3 Viscosity	7
1.1.2.4 Surface tension	8
1.1.2.5 Conductivity	8
1.1.2.6 Process conditions	8
1.1.2.7 Voltage.....	8
1.1.2.8 Feedrate.....	9
1.1.2.9 Collector type	10
1.1.2.10 Needle to collector distance and needle diameter	10
1.1.2.11 Ambient Conditions.....	11
1.1.3 Application of electrospun nanofibers.....	11
1.1.4 Wound dressing.....	12
1.2 Polymer Films and Hydrogels.....	14
1.3 Edible and Biodegradable Films for Packaging Applications	15
1.4 Measurement Systems and Tests.....	16
1.4.1 SEM (Scanning electron microscope)	16
1.4.2 XRD (X-Rays diffraction)	17
1.4.3 FTIR (Fourier transform infrared).....	18
1.4.4 Antibacterial activity test.....	19
1.4.5 Mechanical Properties	20
1.4.6 Contact angle measurement	22
1.4.7 UV-VIS spectroscopy.....	23
1.4.8 Rheometer	24
1.4.9 Conductivity measurement	25
1.4.10 Surface tension measurement.....	26
1.4.11 Gas permeability.....	27

1.4.12 Water vapor permeability (WVP)	29
1.4.13 Swelling behavior and degradation studies	29
1.5 Materials	30
1.5.1 Titanium Dioxide	30
1.5.2 Sol-gel chemistry of Ti alkoxide.....	32
1.5.3 Polyvinylpyrrolidone (PVP).....	33
1.5.4 Polyvinyl alcohol (PVA)	34
1.5.5 Agar.....	35
1.5.6 Aloe vera	36
2. EXPERIMENTAL PROCEDURES	41
2.1 Electrospinning Section.....	41
2.1.1 Sample preparations	41
2.1.2 Preparation of solutions.....	41
2.1.2.1 Solution 1 (Titanium isopropoxide)	42
2.1.2.2 Solution 2 (Titanium (IV) butoxide)	42
2.1.2.3 Preparation of <i>Aloe vera</i> gel	42
2.1.2.4 Solution 2 with <i>Aloe vera</i> gel addition	43
2.1.3 Electrospinning of solutions	43
2.1.4 Annealing	44
2.2 Preparation of Hydrogel Films Section.....	44
2.2.1 Agar/ <i>Aloe vera</i> Films	44
2.2.2 PVA/ <i>Aloe vera</i> Films	46
3. RESULTS AND DISCUSSION.....	47
3.1 Electrospinning Section.....	47
3.1.1 Viscosity, conductivity and surface tension of electrospin solutions	47
3.1.2 Fiber morphology.....	47
3.1.3 XRD analysis	52
3.1.4 Antibacterial activity of fibers	53
3.2 Hydrogel Films Section.....	54
3.2.1 Surface morphology	54
3.2.2 FTIR characterization.....	55
3.2.3 Antibacterial activity of films	56
3.2.4 Mechanical properties	58
3.2.5 Contact angle measurements	62
3.2.6 Transparency of films.....	64
3.2.7 Gas permeability	65
3.2.8 Water vapor permeability	67
3.2.9 Swelling behavior	68
3.2.10 In vitro degradation studies	69
4. CONCLUSION.....	71
REFERENCES	73
CURRICULUM VITAE.....	81

ABBREVIATIONS

<i>A.vera</i>	: <i>Aloe vera</i>
DMA	: Dynamic mechanical analysis
<i>E.coli</i>	: <i>Eschericia coli</i> bacterium
EtOH	: Ethanol
FTIR	: Fourier Transform Infrared
GTR	: Gas transmission rate
PBS	: Phosphate-buffered saline
PVA	: Polyvinylalcohol
PVP	: Polyvinylpyrrolidone
RH	: Relative humidity
SEM	: Scanning Electron Microscope
<i>S. aureus</i>	: <i>Staphylococcus aureus</i> bacterium
TB	: Titanium (IV) butoxide
<i>Tg</i>	: glass transition temperature
TiO₂	: Titanium dioxide
TS	: Tensile strength
TTIP	: Titanium isopropoxide
WVP	: Water vapor permeability
WVTR	: Water vapor transmission rate
XRD	: X-Ray Diffraction



SYMBOLS

min	: minute
nm	: nanometer
μm	: micrometer
cm²	: square centimeter
mL	: milliliter
N	: newton
MPa	: megapascal
kPa	: kilopascal
mg	: miligram
h	: hour
g	: gram
mg	: miligram
mS	: milisiemens
mN	: millinewton
ε	: Elongation
<i>E</i>	: Young's modulus
<i>E'</i>	: Storage modulus
<i>E''</i>	: Loss modulus
δ	: delta
°C	: celcius degree
γ	: interfacial tension
θ_Y	: Young contact angle



LIST OF TABLES

	<u>Page</u>
Table 1.1 : Crystallographic and physical properties of rutile, anatase, brookite.	32
Table 1.2 : The chemical components of Aloe vera.	38
Table 2.1 : Tablo of reagents used in this part of work.....	41
Table 2.2 : The experimentally confirmed conditions for the solutions.	44
Table 3.1 : Physical properties of solutions.....	47
Table 3.2 : Area of inhibitory zones of nanofibers.	53
Table 3.3 : Area of inhibitory zones of films.	57
Table 3.4 : Mechanical analysis of tensile strength (MPa), elongation at break (e%), max. force at break (N) and Young's modulus (MPa) of the films	59
Table 3.5 : Contact angle degrees of the films.	63



LIST OF FIGURES

	<u>Page</u>
Figure 1.1 : Representative photographic and SEM images of a nanofiber.....	2
Figure 1.2 : Producing of nanofiber with drawing technique	3
Figure 1.3 : Phase separation technique for fabricating nanofibrous structure.....	4
Figure 1.4 : Self-assembly of units.	5
Figure 1.5 : Design of a conventional electrospinning set-up.....	6
Figure 1.6 : Average diameter of polyamide fibers as a function of viscosity and the concentration of solution.	7
Figure 1.7 : Digital and cartoon images showing the three stage deformation of the polyvinylpyrrolidone droplet under the influence of increasing electric field	9
Figure 1.8 : Collector types	10
Figure 1.9 : Application areas of electrospun fibers.....	12
Figure 1.10 : The production of nanofibrous mats with biomolecules by electrospinning method for wound healing	13
Figure 1.11 : Different methods of incorporating biocides into electrospun nanofibers	14
Figure 1.12 : SEM system operation diagram.	17
Figure 1.13 : (a) Schematic operation of XRD and (b) XRD instrument.	18
Figure 1.14 : Schematic operation of FTIR.....	19
Figure 1.15 : Changes in the E' or tan delta curves gives transitions in materials....	22
Figure 1.16 : Three-phase boundary where liquid, gas and solid intersect.....	22
Figure 1.17 : Rheometer instrument and representation of parallel plate measurement.	25
Figure 1.18 : Tensiometer instrument and representation of Wilhelmy plate.....	27
Figure 1.19 : General approach of gas or vapour permeation through a film.....	28
Figure 1.20 : Structure of the unit cell of (a) rutile phase (b) anatase phase (c)brookite phase.....	31
Figure 1.21 : A) Hydrolysis, B) alcoxolation, C) oxolation of Ti alkoxide.....	33
Figure 1.22 : Polymerization reaction of PVP	34
Figure 1.23 : Repeating unit of PVA.	35
Figure 1.24 : Chemical structure of agarose and agarpectin	35
Figure 1.25 : Gelling function of agarose	36
Figure 1.26 : The structure of inner leaf pulp of Aloe vera.	37
Figure 1.27 : The ratios of the compounds in Aloe vera gel.....	37
Figure 1.28 : Chemical structures of emodin, aleosin and aloin	39
Figure 2.1 : a) Appearance of solution 2 and b) solution 2 with aloe vera addition .	42
Figure 2.2 : Electrospinning setup.....	43
Figure 2.3 : Agar/A.vera films	45
Figure 2.4 : a) 2% ZnO added Agar/A.vera film and b) 0.3% TiO ₂ solution added Agar film.....	45

Figure 2.5 : PVA/A.vera films	46
Figure 3.1 : Fiber webs of TB solution (on the left) and TB/Aloe vera solution (on the right) on baking paper.	48
Figure 3.2 : Fiber webs of TB solution electrospun on aluminum foil and glasses	48
Figure 3.3 : SEM photographs of nanofiber from Solution 1 at different magnifications, a) before annealing b)after annealing.....	49
Figure 3.4 : SEM photographs of nanofiber from Solution 2 at different magnifications, a) before annealing b)after annealing.....	50
Figure 3.5 : SEM photographs of nanofiber from Solution 2 electrospun with higher voltage and distance at different magnifications	51
Figure 3.6 : SEM photographs of nanofiber from Solution 2 with Aloe vera at different magnifications, a) 5000x b) 10000x c)20000x d)50000x magnification.....	52
Figure 3.7 : X-ray diffraction pattern of electrospun TiO ₂ fibers heat-treated at 500°C for 3 hours	52
Figure 3.8 : Antimicrobial activities of PVP/TiO ₂ /Aloe vera fibers and antibiotic discs against <i>S. Aureus</i>	54
Figure 3.9 : Antimicrobial activities of PVP/TiO ₂ /Aloe vera fibers and antibiotic discs against <i>E. coli</i>	54
Figure 3.10 : SEM photographs of Agar films without Aloe vera (a-b) and with 20% Aloe vera (c-d).....	55
Figure 3.11 : FTIR of agar/aloe vera films	56
Figure 3.12 : Antimicrobial activities of A30 film and antibiotic discs against <i>S. Aureus</i>	57
Figure 3.13 : Antimicrobial activities of A20 film with 4% ZnO nanoparticle (a) against <i>E. coli</i> and (b) against <i>S. Aureus</i>	58
Figure 3.14 : The torn film on the mechanical stress process.....	59
Figure 3.15 : Tensile strength of the aloe vera-added films.	60
Figure 3.16 : Elongation ratios of the aloe vera-added films.....	61
Figure 3.17 : Tan δ curves of A0 (red line) and A20 (black line) films.....	61
Figure 3.18 : Viscoelastic properties of A0 (red line) and A20 (black line) films, storage modules (on the left) and loss modules (on the right).	62
Figure 3.19 : Before water was dropped and after water was dropped onto the film surface	63
Figure 3.20 : Transmittance of Agar/A.vera films	64
Figure 3.21 : Transmittance of PVA/A.vera films	65
Figure 3.22 : Oxygen permeability of some biopolymer films.....	66
Figure 3.23 : WVP values of agar/aloe vera films.	67
Figure 3.24 : Swelling behavior of agar/A.vera films immersed in PBS buffer pH 7.4.	68
Figure 3.25 : Weight loss ratio of agar/A.vera films.....	69

PRODUCTION AND PROPERTIES OF BIOPOLYMER BASED FIBERS AND FILMS

SUMMARY

Advances in science and technology lead to new applications through producing functional and innovative materials. Fabrication and improvement of nanoscale materials are important subjects nowadays. Nanofibers are promising materials due to their particular properties such as large surface-to-volume ratio, porous structure, low weight, and can be easily developed for physical or chemical functionalization. They are valuable and useful materials in medical and technical areas. Nanofibers can be produced by the top-down or the bottom up approach.

Among the nanofiber fabrication techniques, electrospinning is one of the most suitable methods. Electrospinning technique is based on thinning of viscoelastic fluid by pulling it in a route with the use of electrostatic force. Generally, polymer-based materials are used in this process, but also application of different precursors increase fabrication of metal, ceramic and glass nanofibers.

Besides all the promising properties of the nanofiber, the mechanical strength of fibers is not sufficient; therefore, the biopolymer films were added to this study. Polymer films have promising properties for biomedical and food-packaging applications. They are fabricated by natural and synthetic polymers. Flexibility, permeability, thermal and dimensional stability, biocompatibility, biodegradability, mechanical properties and degradation rate are the important properties of suitable polymers for film forming. The use of polymers and natural materials as food packaging materials has increased mainly due to their promising assets over the traditional materials. Desirable quality, extended shelf life, freshness of the food products can be provided with the ease of handle, strong and long-lasting packaging fabricated with lighter, cheaper and recyclable materials.

Aloe vera is one of the important medicinal plants. Chemical analysis reveals that *Aloe vera* contains quite important ingredients and antibacterial agents. It contains water soluble and fat-soluble vitamins, enzymes, organic acids, minerals and phenolic compounds. Extracts of *A.vera* plant is used for medical intents and treatment of skin disorders such as wounds and burns. Furthermore, *Aloe vera* is a safe and environmentally friendly alternative to synthetic preservative substances.

In this study, various fibers containing titanium dioxide (TiO_2) that prepared from titanium (IV) isopropoxide or titanium (IV) butoxide precursors, poly(vinyl pyrrolidone) and *Aloe vera* were obtained by electrospinning process. It is known from the literature, TiO_2 and *Aloe vera* present antibacterial properties. Fibers were annealed in oven at 550°C for 3 hours. Micro and nano structural characterization of fibers were analyzed by SEM and crystallographic characterization was analyzed by XRD. Biopolymer based fibers that contains titanium(IV)isopropoxide as a precursor showed unfavourable structure after heating. So, *Aloe vera* was added to titanium(IV) butoxide solution. The antibacterial activity of the fibers against Gram

negative *Escherichia coli* (*E.coli*) and Gram positive *Staphylococcus aureus* (*S.aureus*) was examined. The addition of *Aloe vera* extremely increased the antibacterial activity of fibers.

Also, *Aloe vera* added agar and poly(vinyl alcohol) films were prepared by solvent casting method. Edible, transparent, strong and antibacterial films were prepared by addition of different amounts of *Aloe vera* (0, 10, 20, 30%) to polymer films. The biopolymer based films were characterized for the dependence of their physical, morphological and antibacterial properties on their *Aloe vera* content. The surface analysis of agar films were made via SEM. Chemical characterization were analyzed by FTIR. Their mechanical testing were examined and obtained tensile strength, elongation at break, Young's modulus and tan delta characters. Hydrophilic features of films were determined with contact angle measurements. *Aloe vera* addition had positive effect on antibacterial activity against Gram negative *Escherichia coli* (*E.coli*) and Gram positive *Staphylococcus aureus* (*S.aureus*). Oxygen permeability and water vapor permeability of agar films were investigated. Light transmissions of films were measured by spectrophotometer. Their swelling and degradation tests were made. Hereby, the biopolymer based films containing *Aloe vera* can be potentially observed as wound dressing and active edible films as packaging materials.

BİYOPOLİMER TABANLI FİBER VE FİLMLEİN ÜRETİMİ VE ÖZELLİKLERİ

ÖZET

Bilim ve teknolojideki gelişmeler, işlevsel ve yenilikçi materyaller aracılığıyla yeni uygulamalara imkan sağlamaktadır. Nano ölçekli malzemelerin imalatı ve geliştirilmesi günümüzde önemli konulardır. Nanofiberler, yüksek yüzey-hacim oranı, gözenekli yapı, düşük ağırlık ve fiziksel veya kimyasal işlevsellik için kolayca geliştirilebilen özelliklerinden dolayı gelecek vaat eden malzemelerdir. Tıbbi ve teknik alanlarda başlıca filtreler, afinite membranları, doku mühendisliği, kontrollü salım sağlayan ürünler, enzim immobilizasyonları, yara iyileştirici maddeler, sensörler ve enerji depolama alanlarında kullanılan önemli ve değerli malzemelerdir. Nanofiberler, tepeden tabana veya tabandan tepeye yaklaşma yöntemleriyle üretilebilir bunlardan bazıları faz ayırma, tel çekme, kendiliğinden toplanma, ıslak eğirme ve elektro eğirme gibi işlemlerdir. Üretim hızı, organizasyonu, lif çapı ve maliyeti, proses tekniğine karar vermede dikkate alınması gereken unsurlardır.

Elektro eğirme, yüksek üretim hızına sahip ve sürekli yapıda nanofiber imal etmek için en uygun yöntemlerden biridir. Ayrıca, lif çapı nanometreden mikronlara kadar ayarlanabilir. Elektro eğirme tekniği, viskoelastik akışkanın elektrostatik kuvvet kullanılarak bir rotada çekilmesi ile inceltilmesine dayanır. Genellikle, polimer esaslı malzemeler bu işlemde kullanılmaktadır, aynı zamanda farklı öncüllerin uygulanması metal, seramik ve cam nanofiberlerin imalatını arttırmaktadır. Çıkan ürünün morfolojisini ve üretim sürecini etkileyen bir çok etken vardır, bu etkenler üç ana grupta incelenebilir bunlar çözelti özellikleri, işlem koşulları ve çevresel faktörlerdir. Konsantrasyon, yüzey gerilimi, viskozite ve iletkenlik gibi çözelti özellikleri işlem sürecinde ve lif morfolojisi üzerinde önemli etkiye sahiptir. Voltaj, besleme hızı, toplayıcı modeli, iğne ucunun çapı ve uç ile toplayıcı arasındaki mesafe süreç etkenlerini tanımlayan kritik özelliklerdir. Bağlı nem ve sıcaklık gibi çevresel faktörler elektro eğirme işleminde etkilidir.

Elektro eğirme ile üretilen nanofiberler, yüksek gözeneklilik ve yüksek yüzey alanı gibi sıvı sızmasının kontrolünü sağlayan özellikleri, gazların matın içinden geçmesini sağlarken mikroorganizmaların istilasını engelleyebilen yararlı özellikleri sayesinde yara örtüsünde kullanılmak üzere iyi bir malzeme olabilir. Ayrıca, tıbbi iyileşme veya antibakteriyel özellik için nanofiberlere ilaç ve katkı maddeleri eklenebilir. Yara iyileşmesi, dinamik bir olay döngüsü içerir. Bakteriyel enfeksiyona maruz kalma riski yaralar için yüksektir, çünkü yara bir süre açık kalır ve dış çevreden mikroorganizmalar kolaylıkla kolonize olabilir. Yara sargı malzemelerinin amacı kanamayı durdurmak, yarayı su ve elektrolitler gibi tahriş edici maddelerden korumak ve mikroorganizmaların yayılmasını engellemektir. Son zamanlarda, yaraların tedavisinde mikrobiyal saldırıyı engelleyen, sürekli nem ve gaz değişim ortamı sağlayan, ek olarak bir enfeksiyon ortaya çıktığında antibakteriyel ajanların veya ilaçların salınmasını sağlayan malzemeler amaçlanmaktadır. Antibakteriyel nanofiberlerin üretimi, liflerde bir biyosit içerme yöntemini kullanır. Antibiyotikler,

gümüş nanopartiküller, metal oksit nanopartikülleri ve çeşitli katkı maddeleri dahil olmak üzere farklı aktif maddeler kullanılabilir.

Nanofiberin umut verici özelliklerinin yanı sıra liflerin mekanik mukavemeti istediğimiz özellikte değil, bu nedenle polimer filmler bu çalışmaya eklenmiştir. Polimer filmlerin biyomedikal ve gıda ambalajlama uygulamaları için umut verici özellikleri vardır. Hidrojeller, sulu çözeltileri hidrofilik özelliklerinden dolayı emebilen ve yapılarını çözünmeden koruyan polimerik ağlardır. Hidrojel filmler doğal ve sentetik polimerler ile üretilir. Polimer bağlantısı, kimyasal veya fiziksel olarak gerçekleştirilebilir. Kimyasal çapraz bağlama, yüksek mekanik dayanımlı hidrojelleri yapmak için çok yönlü bir uygulamadır. Fakat güçlü hidrojel yapı elde etmek için kullanılan çapraz bağlayıcılar tehlikeli olabilir. Fiziksel çapraz bağlanmada toksik çapraz bağlama maddelerinin eklenmesi önlenir. Bu nedenle, fiziksel olarak çapraz bağlanmış hidrojeller üzerinde çalışmalar artmıştır. Esneklik, geçirgenlik, termal ve boyutsal stabilite, biyouyumluluk, biyolojik bozunabilirlik, mekanik özellikler ve bozunma hızı, film oluşturma için uygun polimerlerin önemli özelliklerindedir. Solvent dökme yöntemi ile çözücünün uzaklaşması ile polimer film fiziksel çapraz bağli oluşturulabilir.

Özellikle doğal polimerler, biyouyumlu, biyo-bozunabilir, toksik olmayan, çevre dostu ve kolay üretilen gibi umut verici özellikleri nedeniyle endüstride ve ilaçta yaygın olarak kullanılmaya başlanmıştır. Gıda endüstrileri, tüketicilerin ve pazarın talepleri üzerine ambalaj teknolojisinde çeşitli alternatifler aramaktadır. Yüksek kaliteli, uzun raf ömrüne sahip ve gıda ürünlerinin tazeliğini koruyan, daha kolay, daha ucuz ve geri dönüştürülebilir malzemelerle imal edilen güçlü ve uzun ömürlü ambalajlar üretmek bu talepleri karşılayacaktır. Polimerlerin ve doğal malzemelerin gıda ambalaj malzemesi olarak kullanılması, geleneksel materyallerden üstün özellikleri sayesinde artmıştır. Her bir gıda ürününün özel ihtiyaçları, çok çeşitli malzemeler ve farklı bileşimlerle en uygun paketlenme çözümü ve tasarımı ile sağlanabilir. Gelişen polisakkarit bazlı filmler, yenilebilir ambalaj filmlerinin üretimi için uygundur. Biyobozunur filmler sayesinde petrolden üretilen sentetik plastik yerine doğal ürünlerden biyolojik olarak parçalanabilen plastiklerin kullanımı petrol tüketimini azaltacak, sentetik plastik atık miktarı azalacak ve doğal malzemelerin işlenmesi ekonomik olarak avantajlı olacaktır.

Agar denizel kırmızı alglerden elde edilen bir polisakkarittir. Biyomedikal ve gıda uygulamalarında iyi biyo-uyumluluk, biyo-bozunabilirlik ve toksik olmamaları nedeniyle yaygın olarak kullanılmaktadır. Agaroz ve agaropektinin karışımından oluşan jelleşen bir maddedir, içindeki agaroz katkı maddesine gerek olmadan hidrojen bağları ile polimer moleküllerini bir araya getirerek jel oluşturur. Polivinil alkol (PVA), tekstil, kağıt ve biyomedikal alanlarda yaygın olarak kullanılan renksiz, suda çözünebilir, toksik olmayan, biyo-uyumlu ve biyolojik olarak parçalanabilen sentetik bir polimerdir.

Aloe vera önemli şifalı bitkilerden biridir. Kimyasal analizler, *Aloe vera*'nın oldukça önemli bileşenleri ve antibakteriyel maddeleri içerdiğini ortaya koymaktadır. Suda çözünen ve yağda çözünen vitaminler, enzimler, organik asitler, mineraller ve fenolik bileşikler içerir. *A. vera* bitkisinin özleri tıbbi amaçlarla, yaralar ve yanıklar gibi deri hastalıklarının tedavisinde kullanılır. Antimikrobiyal, yara iyileşmesi, anti-enflamatuar, antioksidatif ve immüno-aracılık gibi önemli etkileri ile bilinir. Yaranın nemli kalması, epitel hücre göçünü arttırması, kollajenin daha hızlı olgunlaşması ve inflamasyonda azalmayı sağlar. *Aloe vera* jelinin Gram-pozitif ve Gram-negatif

bakterilere karşı antimikrobiyal özellikleri çeşitli yöntemlerle incelenmiştir. Ayrıca, *Aloe vera*, sülfür dioksit gibi sentetik koruyucu maddelere karşı güvenli ve çevre dostu bir alternatiftir.

Bu çalışmada, elektro eğirme işlemi ile titanyum (IV) izopropoksit veya titanyum (IV) bütoksit öncül maddelerinden sol-jel yöntemi ile elde edilen TiO₂, Polivinilpirolidon ve *Aloe vera* içeren çeşitli biyopolimer tabanlı fiberler hazırlandı. İşlemi etkileyen parametreler optimize edilmiştir. Literatürde, TiO₂ ve *Aloe vera*'nın antibakteriyel özellikleri mevcut olduğu bilinmektedir. Fiberler fırında 500 ° C'de 3 saat süreyle tavlandı ve polimer yapı uzaklaştırılarak anataz fazda TiO₂ fiberler elde edildi. Liflerin mikro ve nano yapısal karakterizasyonu SEM ile analiz edildi ve kristalografik karakterizasyon XRD ile yapıldı. Öncül madde olarak titanyum (IV) izopropoksit içeren fiberler, ısıtmadan sonra olumsuz yapı sergiledi. Böylece *Aloe vera* titanyum (IV) bütoksit solüsyonuna ilave edildi. Fiberlerin Gram negatif *Escherichia coli* (*E.coli*) ve Gram pozitif *Staphylococcus aureus* (*S.aureus*) 'a karşı antibakteriyel etkinliği incelendi. *Aloe vera*'nın eklenmesi fiberlerin antibakteriyel etkisini son derece arttırmıştır.

Ayrıca, *Aloe vera* eklenmiş agar ve PVA filmleri solvent döküm yöntemi ile hazırlanmıştır. Yenilebilir, şeffaf, kuvvetli ve antibakteriyel filmler, farklı miktarlarda *Aloe vera* jelinin (0, 10, 20, 30%) polimer filmlere ilave edilmesiyle hazırlandı. Biyopolimer tabanlı filmler fiziksel, morfolojik ve antibakteriyel özelliklerinin *Aloe vera* içeriğine bağlılığı ile karakterize edildi. Agar filmlerin yüzey analizi SEM ile yapılmıştır ve *Aloe vera* eklenmesinin film yapısına zarar vermediği gözlemlenmiştir. Kimyasal karakterizasyonları FTIR ile analiz edildi. Mekanik testleri incelendi ve kopma mukavemeti, kopma uzaması, Young modülü ve tan delta değerleri elde edildi. Filmlerin hidrofilik özellikleri temas açısı ölçümleriyle belirlendi. *Aloe vera* eklenmesi, Gram negatif *Escherichia coli* (*E.coli*) ve Gram pozitif *Staphylococcus aureus* (*S.aureus*)'a karşı antibakteriyel aktiviteyi arttırdı. Agar filmlerinin oksijen geçirgenliği ve su buharı geçirgenliği araştırıldı. Filmlerin ışık geçirimi spektrofotometre ile ölçüldü. Şişlik ve bozunma testleri yapıldı. Böylelikle, *Aloe vera* içeren biyopolimer tabanlı filmlerin, yara örtüsü veya aktif yenilebilir filmler şeklinde ambalaj malzemeleri olarak potansiyel kullanımları gözlemlendi.



1. INTRODUCTION

Nanotechnology arise from the term “nanometer” that defines one billionth of a meter in length measuring [1]. Fabrication, manipulation and characterization of materials at the nanoscale are subjects of nanotechnology [2]. Nanotechnology applications have extensive significance due to producing functional and advanced materials [1]. Nanoparticles have been used for developing nanomaterials. High surface area to volume ratio brings considerable advantage to nanomaterials. Materials that are porous, selectively permeable, high surface area can be chosen for several applications. Nanofibers are determined as fibers having less than one micrometer of diameter. These nanofibers can be produced from both organics such as polymers and inorganic materials like metals or ceramics. They have advantages for applications which need large surface area and porosity owing to their small diameters [3,4].

Filtrations, affinity membranes, tissue engineering, release control, enzyme immobilizations, wound healing, sensors and energy storage are major application areas of nanofibers [4].

Nanofibers can be fabricated by different processes such as phase separation, drawing, self-assembly, wet spinning and electrospinning. Production rate, organization and diameter of fibers and cost are elements that should taking into consideration for deciding on process technique. Electrospinning is one of the most suitable method which has high production rate and inexpensive to fabricate continuous nanofibers. Also, fiber diameter can be regulated from nanometers to microns [4,5].

Electrospun nanofiber mats have benefits as wound dressing prospect through its favorable properties such as the high porosity and high surface area facilitate the control of fluid effusion, fluids and gases can move through the mat while prevent the microorganism influx. Additionally, drugs and additives can be added into nanofibers for medical healing or antibacterial property [4].

1.1 Nanofibers

A fiber is a 1Dimensional object, which has a particular diameter, a definite axial ratio and a length. Natural fiber-form pattern examples are cotton, wool and hairs. In most cases, the fibers form a non-woven nanofiber mat by randomly deposition as shown in Figure 1.1 [4].

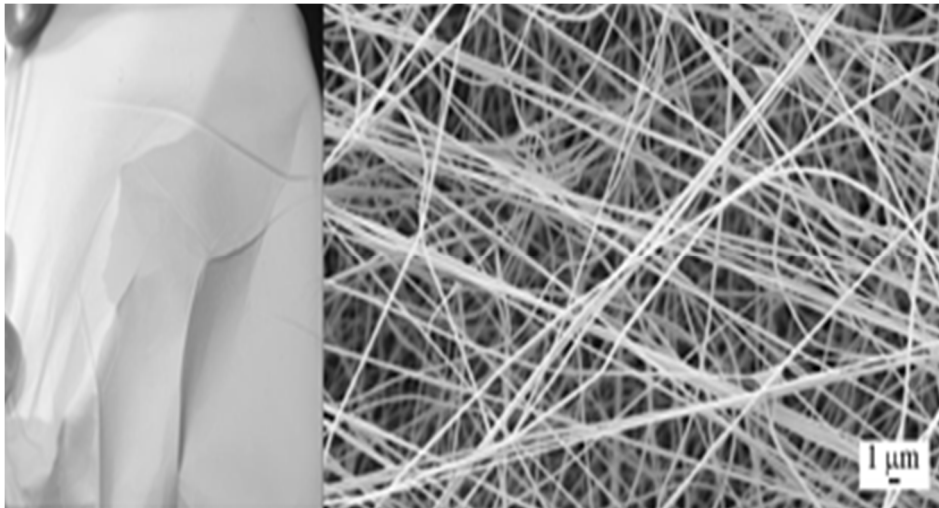


Figure 1.1 : Representative photographic and SEM images of a nanofiber [4].

Nanofibers are worthful and extremely useful materials in technical and medicinal areas. A number of feasible applications are membrane and filter practices, functionalization and enrichment of fibers, catalysis, drug delivery, tissue engineering or wound dressing [6]. Nanofibers present various particular features such as large surface-to-volume ratio, excessive porous structure, very low weight, and ability to easily develop for certain physical or chemical functionalization. Antibiotics or antibacterial agents can be contributed to raw material for designing nanofibers with antibacterial effect [1,4-7].

One of the most important detail is the selection of the material with a known prominent such characteristics as mechanical, optical, electrical, thermal, and magnetic. A large variety of polymers, metals, organic and inorganic materials have been chosen according to sort of application for the production of nanofibers. Adjusting the basic structure of the fiber is another significant factor, suitable fiber preparation method is selected for desired qualities intending at the objective utilization [6].

1.1.1 Nanofiber production techniques

Nanofibers can be produced by different techniques such as drawing, phase separation, self-assembly, wet spinning and electrospinning.

1.1.1.1 Drawing

Drawing method demands very few apparatus for producing nano, micro and macrofibers. As pictured in Figure 1.2, a few micrometer diameter micropipette or a needle is dipped into the millimetric droplet towards the contact line by use of micromanipulator. Nanofibers being pulled by drawing back the micropipette from the liquid. The end of the micropipette is adjoined on the surface to deposit the produced fibers. The fibers are drawn repeatedly on each droplet. The material should be viscoelastic in such a way that can sustain hard deformations and promote the stresses brought out while pulling [1].

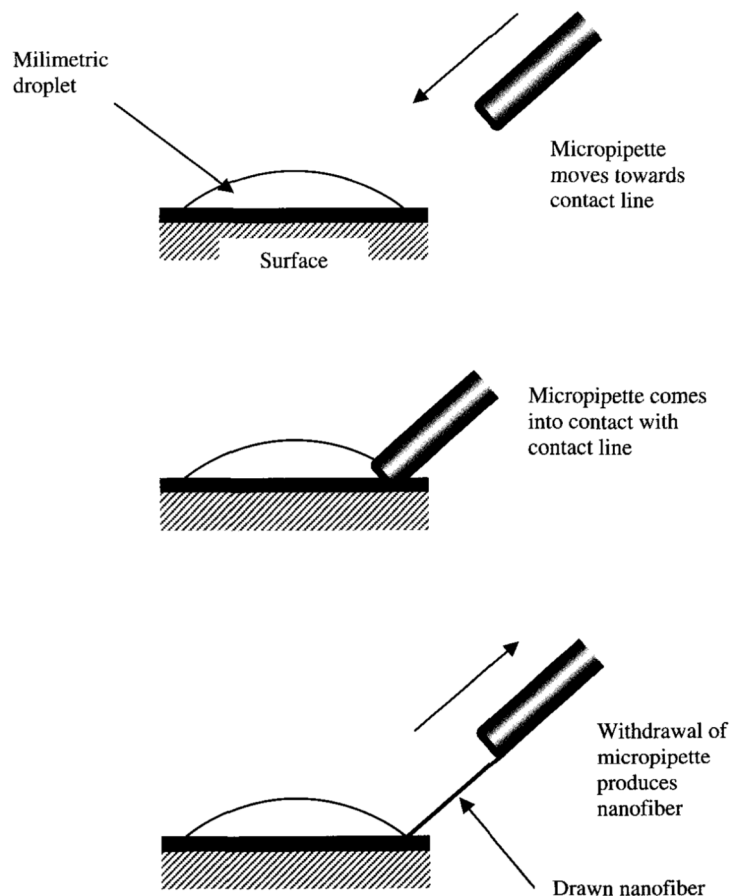


Figure 1.2 : Producing of nanofiber with drawing technique [1].

1.1.1.2 Phase separation

The principle of phase separation method is the separation of phases based on physical difference. Firstly, a polymer is blended with a solvent. After the gelation, solvent is extracted, in this way the other phase is remained as illustrated in Figure 1.3. Nanofiber matrix can be instantly created with minimum equipment by this technique. Polymer concentration is changed for controlling of mechanical features [1].

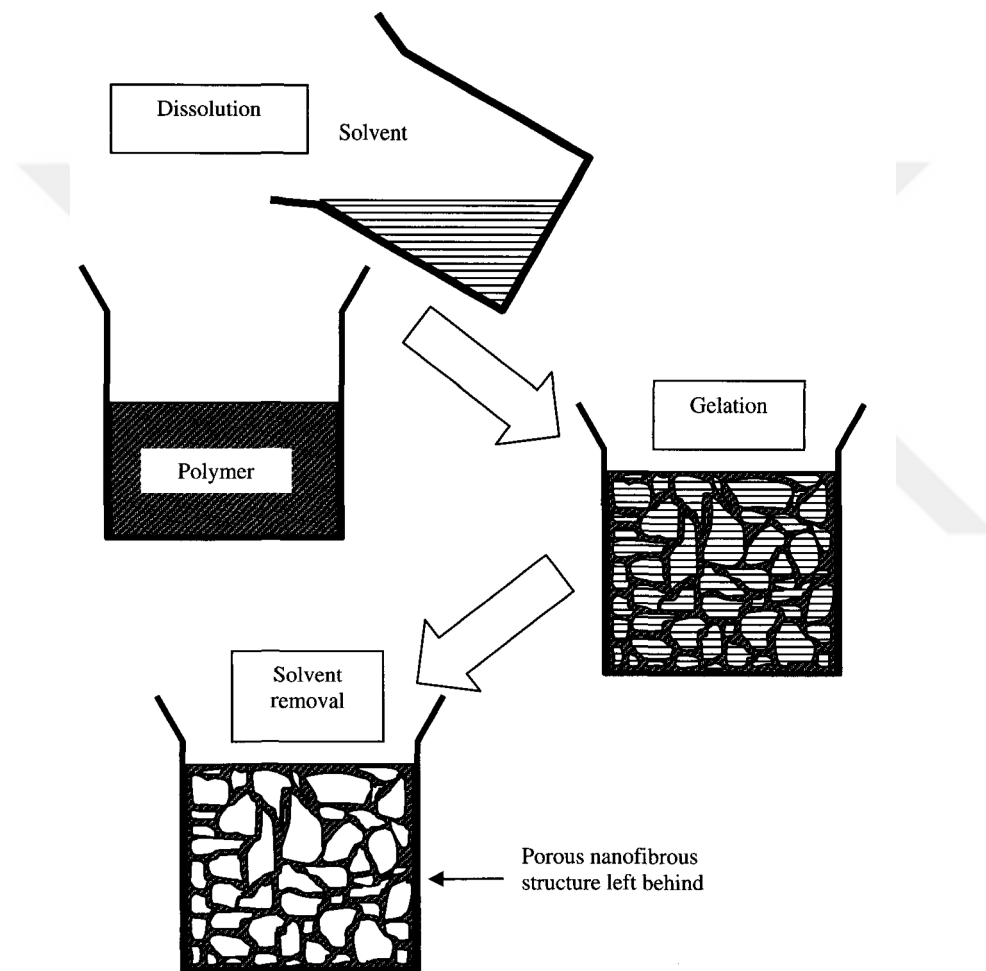


Figure 1.3: Phase separation technique for fabricating nanofibrous structure [1].

1.1.1.3 Self-assembly

In self-assembly technique, smaller molecules are used as prime building blocks to constitute nanofibers. The basic process is that smaller units are brought together via intermolecular forces and the structure of the block units form the complete shape of the macromolecular nanofiber as described in Figure 1.4 [1].

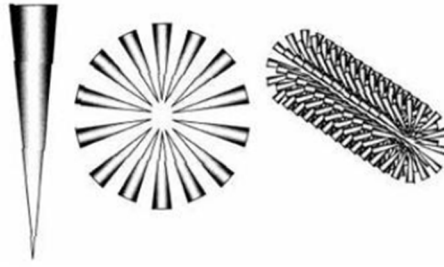


Figure 1.4 : Self-assembly of units [1].

1.1.1.4 Electrospinning

Electrospinning is one of the most efficient methods for the fabrication of nanofibers. This process is based on getting thin of viscoelastic fluid by pulling it in a route using electrostatic force. The precursor researches were in 1700's with liquids in electrical fields [1,6]. In 1885 Raleigh defined the desired amount of charge for transformation of droplets. Droplet is affected by two forces, which are electrical and surface tension, electrically charged jet of droplet is created when the electrical force overcame the surface tension [8]. Electrospinning was patented in 1934 by Formhals as preparation of polymer fibrils employing electrostatic forces [9]. This method is utilized mostly to polymer-based elements, but also application of different precursors amplifies fabrication of metal, ceramic and glass nanofibers [6].

The basic electrospinning setup consists of 3 components as shown in Figure 1.5 [10]:

- A syringe and needle
- A high voltage power supply
- A collector

The process initiates with movement of electric charges into the polymer fluid held in a syringe. The polymer drop is arised on the needle and exposed to high voltage. A collector, which is a counter electrode, is located at a proper distance from the tip of needle, so a high electric field is created. The charges induce instability within the solution, the solution is also under surface tension forces and the droplet forms a conical shape which is named as "Taylor cone" [11]. When the voltage is increased and reached a critical value, the electrostatic forces exceed the surface tension of the cone-shaped droplet, a polymer jet is produced and it started to move forward to the collector. Jet travels linearly for the first some centimeters, then an unstable and fast

whipping of the jet occurs. Rapid whipping motion cause evaporation of the solvent, the diameter of the viscoelastic jet is reduced by drawing and continuous, dry, ultra-thin fibers are formed on the collector. The procedure can be changed to control the fiber diameter by altering the strength of electric field and concentration of polymer solution [10,12].

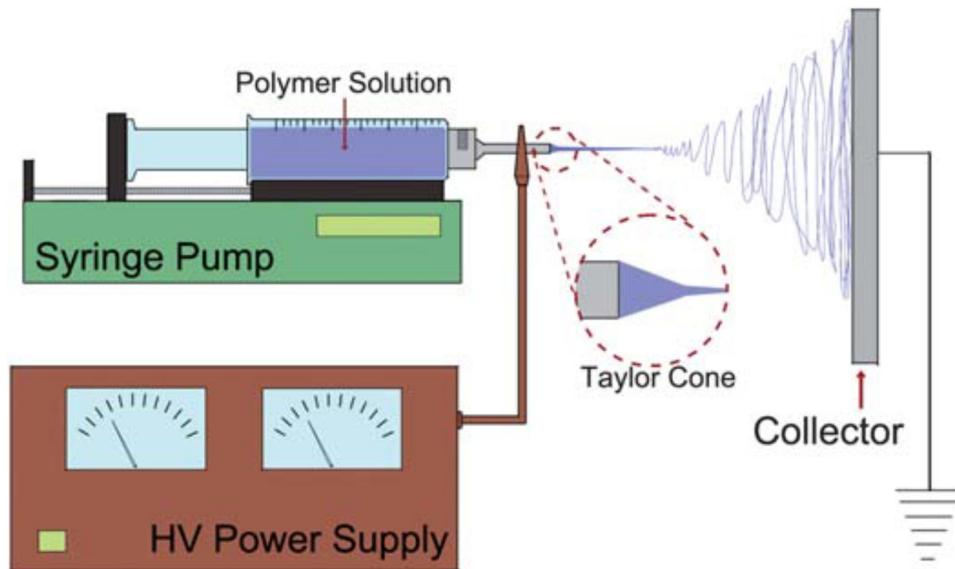


Figure 1.5 : Design of a conventional electrospinning set-up [10].

1.1.2 Factors affecting electrospinning process and nanofiber properties

Parameters that affect the final morphology of the production and the process dynamics can be examined in three main groups. Solution properties, setup and process conditions and the environmental ambient conditions are determinant parameters.

1.1.2.1 Solution properties

The properties of the solution have an important impact on the electrospinning operation and fiber morphology. Concentration, surface tension, viscosity and conductivity are critical parameters that identify the solution properties.

1.1.2.2 Concentration

The concentration of solution should be adjusted at the optimum level. Formation of beads is monitored in low concentrations, and larger fibers are observed as a result of high concentrations because run of the solution from the tip of the needle is inhibited; thereby, generation of continuous fibers cannot be possible [13]. The

viscosity of a solution is altering as the concentration changes. Increasing the concentration of solution causes the fiber jet to contain more polymer and finally production of larger fibers [14].

1.1.2.3 Viscosity

Viscosity is one of the most significant parameter that affects fiber morphology and size in electrospinning process. The viscosity of the solution should be within a certain range to produce continuous nanofiber. Production of continuous fiber is not possible with low viscosity because of formation of nano- and micro-particles. In contrary, generation of jets from polymer fluid is difficult with high viscosity. Concentration and molecular weight of polymer play the most important role on viscosity. Moreover, additives, which are organic or inorganic and intermolecular interactions in solvent, are contributing factors that have an impact on viscosity. Surface tension is prime factor for solutions with low viscosities, therefore, formation of beads ruin the fiber morphology. Jet continuity is provided when enough viscoelasticity is supplied [15,16].

It is claimed that there is an exponential relevance between fiber diameter and viscosity as seen in Figure 1.6. [17].

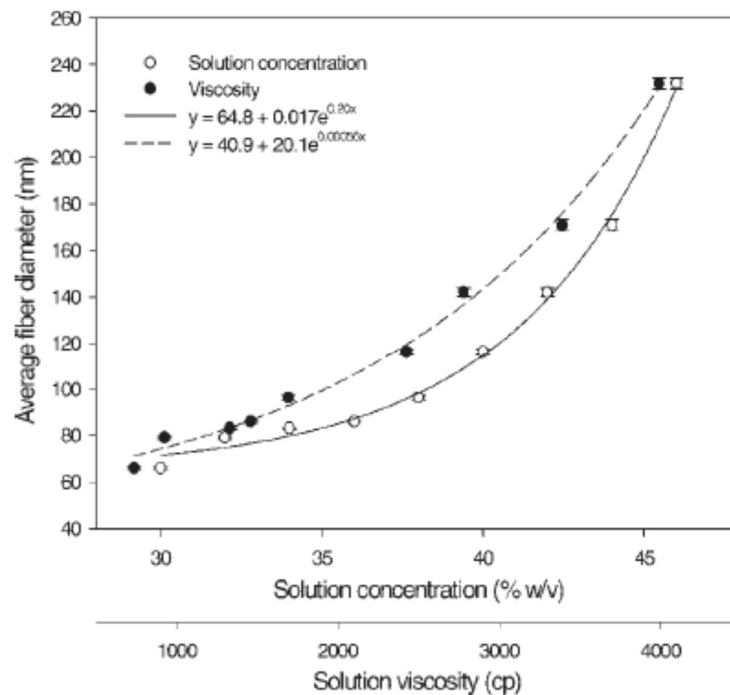


Figure 1.6 : Average diameter of polyamide fibers as a function of viscosity and the concentration of solutions [17].

High motility of polymer chains and infirm intermolecular forces in low viscosity solutions cause unsteadiness during electrospinning process. Because of that, the jet is subject to more stretch, so small diameter fibers are generated. Diameter of fibers is increasing because polymer molecules have firmer structure in high viscosity; thereby jet is exposed to less elongation [15].

1.1.2.4 Surface tension

Solvents present in solution form surface tension, which has a crucial role in the formation of beads, droplets and fibers. The high surface tension of a solution leads unstable jets and formation of sprayed droplets in the electrospinning operation. The electrostatic forces constrain the polymer droplet to elongate while the surface tension maintains the droplet at minimum surface area. Fibers can be generated without bead by a lower surface tension. Surface tension depends on the kind of solvents [18,19].

1.1.2.5 Conductivity

Electrospin solution must carry charges to overcome the surface tension and following stretching. Solution with lower conductivity has not enough charge to generate a Taylor cone, causes failure in electrospinning. A solution with higher conductivity rate leads to carry more charges in the electrospinning. By adding ions to the solution, higher conductivity rates can be obtained. By increasing conductivity, stretch will be increased in the solution and the bead formation can be prevented. Increased stretch will yield to structures with smaller diameter. The conductivity increase will lead to a decrease in the critical voltage for electrospinning process starts and a formation of greater bending [1].

1.1.2.6 Process conditions

The processing conditions that change the products properties are voltage, feedrate, collector type, diameter of the needle tip, distance between tip and collector.

1.1.2.7 Voltage

The application of a high voltage is a vital factor in electrospinning. The high voltage inducts the charges on the solution and triggers the electrospinning process together with the external electric field, so the electrostatic force in the solution overcomes

the surface tension of the solution (Figure 1.7). The solution forms a droplet at the tip of the needle to bend into the shape of a Taylor Cone above voltage of 6 kV during jet formation. If the voltage is higher than a necessary value, smaller and less stable Taylor cone forms. Higher voltage will lead to greater stretching of the solution, reduces the diameter and promotes faster solvent evaporation to produce drier fibers but possibly leads to bead formation. If lower viscosity is used, a higher voltage must be applied for reducing the diameter. At a lower voltage, there is enough flight time for the stretch and elongate process. Increasing voltage will increased the beads density, which at an even higher voltage; the beads will join to form a thicker diameter fiber [1,20].

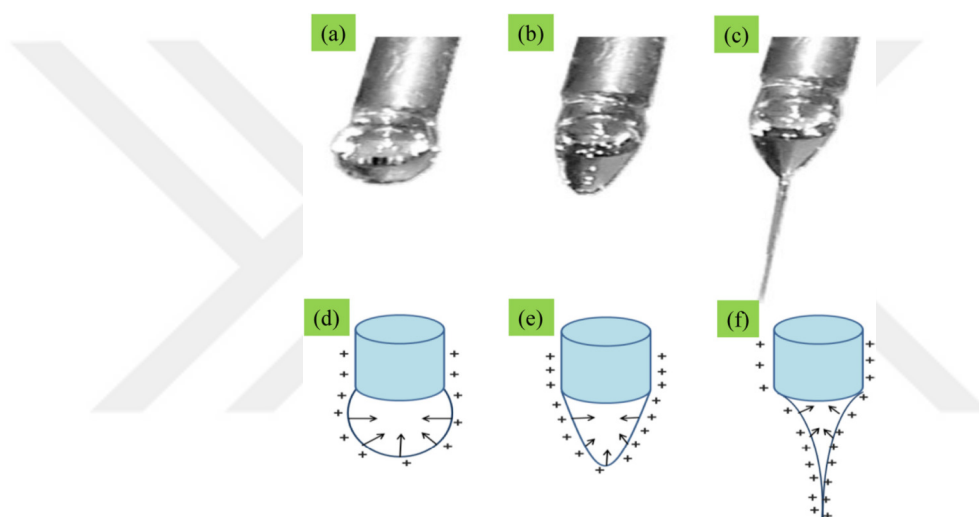


Figure 1.7 : Digital (a-c) and cartoon (d-f) images showing the three stage deformation of the polyvinylpyrrolidone droplet under the influence of increasing electric field; (a,d) hemispherical drop, (b,c) conical shape, (c,f) Taylor cone [20].

1.1.2.8 Feedrate

The feedrate regulates the amount of solution flowed through the needle tip and affects the morphology of the fibers. Necessary feed rate can be distinguished from a qualified Taylor cone formation. There is a critical flow rate for each polymeric solution; uniform beadless nanofibers can be obtained via this critical value. Increase in the feed rate increases the fiber diameter while there is a maximum point had affects the product. If unnecessarily increased feed rate shows up, greater volume of solution ejaculated and it cannot find any time to evaporate. It causes increase not only the fiber diameter but also bead formation. A lower feedrate is more desirable as the solvent will have more time for evaporation. A balance between the flowing

solution and replacement of that solution with the fresh one is maintained with a minimum flow rate during jet formation [1,11].

1.1.2.9 Collector type

For creating a stable potential difference between source and collector, conductive materials are used as collector plates. In case of non-conducting material used as collector, charges of the jet will quickly collect on the plane and fewer fibers are produced [1]. There are various types of collectors as seen in Figure 1.8. Stationary metal plate or a foil placed at a fixed distance from the tip is the simplest type of collector that results with symmetric circular patch of nanofiber on the surface of the metal. A moving collector surface allows some control in the areal density. Using a rotating drum surface allows uniform fiber production. Rotating collector is useful in getting dry fibers as it provides more time to the solvents to evaporate. Tubular fiber mats with a range of diameters were fabricated by the technique that also yielded good control over wall thickness. Open frame collectors (rectangular, pyramidal, or cylindrical) have been used for years to obtain aligned nanofibers [21].

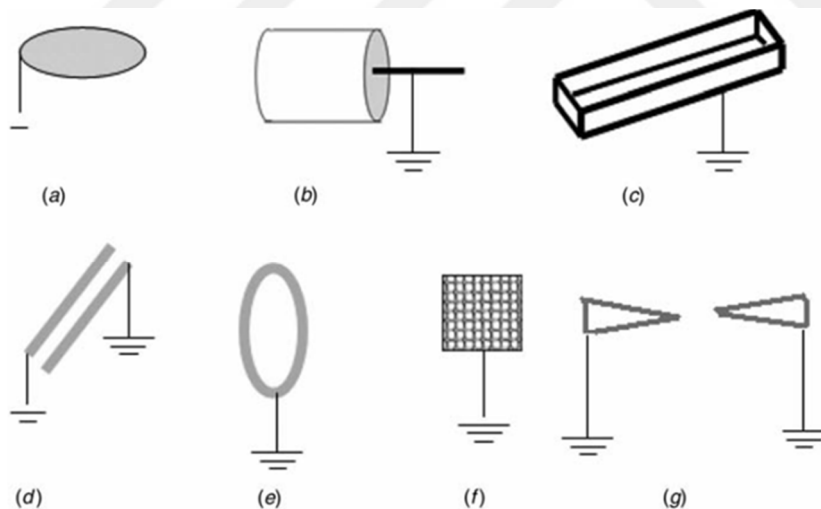


Figure 1.8 : Collector types; (a) flat plate, (b) rotating drum, (c) rectangular, triangular or wire cylinder frame, (d) electrode pair arrangements, (e) single or multiple ring electrodes, (f) mesh electrode, (g) pair of cone shaped [21].

1.1.2.10 Needle to collector distance and needle diameter

The distance between the tip and the collector affects the electric field strength and the flight time of the solution. The morphology of the nanofibers can be affected by the distance because the accumulation time, evaporation rate, and whipping or instability interval varies with the distance. Hence, producing smooth and uniform

nanofibers is depend on sustain a critical distance. The electrospinning jet needs time for the evaporation of solvents to form separated fibers. If the distance between collector and the tip is too short, the fiber will not have enough time to solidify, and if the distance is too long, beads can be observed. However, a sufficient increase in the distance will result with fibers with smaller diameter [1,11]. In addition, a smaller internal diameter of needle leads to reduce blockage and beads on the fibers. The solution is less exposed to the atmosphere in case of a small diameter needle tip, so the clogging is reduced. The reduction of the diameter of the electrospun fibers can be observed due to the smaller holes. Nevertheless, it may not be possible to subtract a drop of solution at the tip of the needle when the diameter of the hole is too small [1].

1.1.2.11 Ambient Conditions

Environmental factors such as relative humidity and temperature have an effect on the electrospinning process. High humidity causes accumulation of water on the fiber surface. Increased humidity also induces creation of pores on the surface of the electrospun fibers and they merge to generate non-uniform, large structures. The diameter of the nanofibers is changed with humidity by managing the solidification process of the jet [11].

In higher temperature, evaporation rate is increased and the viscosity is reduced. This procedure leads to form uniform diameter. With lower viscosity of the solution and greater solubility of the polymer in the solvent, more stretching of the solution will result in fibers of smaller diameter. However, if biological substances are used high temperature may cause loss of functionality [1].

1.1.3 Application of electrospun nanofibers

A broad range of technical parts managing our daily lives in the area of both private and technical, also large number of currently revealed technologies have fibers in their basic structural and operational elements or are based on fiber-type structures. Nanofibers are unrivaled nanostructures have a magnificent potential in medical and technical areas such as filter applications, fiber reinforcement as in transportation, drug delivery, wound healing, tissue engineering, functionalization of textiles. Furthermore, electric cables carrying electric energy comprised of fibers and objects

supply clean air, water, and gas are also some examples of application of fibers in technical area. The application areas of nanofibers were shown in Figure 1.9 [4].

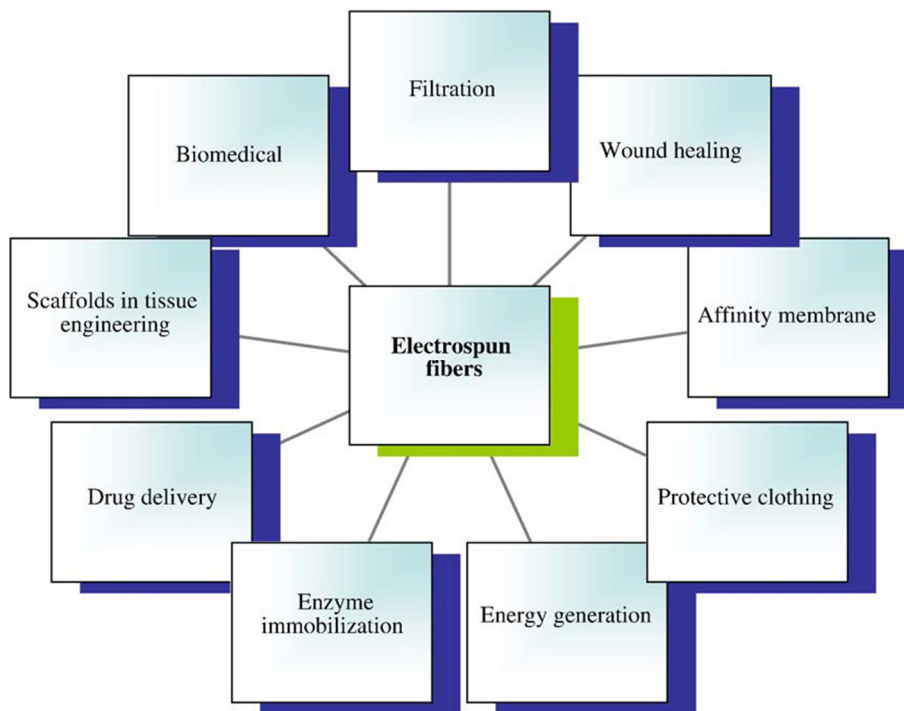


Figure 1.9 : Application areas of electrospun fibers [4].

1.1.4 Wound dressing

Wound healing incorporate a dynamic cycles of events involved chemotaxis, cell division, neovascularization, synthesis of new extracellular matrix, and the formation and remodeling of the scar tissue. Platelets, inflammatory cells, cytokines, growth factors, matrix metalloproteinases and their inhibitors are regulation agents of these events. Haemostasis, inflammation, proliferation, and remodeling are the wound healing phases [22]. The risk of exposure to bacterial infection is high for wounds because the wound stay opened and unhealed for a time and it results that microorganisms from various sources such as external environment, skin region and endogenous basis can easily colonize [23].

The aims of wound dressing materials are block bleeding, insulate the wound from external irritants along with water and electrolytes, and protect from invasion of microorganisms [24]. Treatment of wounds presently focuses on dressings that inhibit microbial invasion and perform a steady moisture and gas exchange environment. In addition, delivery of antibacterial agents is aimed when an infection arise. Enhancement of cell proliferation is another point of the wound dressings [25].

Progress of wound dressings ground on fabrication of polymeric nanofibrous mats. They have advantages for applications, which need large surface area and porosity owing to their small diameters. Nanofiber mats have benefits as wound dressing prospect through its favorable properties such as the high porosity and high surface area facilitate the control of fluid effusion, fluids and gases can move through the mat while prevent the microorganism influx. Additionally, drugs and additives can be added into nanofibers for medical healing or antibacterial property. Antibiotics or antibacterial agents can be added to raw substance for designing nanofibers with antibacterial effect. In addition, nanofibers are presenting as a scaffold for cell proliferation [4].

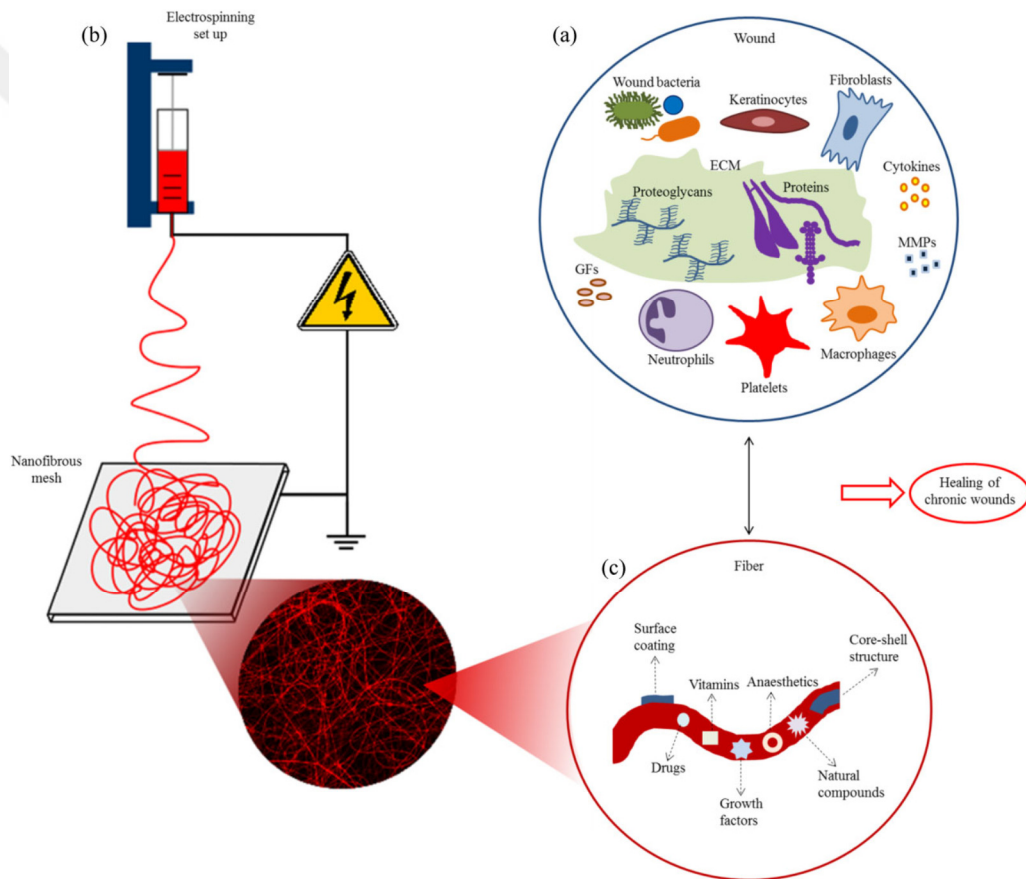


Figure 1.10 : a) Biomolecules existing in the wound bed and implied in the healing process; b) the production of nanofibrous mats by electrospinning method; and c) the main advances to get electrospun fibers for the necessary features for wound healing applications [25].

Fabrication of antibacterial nanofibres employs the method of containing a biocide in the fibers. Different active agents can be used, including antibiotics, silver nanoparticles, metal oxide nanoparticles and several additives. Various methods can

achieve the incorporation of biocides into fibers. They can be summarized as blending the active agent in the polymer solution prior to electrospinning, enclosing the active agent in the core of the fiber by way of coaxial electrospinning, encapsulating the active agent in nanostructures before dispersing them in the electrospinning solution, post-treatment of the fiber after electrospinning to transform a precursor to its active form and attachment of the active agent onto the fiber surface (Figure 1.11) [26].

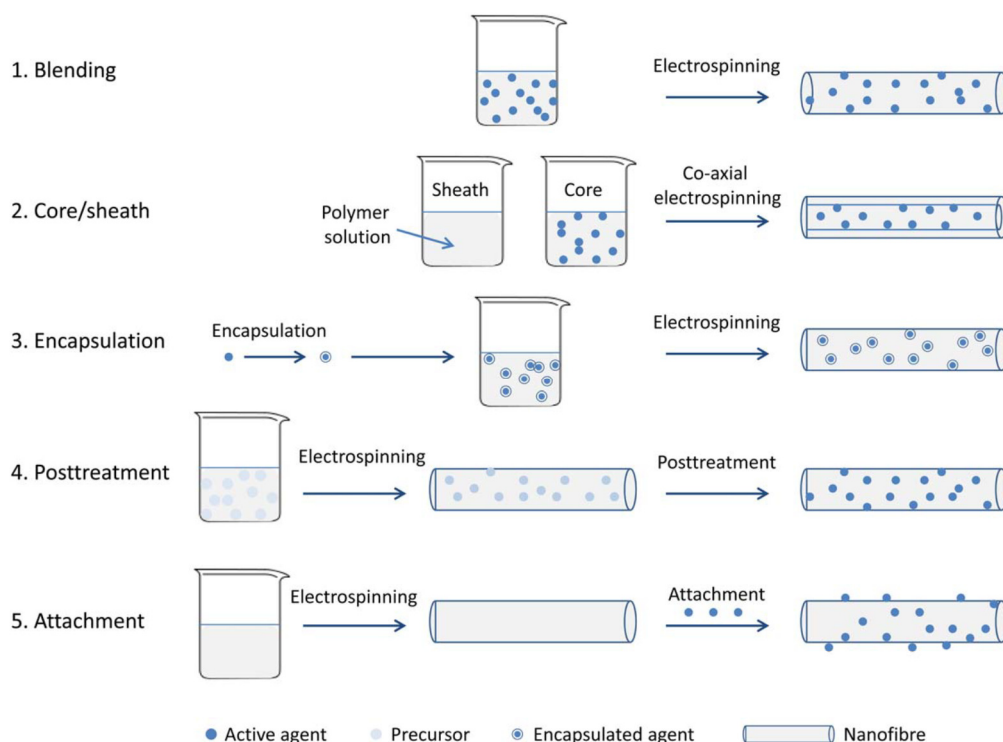


Figure 1.11 : Different methods of incorporating biocides into electrospun nanofibers [26].

1.2 Polymer Films and Hydrogels

Polymer films have promising properties for biomedical and food-packaging applications. Hydrogels are polymeric networks that are able to absorb aqueous solutions through their hydrophilic properties and sustain their structure without dissolution. Hydrogel films are fabricated by natural and synthetic polymers such as chitosan, alginate, gelatin, poly(vinyl alcohol) (PVA), poly(vinylpyrrolidone) (PVP). The important features of suitable polymers for film forming are flexibility, permeability, thermal and dimensional stability, biocompatibility, biodegradability, mechanical properties and degradation rate [27]. The polymer linkage can be

accomplished either chemically or physically. The chemical crosslinking is a versatile practice to make hydrogels with great mechanical behavior. Nevertheless, the crosslinkers used to obtain strong hydrogel structure are generally hazardous. The addition of toxic crosslinking agents is prevented in physical crosslinking; hence, studies on physically crosslinked hydrogels has increased. Methods for synthesizing chemically crosslinked hydrogels are;

- Polymerization
- Radiation (e.g. γ -ray)
- Small-molecule crosslinking (e.g. glutaraldehyde)
- Polymer–polymer crosslinking (such as condensation reaction)

Methods for synthesizing physically crosslinked hydrogels are;

- Ionic interactions (like alginate with Ca ions)
- Hydrophobic interactions (PEO–PPO–PEO etc.)
- Hydrogen bonding interactions (PAAc etc.)
- Stereocomplexation
- Supramolecular chemistry (e.g. inclusion complex)[28]

Casting-solvent evaporation and freeze-thaw techniques are performed for physical crosslinking of hydrogels. The physical hydrogels, particularly those containing natural polymers have started to be commonly used in industry and medicine because of their promising features such as biocompatibility, biodegradability, non-toxicity, eco-friendly and easy producibility [29,30].

1.3 Edible and Biodegradable Films for Packaging Applications

The food industries have searched various alternatives in packaging technology because demands of consumers and market have been changing in recent years. These desires can be outlined in high quality, extended shelf life and freshness of the food products, the ease of handle, strong and long-lasting packaging fabricated with lighter, cheaper and recyclable materials. The active packaging technologies concern these requirements; they interact with the food, extend the shelf life and enhance the quality of the food [31].

The use of polymers and natural materials as food packaging materials has increased mainly due to their promising assets over the traditional materials. The specific needs of each food product can be supplied with the most appropriate packaging solution and design by a wide variety of materials and different compositions.

Polysaccharides are natural and edible polymers of sugars. Many of them are cheap and abundant; some of them have film-forming properties. Developing polysaccharide-based films is suitable for requirement of edible packaging films [32].

The significance of biodegradable films can be expressed as:

- The usage of biodegradable plastics from natural products instead of synthetic plastics produced from petroleum reduces the consumption of petroleum.
- The amount of non-biodegradable synthetic plastic waste decreased by changing them with biodegradable plastics because biodegradable plastics are environmentally friendly.
- Processing of biodegradable plastics from natural materials can be economically advantageous [32].

1.4 Measurement Systems and Tests

1.4.1 SEM (Scanning electron microscope)

Scanning electron microscopy facilitates the examination of specimens with a resolution down to the nanometer scale. A basic SEM device includes a light source, an illumination section, a magnification section and a detector. Scanning electron microscopes function at a high vacuum level. The basic principle is that an electron gun generate a beam of electrons and the beam is accelerated with a high voltage between the range of 0,1-30 keV. Beam move through an array of lenses and apertures to control the diameter of the beam for producing thin beam of electrons. Then, the beam arrives in specimen and scans the surface of the sample. Secondary electrons and back-scattered electrons are emitted from the surface and the signals are collected by a detector. They are transformed to an image or spectra on the display screen [33].

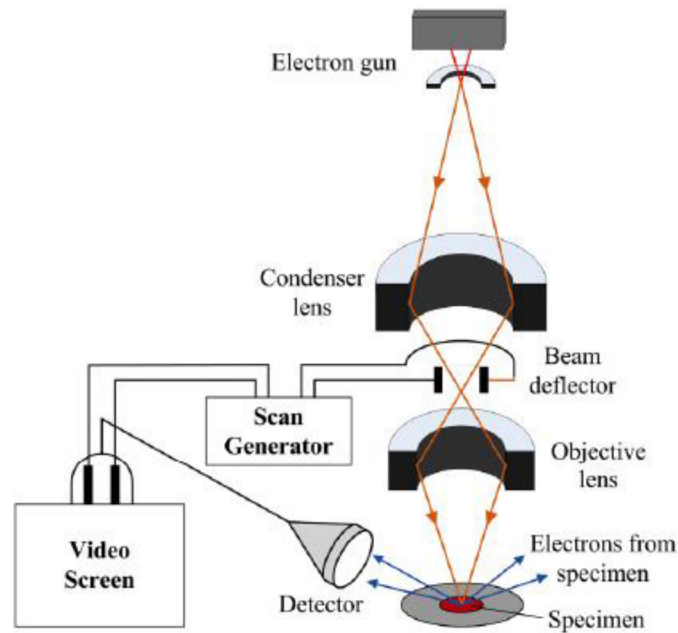


Figure 1.12 : SEM system operation diagram [34].

1.4.2 XRD (X-Rays diffraction)

X-rays are a type of high frequency electromagnetic radiation which range between ultraviolet light and gamma rays in the electromagnetic spectrum. X-rays have very small wavelengths between the 0.01 to 10 nanometers. There are two ways of generating X-rays; a continuous spectrum of X-rays is produced with the transition of the kinetic energy of charged atoms into radiation, and characteristic lines of about monochromatic X-rays are generating via the excitation of atoms in a target by striking of accelerated electrons [35].

X-ray diffraction is a non-destructive, multi-purpose and powerful technique that determines specific information about the chemical structure and crystallographic nature of materials. It is an ideal method for studying structure of nano-materials owing to the atomic level of wavelength of X-rays. Elastic scattering is the basis of X-ray diffraction, the direction of the electromagnetic waves motion changes but there is no energy loss in this mode of scattering. The sum total of the electromagnetic waves that are diffused from the atoms in phase results in diffraction [35,36].

A standart XRD apparatus composes of four basic tools such as X-ray source, sample stage, receiving optics and X-ray detector as shown in figure. The basis of XRD analysis is Bragg's law. Crystal structures are detected with certain quantifications of

experimental findings through this law. The formula of Bragg's law is shown in equation 1.1.

$$2d \sin \theta = n\lambda \quad (1.1)$$

θ is the angle between the plane of the sample and the X-ray beams. The distance between successive atomic planes in a crystal is d , λ is the wavelength of the X-ray and n is the order of diffraction. Powdered specimen is fixed on the specimen holder for the XRD assay. The arrival of an X-ray beam onto a specimen causes scattering from all atoms. When the scattered beams have identical phases, constructive interference arises and the intensity of scattered waves reach maximum at that angle. That intensity is evaluated as the function of the angle to get a diffraction pattern. The crystal configuration, orientation, and the mean size of crystal are obtained with X-ray diffraction analysis. Almost 25,000 organic and 50,000 inorganic single elements, diffraction patterns and crystalline phases have been studied and kept as references on an optical or magnetic context [36,37].

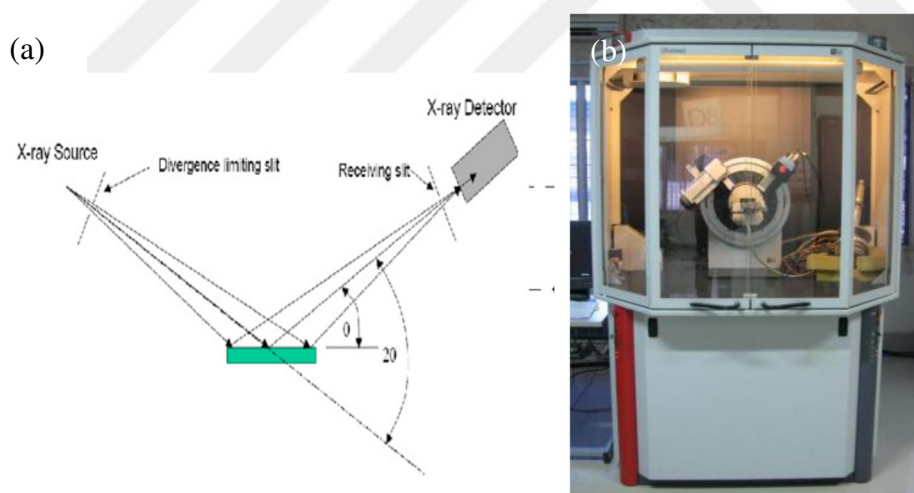


Figure 1.13 : (a) Schematic operation of XRD and (b) XRD instrument [36].

1.4.3 FTIR (Fourier transform infrared)

Infrared Spectroscopy (IR) investigates the molecular vibrations. Absorption in the infrared region creates changes in vibrational and rotational states of the molecules. Functional groups can be linked to characteristic infrared absorption bands which comply with the fundamental vibrations of the functional groups. The molecule absorbs the incident infrared light, if the dipole moment of the molecule change

during the vibration. The absorption frequency depends on the vibrational frequency of the molecules. Two particular types of vibrations are monitored in the mid-infrared region ($400\text{-}5000\text{ cm}^{-1}$); stretching vibrations (ν) that are vibrations along chemical bonds containing bond-length changes and bending vibrations (δ —in plane, π —out of plane) including changes in bond angles [38,39].

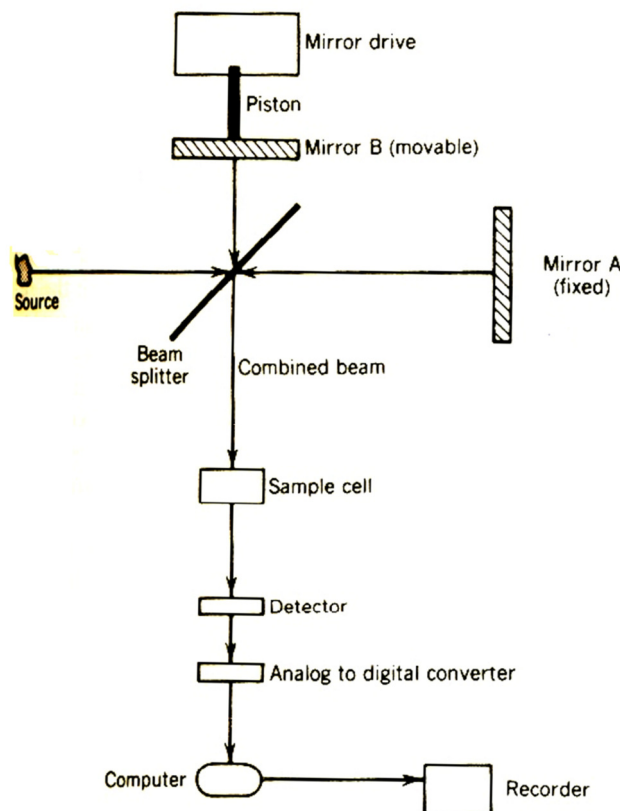


Figure 1.14 : Schematic operation of FTIR [38].

Conventional dispersive infrared analysis or Fourier Transform Infrared (FTIR) spectroscopy can be used for quantification of various components absorbing in the mid-infrared region ($400\text{-}5000\text{ cm}^{-1}$). Considering the dispersive IR analysis, FTIR analysis is faster and has a better signal-to-noise ratio [38].

1.4.4 Antibacterial activity test

Different techniques are used to detect antimicrobial activity of samples; the agar diffusion assay is one of the most conventional methods. This technique relies on the diffusion of compounds from a disk into agar plate where bacteria have been seeded. If the compounds are antimicrobial, it prohibits the bacteria from growing so a clear zone seems around the disk after the microbial growth on agar. The area of zone

depends on the antimicrobial activity of the sample. The agar diffusion assay is an inexpensive, simple and easy to interpret results. The results are obtained within 24-48 hours [40]. After agar is dissolved in distilled water, the medium is prepared by placing in autoclave at 121 °C. Then the bacteria are inoculated on the prepared medium and the test samples are placed on them. The plates are incubated at 37 °C for 18-48 h and the area of inhibition zone was measured.

Staphylococcus aureus (Gram +) and *Escherichia coli* (Gram -) are the microorganisms used for the antimicrobial test. Bacteria can be divided into two main subclasses as Gram positive and Gram negative according to how they respond to the basic dyes used in a Gram stain. The cell walls of Gram positive and Gram negative bacteria both are formed from peptidoglycan. The cell walls of Gram positive bacteria are very thick (up to 80 nm thick); the peptidoglycan of Gram positive bacteria is highly crosslinked. The cell walls of Gram-negative bacteria are thinner (10 nm or less); the peptidoglycan is not as fully crosslinked [41].

Staphylococcus aureus is a Gram-positive, round-shaped commensal bacterium. It causes skin infections and food-borne illness [42]. Wounds should be protected from *S.aureus* infection.

Escherichia coli are Gram-negative, rod-shaped bacteria that found in the environment and intestines of animals. Most strains of *E. coli* are harmless, but some kinds of *E. coli* can cause diarrhea, urinary tract infections, respiratory illness and other illnesses [43].

1.4.5 Mechanical Properties

The mechanical properties such as tensile strength, elongation and elastic modulus express strength, flexibility and toughness of a film and indicate the ability of sustain film integrity [44]. The mechanical features of films depend on their composition, structure, crosslinking density and polymerization conditions. Experimental methods were used to characterize the mechanical properties such as Young's modulus. Simple tensile testing is employed to detect the behavior; the test specimen cut and placed between the sample clamps. The sample is pulled with constant extension speeds at different loads until it ruptured [45].

In this work, the thickness of the film samples was measured by handheld micrometer with a sensitivity of 0.01 mm. Thickness was taken in five random points

of the film and the average values were used. The films cut into rectangular strips with 20 mm width. The two ends of each sample were fixed into the sample holders. Shimadzu Autograph AGS-10kNJ with TRAPEZIUM2 data processing software was used with the crosshead speed of 15 mm/min. The tensile strength (TS) was calculated by dividing the maximum load (N) by the initial cross-sectional area (mm²) of the films as seen in equation 1.2 and expressed in MPa. The elongation (ε)(%) was determined by dividing the extension at the rupture of the film by the initial length of the film multiplied by 100 as shown in equation 1.3. The elastic modulus (*E*) was determined from the slope of the linear portion of the stress–strain curves.

$$TS = F_{max} / A \quad (1.2)$$

$$\% \epsilon = (L / L_0 - 1) \quad (1.3)$$

Also, dynamic mechanical analysis (DMA) can be employed under tension or shear to find the viscoelastic properties. It is a commonly used technique to characterize properties of materials as a function of temperature, time, frequency, stress, atmosphere or a combination of these factors. A sinusoidal deformation is enforced to a specimen, the stiffness of the sample determine its deformability [46].

DMA estimates stiffness and damping that are examined as modulus and tan delta. The modulus is stated as an in-phase component, the storage modulus, and an out of phase component, the loss modulus. The storage modulus, showed as *E'* or *G'*, is the measure of elastic behavior. The ratio of the loss to the storage gives the tan delta which is called damping. It is a measurement of the energy loss of a material and states that its succeeding at absorbing energy. Figure 1.15 shows transition in materials, which can be observed as changes in the *E'* or tan delta curves, these are changed with temperature [46].

The viscoelastic properties of agar films were determined by Perkin Elmer Diamond dynamic mechanical analyzer (DMA) operating in tensile mode. The spectrum was scanned from 25 to 160 °C with a frequency 1 Hz and heating rate of 3 °C/min.

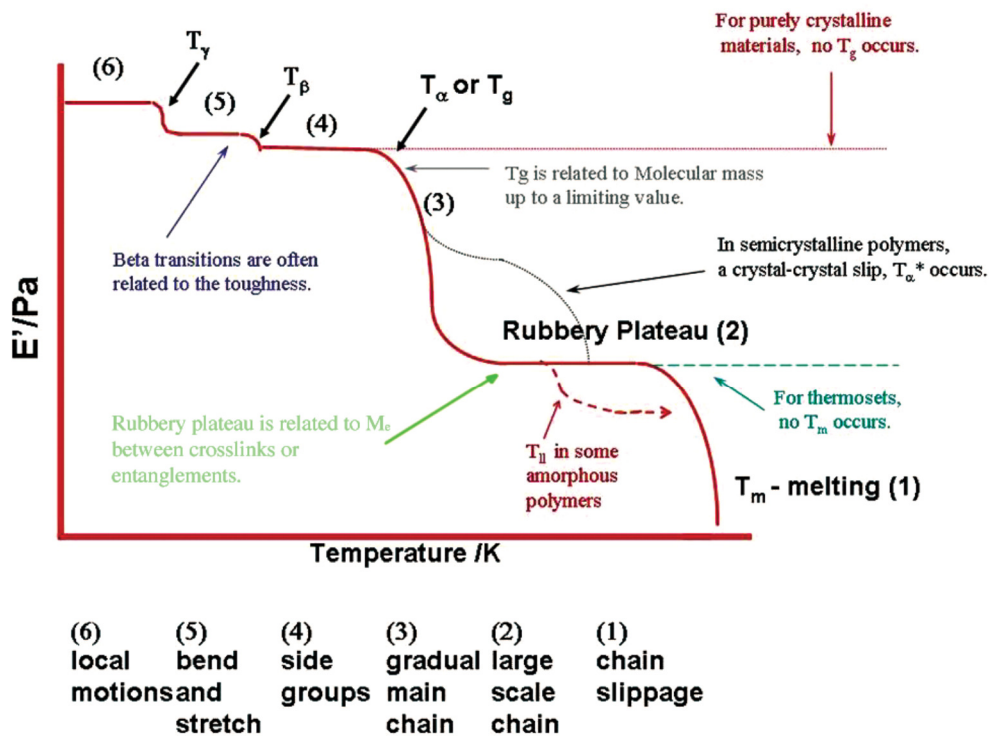


Figure 1.15: Changes in the E' or $\tan \delta$ curves gives transitions in materials [46].

1.4.6 Contact angle measurement

Contact angle is described as the angle originated by a liquid at the three-phase boundary where a liquid, gas and solid intersect. The interfacial tensions, which are between solid and vapour (SV), solid and liquid (SL) and liquid and vapour (LV), balance a liquid drop on solid surface and form the contact angle equilibrium as shown in Figure 1.16. The Young equation (1.4) defines the state of equilibrium at the three-phase contact;

$$\gamma_{sv} = \gamma_{sl} + \gamma_{lv} \cos \theta_Y \quad (1.4)$$

where γ is the interfacial tension and θ_Y is Young contact angle [47,48].

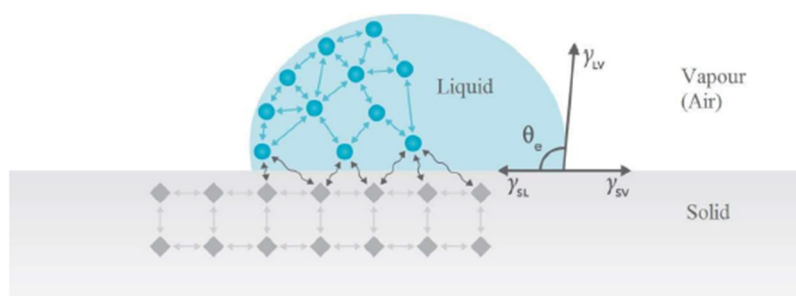


Figure 1.16 : Three-phase boundary where liquid, gas and solid intersect [47].

The focus of contact angle studies is to find out the wetting properties of an individual liquid on a solid substrate. If the solid layer has high surface energy, $\cos\theta$ becomes close to 1 as the contact angle approaching zero, which show that liquid is spreading on the surface of solid. In samples where the solid has a much lower surface energy compared to the liquid, the contact angle exceeds 90° and the surface displays hydrophobic properties [47,48].

The measurement of contact angle can be performed by two methods as static contact angle measurement and dynamic contact angle measurement. Static contact angle is measured with sessile drop when three-phase boundary is not moving by using video recorder with high frame rate. Dynamic contact angle is measured when the three-phase boundary is moving via tensiometry. Preparation of substrates with smooth and homogen surface, usage of pure liquids for drop formation, adjusting of drop size, fast measurement to prevent drop evaporation, needle location, and obtaining sharp images are important parameters that must be considered during contact angle studies [47,49].

In this study, we measured contact angles by static sessile drop method. KSV Instruments CAM200 contact angle meter was used to measure contact angles of films with high-resolution cameras. 3 μL water was dropped onto the film surfaces from syringe. 10 images for each sample were taken with 1 second frame interval. Final contact angle were calculated by taking the average on left and right side contact angles of water droplet.

1.4.7 UV-VIS spectroscopy

UV-vis spectrophotometer technique is based on the transmittance and absorbance of the light by the material that is to be examined. The ultraviolet range (185 – 380 nm) and visible range (380-780 nm) of the light is used for analyzing. When light falls upon a sample, the light may be reflected or absorbed. Absorption measurements can be at a single wavelength or over an extended spectral area. The components of spectrophotometer are the light source, monochromator, sample chamber, detector and recorder. The difference between the incident radiation (I_0) and the transmitted radiation (I) gives the amount of light absorbed [50]. Transmittance is defined as;

$$T = I/I_0 \text{ or } \%T = (I/I_0) \times 100 \quad (1.5)$$

Absorbance is defined as;

$$A = -\log T \quad (1.6)$$

In this study, the transparency of the films was estimated by spectrophotometry. Agilent 8453 UV-visible Spectroscopy System was used for light transmission works. Film samples were analyzed at between 200 nm-800 nm.

1.4.8 Rheometer

The viscosity is internal friction of a fluid and is a measure of resistance to flow. The molecules of fluid create a friction and this friction arises when a layer of liquid is moved relative to another layer. If the fluid has great friction, the amount of force, which is called shear stress, to overcome the friction and keep the fluid moving increases. Rheology is examination of flow of material and reaction of material to being sheared, and a rheometer is a device used to measure the rheology of the fluid. Two types of viscosity that are absolute/dynamic viscosity (η) and kinematic viscosity (ν) are measured in general manner [51,52]. Viscosity can be defined as in equation 1.7;

$$\eta(\text{viscosity}) = \frac{\tau (\text{shearing stress in fluid } (N/m^2))}{\gamma (\text{shear rate } (s^{-1}))} \quad (1.7)$$

The dynamic viscosity units are Pascal-second (Pa.s) in the SI system or Poise (P) in the metric CGS system where 1 poise = 1 g/(cm s) = 1/10 Pa s = 1/10 N s/m²

If the shearing stress is linearly related to shear rate, these group of fluids is termed Newtonian liquids. Fluids that have non-linear relationship between shear stress and shear rate are called non-Newtonian [51].

Viscosity is one of the most important parameter that modifies fiber size and morphology in electrospinning process. During this study, viscosity of electrospin solutions were measured by Thermo Scientific™ HAAKE RheoStress 1 Rheometer by using 35 mm parallel plate (Figure 1.17) with 0.01-300 1/s shear rate for 2 minutes at 25 °C constant temperature.

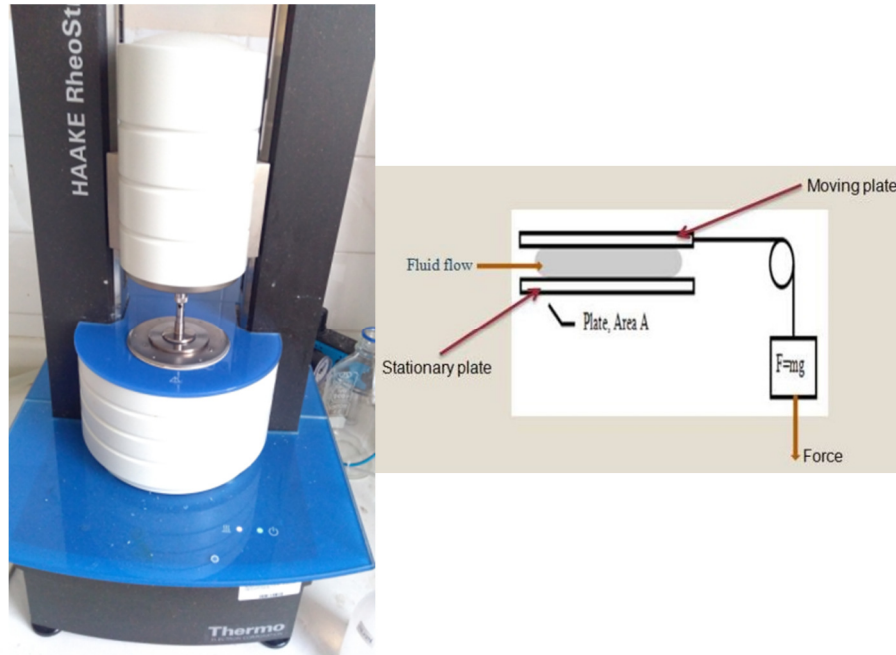


Figure 1.17: Rheometer instrument and representation of parallel plate measurement.

1.4.9 Conductivity measurement

Conductivity is the measure of the ionic concentration and the ability to carry an electric current of a material. The current is carried by electrons in metals whereas it is carried by cations and anions in solutions. The SI unit of conductivity is Siemens per meter (S/m). The level of ionic strength of aqueous solutions begins with ultra-pure water at a conductivity of $0.05 \mu\text{S}/\text{cm}$ (25°C) and changes to the high conductivity of concentrated acids and bases. Concentration, mobility of ions, valence of ions and temperature are the factors that affect the conductivity. Conductivity is evaluated by measuring the electrical resistance. Two electrodes are submerged in a solution, an alternating voltage imparted, the cations moves to the negative electrode, the anions to the positive electrode, and the solution reacts as an electrical conductor [53,54]. The instrument assesses the voltage and applies Ohm's law to calculate the conductivity of the solution as shown with these formulas [54]:

$$\kappa = G \cdot K \quad (1.8)$$

$$G = 1/R \quad (1.9)$$

$$R = V/I \quad (1.10)$$

where:

κ = conductivity (S/cm), G = conductance(S), K = cell constant (cm^{-1})

R = electrical resistance (ohms), V = voltage (volts), I = current (amperes)

Electrospin solution must carry charges to overcome the surface tension and following stretching [1]. During this study, the conductivity of electrospin solutions was measured by Wissenschaftlich-Technische-Werkstätten WTW LF-95 Conductivity Temperature Meter.

1.4.10 Surface tension measurement

Surface tension is the cohesive energy of a fluid at an interface that allows having a minimum surface area. Liquid molecules attract each other. The interactions of a molecule in a volume of a liquid are balanced by same forces in each direction. The molecules at the surface receive imbalanced forces so are proceeded toward the inside. It cause internal pressure and acts to contract and reduce liquid surface. Surface tension σ has the units of force/length or energy/area. The measurement of surface tension is done by a tensiometer; it is based on force quantifications of the interaction of a probe with the surface of fluid. The mathematical analysis of the force measurements subjects to the shape of the probe. Du Nouy Ring and the Wilhelmy Plate are two types of probes that usually used [55,56].

Surface tension has an important role in the formation of beads, droplets and fibers in the electrospinning operation. In this study, Dataphysics DCAT 11EC Dynamic Contact Angle Measuring Instrument and Tensiometer was used to measure surface tension of electrospin solutions. 19.90x0.20 mm Wilhelmy plate was utilized as the test body (Figure 1.18). The plate is fixed to the weighing system of the tensiometer and set at the liquid surface so that a liquid lamella forms. The motor speed was 1 mm/s and immersion depth was 3 mm. The vertical portion of the tensile force because of the surface tension is measured. Wilhelmy equation is obtained with the definition of the surface tension as tensile force per length of the interaction border [56]. The unit of surface tension is mN/m.

$$\sigma = \frac{F_{tens}}{L} = \frac{F_{\perp}}{L \cos \Theta_c} \quad (1.11)$$

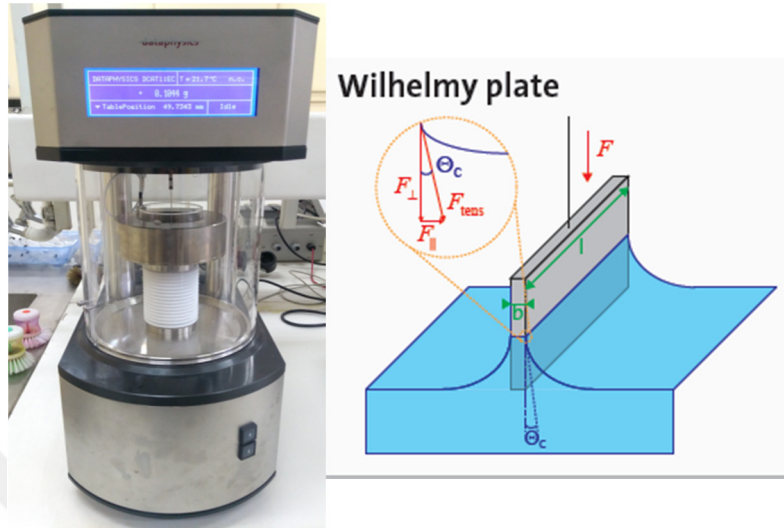


Figure 1.18: Tensiometer instrument and representation of Wilhelmy plate [56].

1.4.11 Gas permeability

Polymer materials, which are preferably used for food packaging, are permeable at distinctive degrees to water vapour, gases and organic compounds. The barrier features of these materials depends on polymer film structure, degree of crystallinity, thickness, area, thermal and mechanical treatment, degree of crosslinking, chemical groups into the polymer and glass transition temperature (T_g) [57].

Information about the solution, diffusion, and permeation behaviors of these molecules through packaging film has more importance day by day, particularly where contamination from the outside must be prevented and extending shelf life provided with modified atmosphere packaging (MAP) methods [58].

Diffusion is the main mechanism for gas flow through a film. Diffusion is affected by:

- the molecular size and phase of the diffusant molecule
- the morphology of the polymer
- crystallinity, degree of cross-linking and polymer chain motion
- the solubility limit of the solute within the polymer
- the volatility of the permeant

- the surface or interfacial energies of the films

Gas molecules cannot permeate through the polymer crystallites, because they are insoluble into the material. Thus, the decrease in the permeability value is relative to the volume portion of the crystalline phase. The permeation of gas through a polymer is depicted by a diffusion model, using Henry and Fick's laws. Figure 1.19 gives a homogeneous polymer film with thickness of l and p as the permeant pressure ($p_1 > p_2$) and c as the different permeant concentration through the film ($c_1 > c_2$) [58].

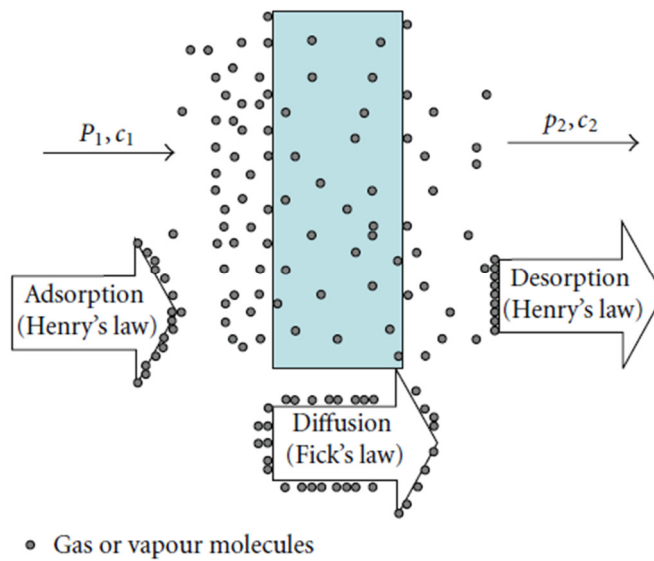


Figure 1.19: General approach of gas or vapour permeation through a film [58].

If the diffusion coefficient is assumed as constant, the relationship between the diffusion coefficient, the permeation coefficient, and the solubility coefficient is described as equation 1.12:

$$P = D \cdot S \quad (1.12)$$

where P is permeability constant, D is diffusion constant, S is solubility constant.

Gas transmission rate or permeance (q) is determined as the volume of gas passing across a test film, per unit area and time under defined conditions.

$$\text{GTR (or } q) = k_1 \left[\frac{V}{T(29N - t_L)} \right] \quad (1.13)$$

where $k_1 = 9.89 \cdot 10^8$, GTR(or q) is the permeance ($\text{cm}^3/\text{m}^2 \text{ day bar}$), V is the measured volume (mL), N is the slope of the measured curve (sec), T is the temperature (K), and t_L is the time-lag value (sec) [58].

Oxygen gas permeability of the agar films was measured with Brugger GDP-C 2000 gas permeability tester device using the manometric method. The device operates according to the "constant volume - variable pressure" principle (ASTM D1434) and calculates the gas permeability (P) value. It is based on differential pressure method, the lower pressure chamber is evacuated and the passage of the gas through the sample is indicated by the evaluation of the increase in pressure [59]. Gas permeability measurements were made at room temperature (25 ± 2 °C, 50% RH) and 1 atm pressure. The O_2 flow rate was $80 \text{ mm}^3/\text{min}$.

1.4.12 Water vapor permeability (WVP)

The water vapor permeability (WVP) of the films was determined gravimetrically according to the standard method of ASTM E96-05 with slight modifications to give an estimate [60]. The films were cut into circle pieces and circular glass beakers with a diameter of 55 mm were applied. The film samples were applied onto the beaker mouth containing 50 ml distilled water. The beakers were placed at a room temperature (20.5 ± 1 °C) and $50 \pm 5\%$ humidity. The weight of the beaker was measured every hour for 8 h and weight loss was measured. Water vapor transmission rate (WVTR) was calculated by dividing the slopes of weight loss over time curve by the film area. Then, the WVP of the films were calculated in g mm/kPa h m^2 as follows:

$$WVP = WVTR \times L / \Delta P \quad (1.14)$$

where WVTR was the measured water vapor transmission rate ($\text{g}/\text{m}^2 \text{ h}$), L was the mean thickness of the film (mm), and ΔP was partial water vapor pressure difference (kPa) across the film.

1.4.13 Swelling behavior and degradation studies

One of the important parameter is the swelling behavior to exploring the application of hydrogels in pharmaceutical and biomedical areas. Polymer chains are involved in an interaction with the solvent and can be dissolved but crosslink structures resist this

behavior. When these opposing forces are balanced, equilibrium is accomplished [28]. The swelling behavior of the films was detected through the immersion of pre-weighted samples into 20 mL of phosphate buffered saline (PBS) solution pH 7.4 simulating the body fluid. The samples were collected from solution at determined periods of time, the excess of water was dried by a filter paper and its wet weight measured [61]. The following equation 1.15 gives the swelling ratio of the films:

$$\text{Water absorption (\%)} = \left(\frac{W_h - W_i}{W_i} \right) \times 100 \quad (1.15)$$

where W_h is the hydrated weight of film, and W_i represents the initial weight of the film.

The in vitro degradation behavior of the films was figured via measuring the weight loss after keeping in PBS during 14 days. A piece of films were immersed in PBS and on days 1,2,3,7 and 14 the samples were taken from the solution, remaining water on the samples were dried with filter paper. Then, the samples were placed in an oven and dried at 37 °C until the masses were constant [61]. The degradation ratio was calculated based on weight losses with the following equation 1.16:

$$\text{Weight loss (\%)} = \left(\frac{W_i - W_f}{W_i} \right) \times 100 \quad (1.16)$$

where W_i is the initial weight of the sample and W_f is the final sample when it is dried.

1.5 Materials

The materials used in experimental section of the work are presented in this part. These materials are metal oxides and their initiators, polymers and solvents. Titanium dioxide, PVP, PVA, Agar and *Aloe vera* are introduced in this section.

1.5.1 Titanium Dioxide

TiO₂ has 8 crystalline phases in principle, 5 phases are formed only by process with high pressure while other 3 phases exist as stable. These structures are rutile, anatase and brookite that have different crystal structures [62]. Pure titanium dioxide does

not occur in nature but is derived from ilmenite or leucosene ores. Titanium dioxide, formed by the combination of the Titanium atom in the IV column of the periodic table and the Oxygen atom in the VI column, is one of the binary compound semiconductors IV-VI [63]. Titanium is in the 4th group of the periodic table in which dominant bond strength is the covalent bond and has an atomic number of 22, an atomic weight of 47.9, and hard, white, bright structure [64].

Among the crystal structures, the rutile phase is thermodynamically the most stable form. For that reason, anatase and brookite rearrange at elevated temperatures of 750 °C (brookite) or 915 °C (anatase), respectively, monotropically to rutile. This modification is stable all the way up to its melting point at approximately 1830 °C to 1850 °C [65]. Anatase and rutile structure are both tetragonal, brookite has orthorhombic crystal structure as shown in Figure 1.20.

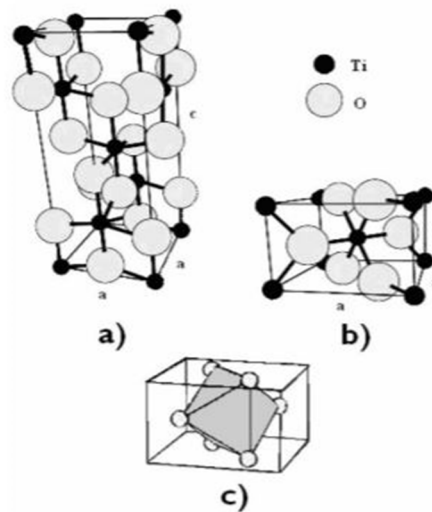


Figure 1.20: Structure of the unit cell of (a) rutile phase (b) anatase phase (c) brookite phase [64].

Crystallographic and physical properties of rutile, anatase, brookite are given in Table 1.1. The phase transformation of TiO_2 to the anatase is achieved with heat treatment at 500-600 °C. Anatase phase is the most convenient phase because it is promising photocatalytic material because of the large bandgap of 3.2 eV, applicable in photovoltaic cells and has antimicrobial activity. Electromagnetic wave in the range of microwave can easily heat up anatase TiO_2 owing to its high dielectric permittivity. TiO_2 nanoparticles have been a subject of a new generation of advanced materials because of their potential utilization in electronic, photonic and mechanic

fields. It is commonly used as a self-cleaning and self-disinfecting surface coating materials due to its photo-induced properties. Furthermore, nano-scaled inorganic oxides that are formed by the sol-gel process have been presented as biocompatible and appropriate supports for a wide range of compounds [66].

Table 1.1. Crystallographic and physical properties of rutile, anatase, brookite [65].

Properties	Rutile	Anatase	Brookite
Chemical formula	TiO ₂	TiO ₂	TiO ₂
Crystal system	tetragonal	tetragonal	orthorhombic
Point group according to Schönflies	D _{4h}	D _{4h}	D _{2h}
Point group according to Hermann-Mauguin	4 mmm	4 mmm	mmm
Volume of the elementary cell (nm³)	62.07	136.25	257.38
Molar volume (cm³/mol)	18.693	20.156	19.377
Moh's hardness	6.5-7	5.5-6	5.5-6
Density (g/cm³)	4.2-4.3	3.8-3.9	3.9-4.1
Melting point (°C)	1830-1850	Transformation to rutile	Transformation to rutile

The sol-gel method is one of the most available methods to synthesize powders for photocatalytic materials. TiO₂ nanoparticles can be prepared by a sol-gel method using different precursors such as titanium isopropoxide, titanium tetrabutoxide, titanium tetrachloride and titanium alkoxide. By this method control the synthesis conditions, sol homogeneity, viscosity and purity are available [67].

1.5.2 Sol-gel chemistry of Ti alkoxide

TiO₂ can be formulated by hydrolysis and condensation reactions involving water molecules and Ti alkoxides as precursor. In the absence of the catalyst, both occur with the S_N2 mechanism in which nucleophilic substitution, S means substitution, N

means nucleophilic and 2 means the bimolecular reaction as determined in Figure 1.21. The alkyl groups of the Ti alkoxide (-OR) have strong electronegativity; it makes the Ti atom a favorite target to be attacked by nucleophiles.

The nucleophile attacks the Ti atom in the alkoxide in the hydrolysis reaction. When the -OR group is cleaved, it takes one of hydrogen atoms in the water molecule to complete the reaction to form Ti with a hydroxyl group (HO-Ti) and an alcohol (R-OH).

There are two different ways of condensation, which are alkoxolation and the oxolation. Alkoxolation is also an oxolation type and forms an oxo bridge (-O-), but it produces alcohol instead of water as a side product. The oxygen atom in the hydroxyl group (-OH) of the hydrolyzed Ti acts as nucleophile in condensation reactions. The nucleophile attacks on the other Ti atom, the alkoxy group in the alkoxolation and the hydroxyl group in the oxolation are removed and take the hydrogen atom in the nucleophile. Ti-O-Ti bond and an alcohol or a water molecule is formed as a result [68].

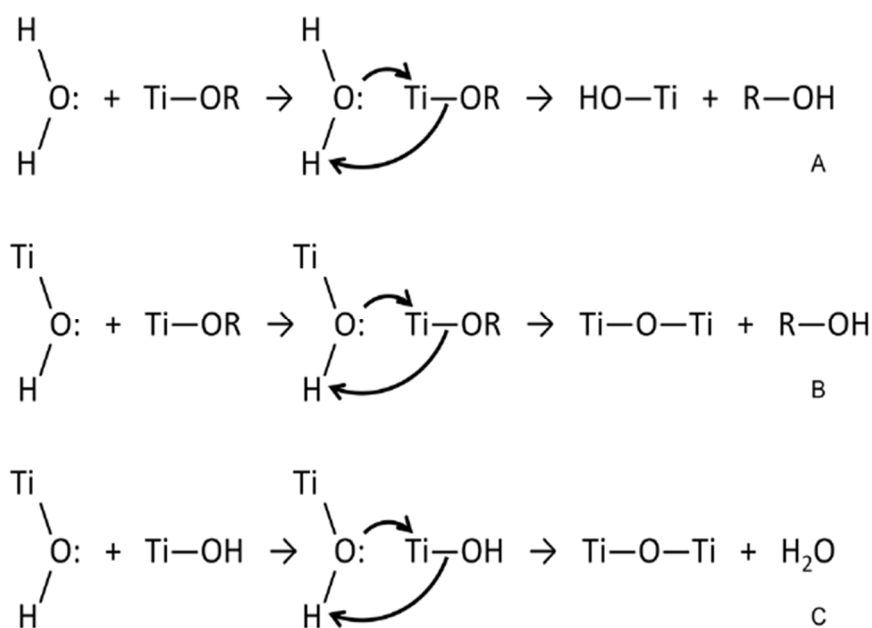


Figure 1.21 : A) Hydrolysis, B) alkoxolation, C) oxolation of Ti alkoxide [68].

1.5.3 Polyvinylpyrrolidone (PVP)

Polyvinylpyrrolidone (PVP) is a synthetic polymer, which is soluble in water and other polar solvents. It is nontoxic, chemically inactive, biocompatible, heat-

resistant, pH-balanced, non-ionic and colorless in solution. These significant features enable its utilization in various applications in cosmetics, medicine, and technical industry. PVP is light white colored powder when it is dry. It has remarkable solubility in different solvents and easily forms films. In addition, it affects as binding texture and suspension or emulsion-stabilizer in solution, so it is considered as a coating or supplement to coatings and pharmaceuticals [69]. Furthermore, PVP is a supporter polymer for electrospinning titania nanofibers as frame of this study [70].

The structure of PVP is more complex than linear polymer, it has branched structure. The composition of PVP is made up of the vinylpyrrolidone (VP) monomers by means of a free radical polymerization reaction. In Figure 1.22, Azobisisobutyronitrile (AIBN) is used as a free radical initiator for synthesis of PVP [71].

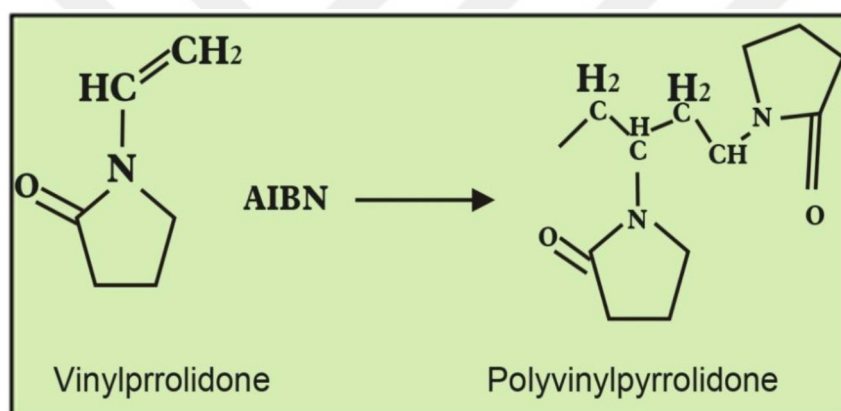


Figure 1.22: Polymerization reaction of PVP [71].

1.5.4 Polyvinyl alcohol (PVA)

Polyvinyl alcohol (PVA) is a colorless, water-soluble, non-toxic, biocompatible and biodegradable synthetic polymer, which is commonly used in textile, paper and biomedical fields. PVA is a specific polymer because it is not formed via polymerization reactions from monomers that are single unit precursor molecule. PVA is synthesized by dissolving PVAc, another polymer, in an alcohol and treating it with an alkaline catalyst like sodium hydroxide. The acetate groups are removed from the PVAc molecules by hydrolysis or alcoholysis while their long chain structures are not disrupted [72,73]. The final repeating unit of vinyl alcohol is observed in Figure 1.23.

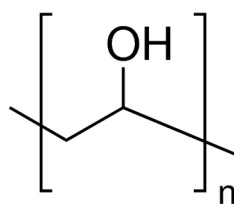


Figure 1.23 : Repeating unit of PVA.

If the reaction is completely processed, the product will be highly soluble in water and insoluble in organic solvents. With the increase in acetate groups, product become less soluble in water whereas more soluble in organic solvents [73].

Polyvinyl alcohol has excellent film forming, plasticizer and adhesive properties. PVA has a number of worthwhile characteristics such as adequate mechanical strength, high flexibility, high hydrophilicity and good biocompatibility and biodegradability. It has a melting point at 230 °C for fully hydrolyzed grades [72,73].

1.5.5 Agar

Agar is a hydrocolloid obtained from marine red algae. It is a gelling substance consisting of a complex mixture of agarose and agarpectin. Agarose is the unbranched gelling segment of the polymer skeleton which is chemically described by 3-linked β -D-galactose (G) and 4-linked 3,6-anhydro- α -L-galactose (LA) units as shown in Figure 1.24. Agarpectin is built by G, LA and 4-linked α -L-galactose (L) residues with various substituent groups such as sulfate esters, methyl ethers, and pyruvate acid ketals [74].

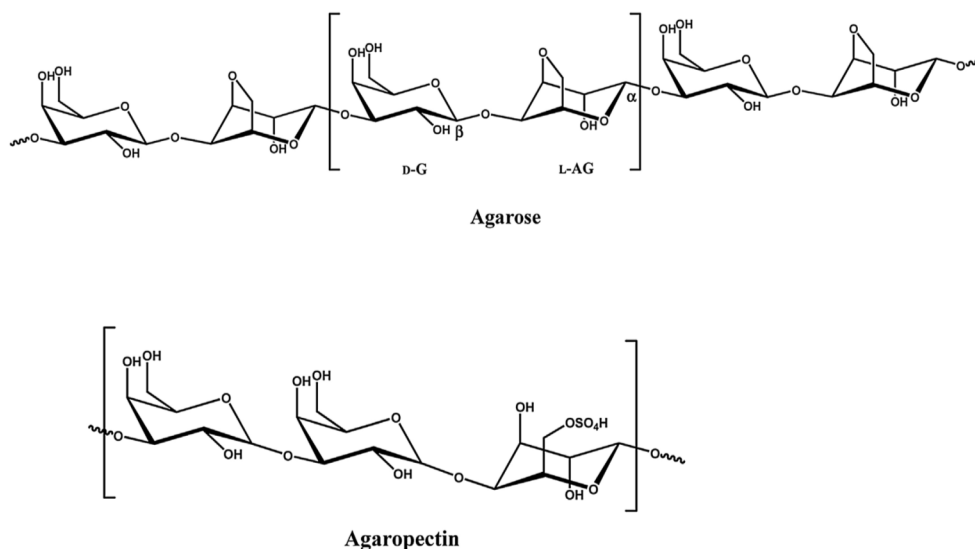


Figure 1.24: Chemical structure of agarose and agarpectin [74].

Agarose generates a 'physical gel' formed by polymer molecules assembled together by hydrogen bonds and does not require additives. These gels can keep large amount of water in the inner structure. Hydrogen bonds occurred between linear galactan chains give the gelling ability to agar and supply an outstanding reversibility. Reversibility is the most notable feature of physical gels. They melt with heating (around 85 °C) and gel again by cooling about 38 °C [75]. The gelling function of agarose can be seen in Figure 1.25 [76]. This is an exothermic process while agarose molecules are dissolved in water.

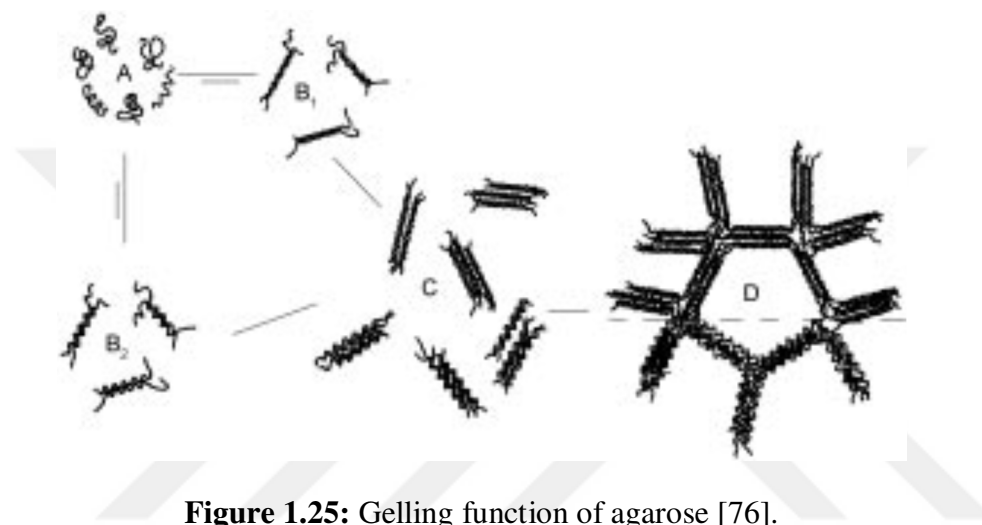


Figure 1.25: Gelling function of agarose [76].

Agar and agar-based components are widely used in biomedical and food applications due to its good biocompatibility, biodegradability and nontoxicity. Also agar films have excellent functional properties such as transparent, flexible, homogeneous and easy to handle [77].

1.5.6 Aloe vera

Aloe vera (*Aloe barbadensis* Miller) is a plant species of the family Asphodelaceae (Liliaceae) which have large, thick, fleshy leaves. It is a cactus-like plant that generally found in hot and dry climates. There are three distinguishable sections of the *Aloe vera* leaves; the outer cover which includes rinds, tips and thorns, the internal mucilaginous gel matrix and yellow latex exudate that have anthraquinones. The inner leaf pulp of *Aloe vera* has three structural parts as cell walls, degenerated organelles and the liquid gel within the cells as shown in Figure 1.26. These components have different sugar formulation and morphology [78].

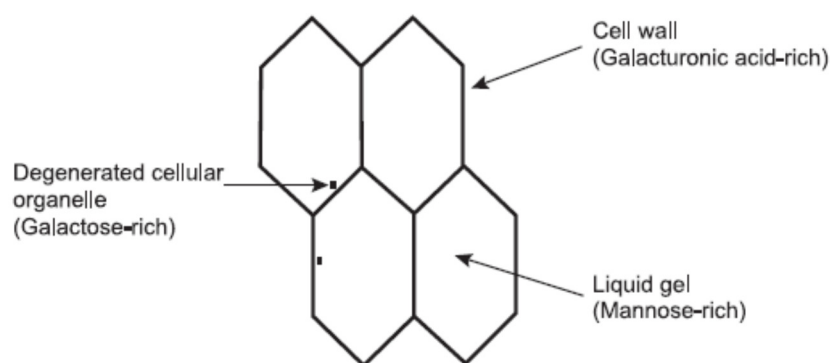


Figure 1.26: The structure of inner leaf pulp of *Aloe vera* [76].

The inner layer of Aloe leaves composed of a luminous gel including 99% of water. The other 1% consists of polysaccharides (0.55%), sugars (0.17%), minerals and trace elements (0.16%), amino acids (0.07%), lipids and sterols (0.04%) and phenolic compounds (0.01%) which include anthraquinones, aloin and emodin as ratios can be observed in Figure 1.27 [79].

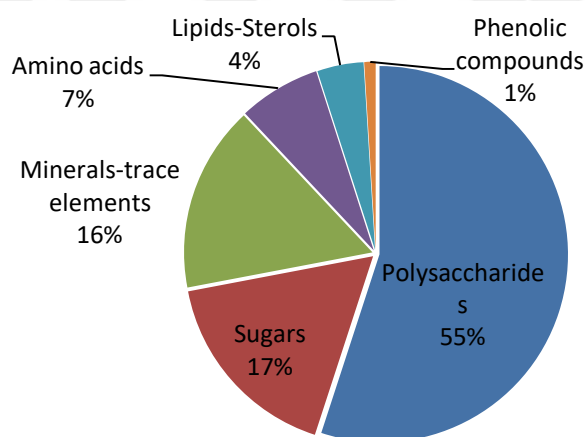


Figure 1.27: The ratios of the compounds in *Aloe vera* gel.

The chemical components of *A. vera* pulp and exudate are given in Table 1.2 [80]. The gel of *A. vera* is known for its important effects such as antimicrobial, wound healing, anti-inflammatory, antioxidative and immuno-mediating. It is used widely in cosmetic, pharmaceutical and food industries. Various mechanisms have been suggested for the wound healing effects of aloe gel, which involve sustaining the wound moist, increase epithelial cell migration, more rapid maturation of collagen and reduction in inflammation [81]. *Aloe vera* gel has high volume of water so

restrains skin dryness. The high percentage of glucose and mannose sugars lead to high osmotic virtue, it results prevention of bacterial growth [82,83].

Table 1.2 : The chemical components of *Aloe vera* [80].

Class	Compounds
Anthraquinones/anthrones	Aloe-emodin, aloetic-acid, anthranol, aloin A and B (or collectively known as barbaloin), isobarbaloin, emodin, ester of cinnamic acid
Carbohydrates	Pure mannan, acetylated mannan, acetylated glucomannan, glucogalactomannan, galactan, galactogalacturan, arabinogalactan, galactoglucoarabinomannan, pectic substance, xylan, cellulose
Chromones	8-C-glucosyl-(2'-O-cinnamoyl)-7-O-methylaloediol A, 8-C glucosyl-(S)- aloesol, 8-C-glucosyl-7-O-methyl-(S)-aloesol, 8-C-glucosyl-7-O-methylaloediol, 8-C-glucosyl-noreugenin, isoaloesin D, isorabaichromone, nealoesin A
Enzymes	Alkaline phosphatase, amylase, carboxypeptidase, catalase, cyclooxygenase, cyclooxygenase, lipase, oxidase, phosphoenolpyruvate carboxylase, superoxide dismutase
Inorganic compounds	Calcium, chlorine, chromium, copper, iron, magnesium, manganese, potassium, phosphorous, sodium, zinc
Miscellaneous including organic compounds and lipids	Arachidonic acid, γ -linolenic acid, steroids (campesterol, cholesterol, β - sitosterol), triglycerides, triterpenoid, gibberillin, lignins, potassium sorbate, salicylic acid, uric acid
Non-essential and essential amino acids	Alanine, arginine, aspartic acid, glutamic acid, glycine, histidine, hydroxyproline, isoleucine, leucine, lysine, methionine, phenylalanine, proline, threonine, tyrosine, valine
Proteins	Lectins, lectin-like substance
Saccharides	Mannose, glucose, L-rhamnose, aldopentose
Vitamins	B1, B2, B6, C, β -carotene, choline, folic acid, α -tocopherol

Some enzymes hydrolyse prostaglandin and bradykinin that are cause pain inflammation, thus reduce pain and inflammation. The amylase enzyme eradicates the dead tissue and aloctin-A possesses cell division and mitosis impact, leads to the

acceleration of healing and exciting macrophage to excrete the dead tissue. Proteins are made with amino acids in *Aloe vera* gel, causing tissue growth and healing. Vitamins, which are used in cell reaction, are consumed as antioxidants to strengthen the immune system [82].

The antimicrobial properties of *A. vera* gel against Gram-positive and Gram-negative bacteria have been showed by various different methods [84]. Anthraquinones isolated from the exudate of *A. Vera* have demonstrated wide antimicrobial activity. It was suggested that the antibacterial activity of emodin against *Escherichia coli* is in connection with inhibition of solute transport in membranes [85]. Chemical structures of some anthraquinones included emodin, aleosin and aloin were shown in Figure 1.28.

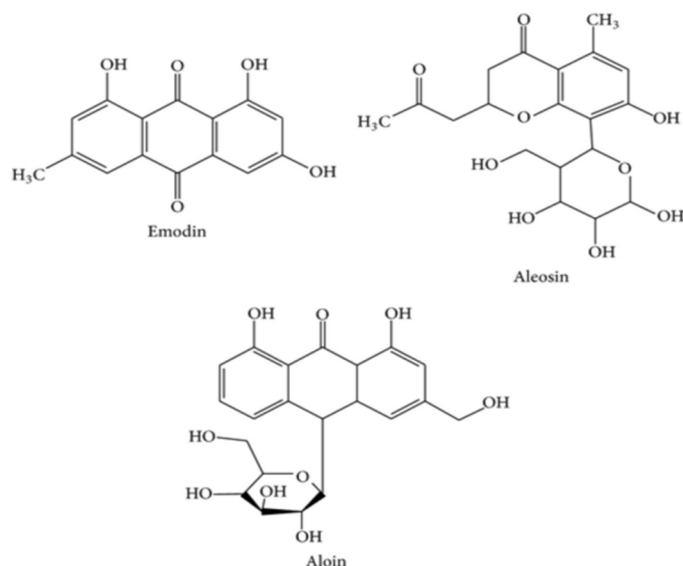


Figure 1.28: Chemical structures of emodin, aleosin and aloin.



2. EXPERIMENTAL PROCEDURES

2.1 Electrospinning Section

2.1.1 Sample preparations

The Isolab glasses are used as substrates for fiber adhesion. The glasses were cut to 1.5x1.5 cm and were cleaned with deionized water and sonicated by Hydra Ultrasonic Cleaner for 20 minutes. Then, the water was drained and the glasses once more immersed in ethanol and sonicated for another 20 minutes. Finally, the substrates were dried and fixed on aluminum foil.

2.1.2 Preparation of solutions

Blends are prepared using numerous precursors and concentrations for two main reasons; first to study the effect of the amount of polymer on fiber formation and second to prepare suitable solutions and blends for electrospinning technique. The reagents used in this part of the thesis study are indicated on the Table 2.1.

Table 2.1: Table of reagents used in this part of work

Chemical Name	Chemical Formula	Purity	Company
Titanium(IV) isopropoxide	Ti[OCH(CH ₃) ₂] ₄	97%	Aldrich
Titanium (IV)butoxide	Ti[O(CH ₂) ₃ CH ₃] ₄	97%	Aldrich
Ethanol	C ₂ H ₅ OH	>99,9	Merck
Acetic acid	CH ₃ COOH	100%	Merck
Polyvinylpyrrolidone (PVP)	(C ₆ H ₉ NO) _n	MW 1,300,000	Aldrich

2.1.2.1 Solution 1 (Titanium isopropoxide)

7 ml of ethanol and 2 ml of titanium isopropoxide were added in a glass beaker and stirred with a magnetic stirrer for 15 minutes. Then 2 ml of acetic acid was added in the beaker and stirred for another 30 minutes. After this solution mixed homogeneously, 1 g of PVP (1,300,000 Mw) was added slowly in the solution thus obtaining 9% wt/v PVP concentration. Finally the solution was mixtured with a magnetic stirrer for at least 3 hours, until the color of the solution became yellowish.

2.1.2.2 Solution 2 (Titanium (IV) butoxide)

7.5 ml of titanium (IV) butoxide was mixed with 2.7 ml of ethanol, with 5.25 ml of acetic acid used as catalyst in a glass beaker and followed by the magnetic stirring for about 2 hours.

24.3 ml of ethanol and 1.35 g of polyvinylpyrrolidone (PVP) were mixed in another beaker with a magnetic stirrer for 2 hours. After individually stirring for 2 hours at room temperature, these two solutions were stirred together for another 3 hours. The overall PVP concentration were 5% w/v total EtOH. The light-yellow colored solution was obtained as shown in Figure 2.1.

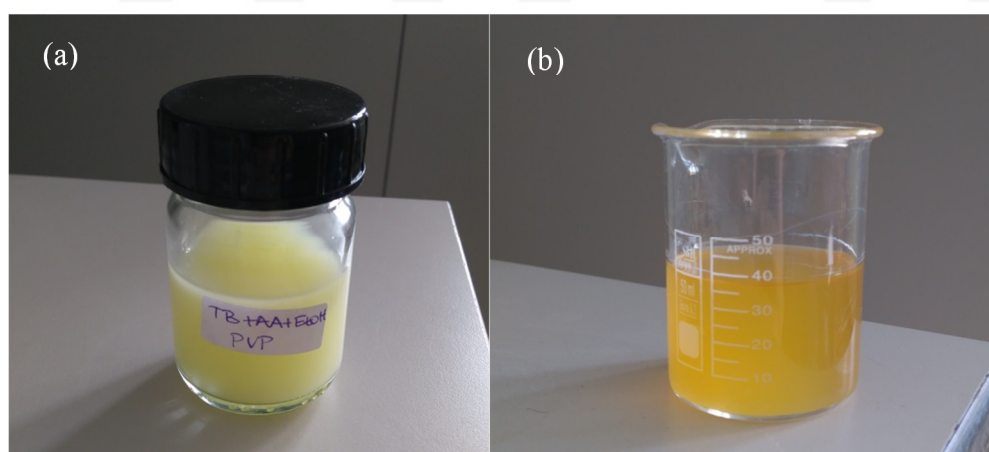


Figure 2.1: a) Appearance of solution 2 and b) solution 2 with *Aloe vera* addition.

2.1.2.3 Preparation of *Aloe vera* gel

Aloe vera gel was prepared from fresh *Aloe vera* leaves. The leaves were cut from the plant and washed with distilled water. Their outer skin was carefully separated and inner gel was drained with a sieve. The resulting *Aloe vera* gel was stored at 4 °C.

2.1.2.4 Solution 2 with *Aloe vera* gel addition

Titanium(IV) butoxide solution was prepared as mentioned above. Differently, 0.405 g of *Aloe vera* gel and 0.945 g of PVP was mixed with 24.3 ml of ethanol to obtain 30% wt *Aloe vera*, so *Aloe vera* /PVP mass ratio was 30/70. After stirring for 2 hours, the solution was added to titanium(IV) butoxide solution and magnetically stirred for another 3 hours. The color of this solution was observed darker than Solution 2 without *Aloe vera* as shown in Figure 2.1.

2.1.3 Electrospinning of solutions

The electrospinning equipment is Inovenso Ne100 Electrospinning Machine, which includes a variable high voltage power supply, a syringe pump and a flat collector plate. A piece of aluminum foil was covered on the collector and the glasses were fixed on it. The collector was placed at the proper distance away from the tip of the needle. The prepared mixture was loaded into a plastic syringe. The syringe pump provide controlling of flow rate. The solutions were electrospun under several conditions such as applied voltage, needle to collector distance and flow rate to determine optimum conditions for nanofiber production as shown in Figure 2.2. The experimentally confirmed conditions for the solutions are given in Table 2.2.

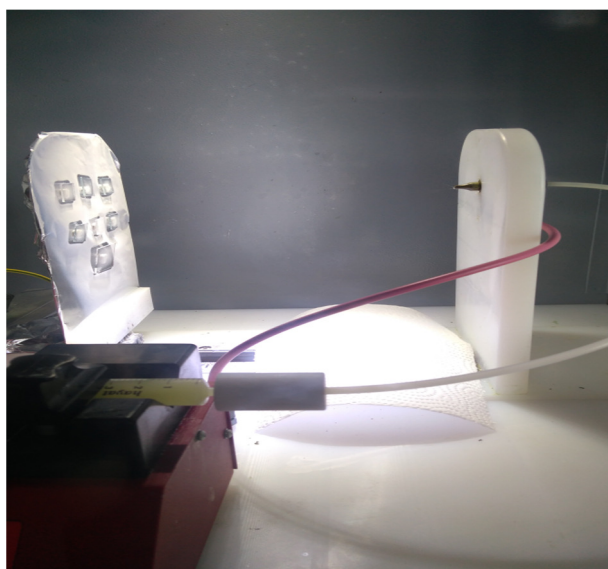


Figure 2.2: Electrospinning setup.

In this experiment, temperature is a parameter that affects the electrospinning procedure, which was performed at room temperature. After performing electrospinning part, nanofibers collected on the glasses and aluminum foil were

stored at room temperature. To prepare titanium oxide nanofibers, some nanofiber samples were annealed.

Table 2.2 : The experimentally confirmed conditions for the solutions.

Solution	Voltage (kV)	Needle- Collector Distance (cm)	Flow rate (ml/h)
Solution 1(TTIP)	11	15	4
	11	12	6
Solution 2 (TB)	11	15	5
	18	20	1
Sol. 2-Aloe vera	16	20	1

2.1.4 Annealing

Following electrospinning, the glasses coated with nanofibers were placed in a furnace for the process of polymer removal and crystallization. The furnace was heated to 500 °C with an increase rate of 5 °C/min and stayed for 90 minutes. Then, it was heated again to 550 °C with the same increase rate as 5 °C/min and stayed for another 90 minutes. After thermal treatment, they were cooled down to room temperature.

2.2 Preparation of Hydrogel Films Section

The hydrogel films were prepared via solvent-casting method. They contained different percentages of *Aloe vera*. PVA (average Mw=145,000 g/mol and 98% hydrolyzed) and Agar-agar ultrapure was purchased from Merck Co. (Germany). *Aloe vera* leaves were collected from a plant.

2.2.1 Agar/*Aloe vera* Films

Solutions of agar (1.5% w/v) were firstly prepared through the dissolution in distilled water at ~90 °C under strong stirring. Homogeneous transparent fluid was observed

when they dissolved completely, and solution was cooled down to ~40-50 °C with stirring for addition of *Aloe vera* gel. The solution begins to gelling and solidifying at colder temperatures. *Aloe vera* gel was added at a percentage of 10, 20, and 30% (w/w, based on the mass of the agar) under stirring for 5 minutes to avoid gelation of solution. After the mixing, 30 ml of solution was casted into petri dishes with diameter of 8.5 cm and left to dry at 60 °C in oven. After drying, flexible and transparent films were ready to use (Figure 2.3).

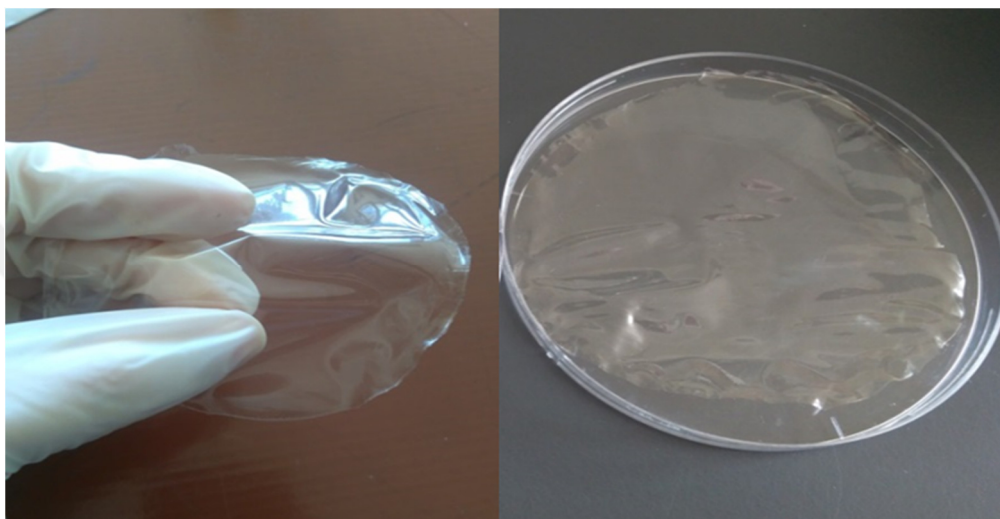


Figure 2.3 : Agar/*A.vera* films.

Also, ZnO nanoparticles were added to the 20% *Aloe vera* contained agar films as 1%, 2% and 4% (w/w based on the mass of the agar) concentrations. In addition, 0.3% TiO₂ solution was added to neat agar film (Figure 2.4).

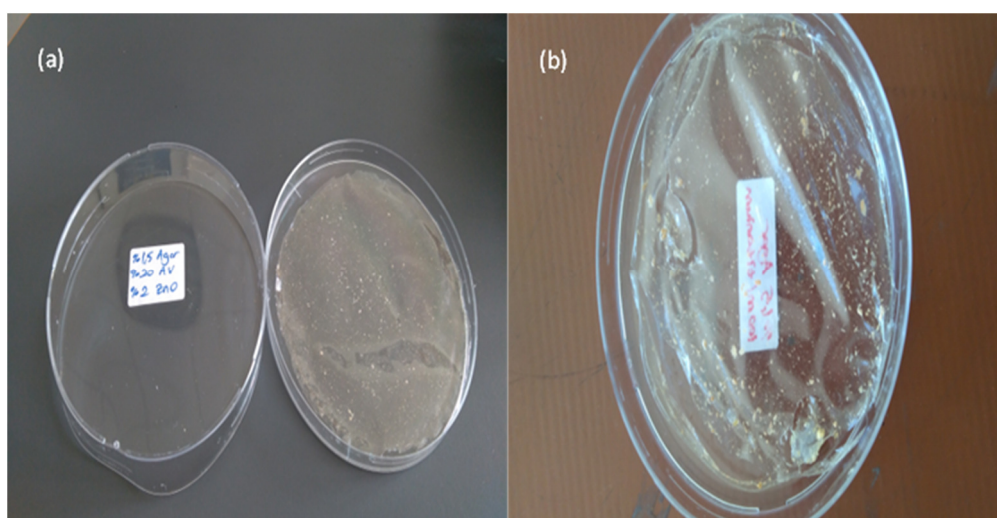


Figure 2.4 : a) 2% ZnO added Agar/*A.vera* film and b) 0.3% TiO₂ solution added Agar film.

2.2.2 PVA/*Aloe vera* Films

PVA films containing different percentages of PVA and *Aloe vera* were prepared similar to agar films. The PVA powder was dissolved in distilled water at ~100 °C to obtain 1% w/v PVA solutions. Then they were cooled down to ~40 °C with stirring for addition of *Aloe vera* gel. *Aloe vera* gel was added at a percentage of 10, 20, and 30% (w/w, based on the mass of the PVA) with mixing for 15 minutes. After the stirring, 30 ml of solution was casted into petri dishes with diameter of 8.5 cm and left to dry at 60 °C in oven. Elastic and transparent films were obtained after drying (Figure 2.5).

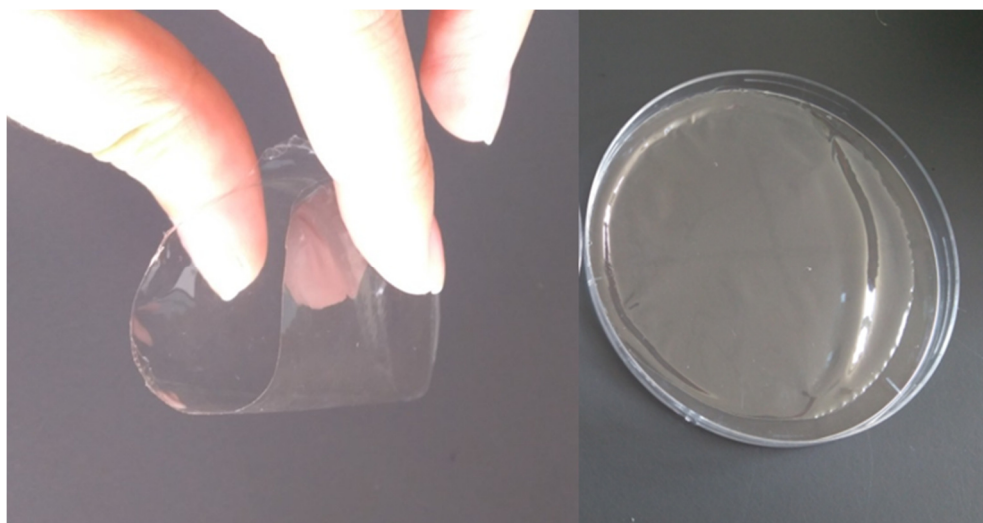


Figure 2.5 : PVA/*A. vera* films.

3. RESULTS AND DISCUSSION

3.1 Electrospinning Section

3.1.1 Viscosity, conductivity and surface tension of electrospin solutions

Viscosity, conductivity and surface tension of the solutions were measured by the Thermo Scientific™ HAAKE RheoStress 1 Rheometer, Wissenschaftlich-Technische-Werkstätten WTW LF-95 Conductivity Temperature Meter, and Dataphysics DCAT 11EC Dynamic Contact Angle Measuring Instrument and Tensiometer, respectively. Viscosity and surface tension tests were carried out in three replicates. The measurements were shown in Table 3.1.

Table 3.1: Physical properties of solutions

Sample Name	Viscosity (mPa.s)	Surface Tension (mN/m)	Conductivity (mS/cm)
TB	12.09±1.58	24.62±0.03	0.03
TB+AV	9.27±2.00	24.68±0.02	0.02

The amount of PVP decreased with the addition of *Aloe vera*, it may cause the slight decrease of viscosity from 12.09±1.58 mPa.s to 9.27±2.00 mPa.s. Conductivity of TB solution was measured as 0.03 mS/cm and TB/*Aloe vera* solution was 0.02 mS/cm. Surface tension was evaluated as 24.624±0.025 mN/m for TB solution and 24.682±0.020 mN/m for TB/*Aloe vera* solution. The almost same values showed that the addition of *Aloe vera* have not affected the surface tension property of solution.

3.1.2 Fiber morphology

Nanofiber webs were produced on glasses and aluminum foil, also on baking paper by optimal electrospinning conditions as seen in Figure 3.1 and 3.2. *Aloe vera* gel added fiber webs appeared smoother than the fibers without *Aloe vera* gel.



Figure 3.1 : Fiber webs of TB solution (on the left) and TB/*Aloe vera* solution (on the right) on baking paper.



Figure 3.2 : Fiber webs of TB solution electrospun on aluminum foil and glasses.

A scanning electron microscope (FEI - Quanta FEG 450 and ZEISS EVO LS15) was used to visualize TiO_2 -PVP nanowebs. SEM images were obtained with different magnifications. Fiber diameters of nanofibers were measured using Image J image visualization software. SEM photographs of nanofibers obtained from Solution 1 are given in Figure 3.3.

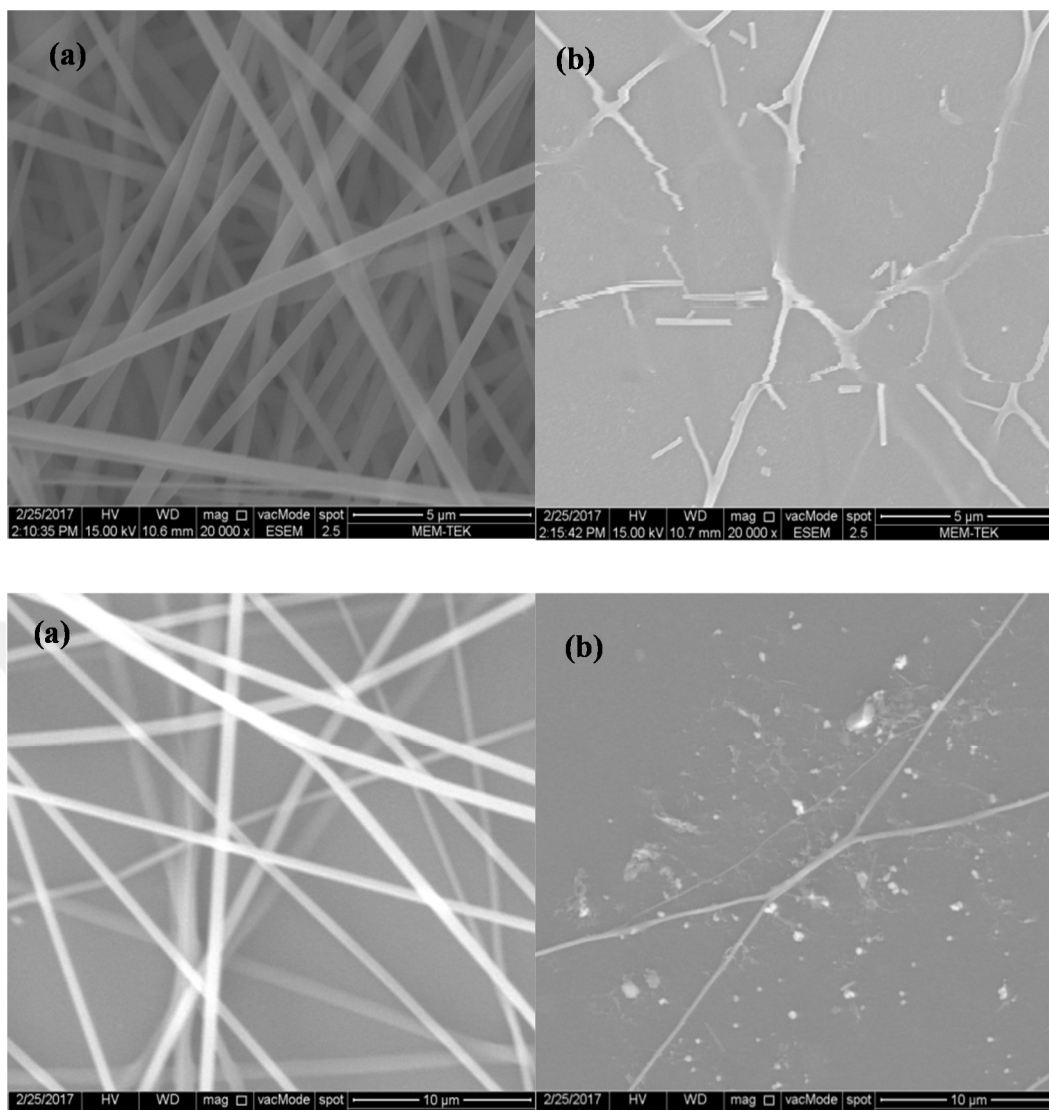


Figure 3.3 : SEM photographs of nanofiber from Solution 1 at different magnifications, a) before annealing b)after annealing

Nanofiber web obtained from Solution 1 have smooth continuous morphology and overlapped each other before annealing as seen in Figure 3.3. Average diameter of nanofibers is 410 nm. Diameters of the nanofibers are in the range of 250 nm to 565 nm. Collected nanofibers were calcinated at 500-550 °C for 3 hours. PVP is reported to be thermally degraded at around 420°C [86]. However, the nanofiber structure was not observed after annealing. Unconnected, very rare fiber-like structures were seen.

Electrospun fibers obtained from Solution 2 have more dense and uniformly distributed morphology than Solution 1. SEM photographs of nanofibers obtained from Solution 2 with 11 kV voltage, 15 cm needle to collector distance and 5 ml/h feedrate are given in Figure 3.4.

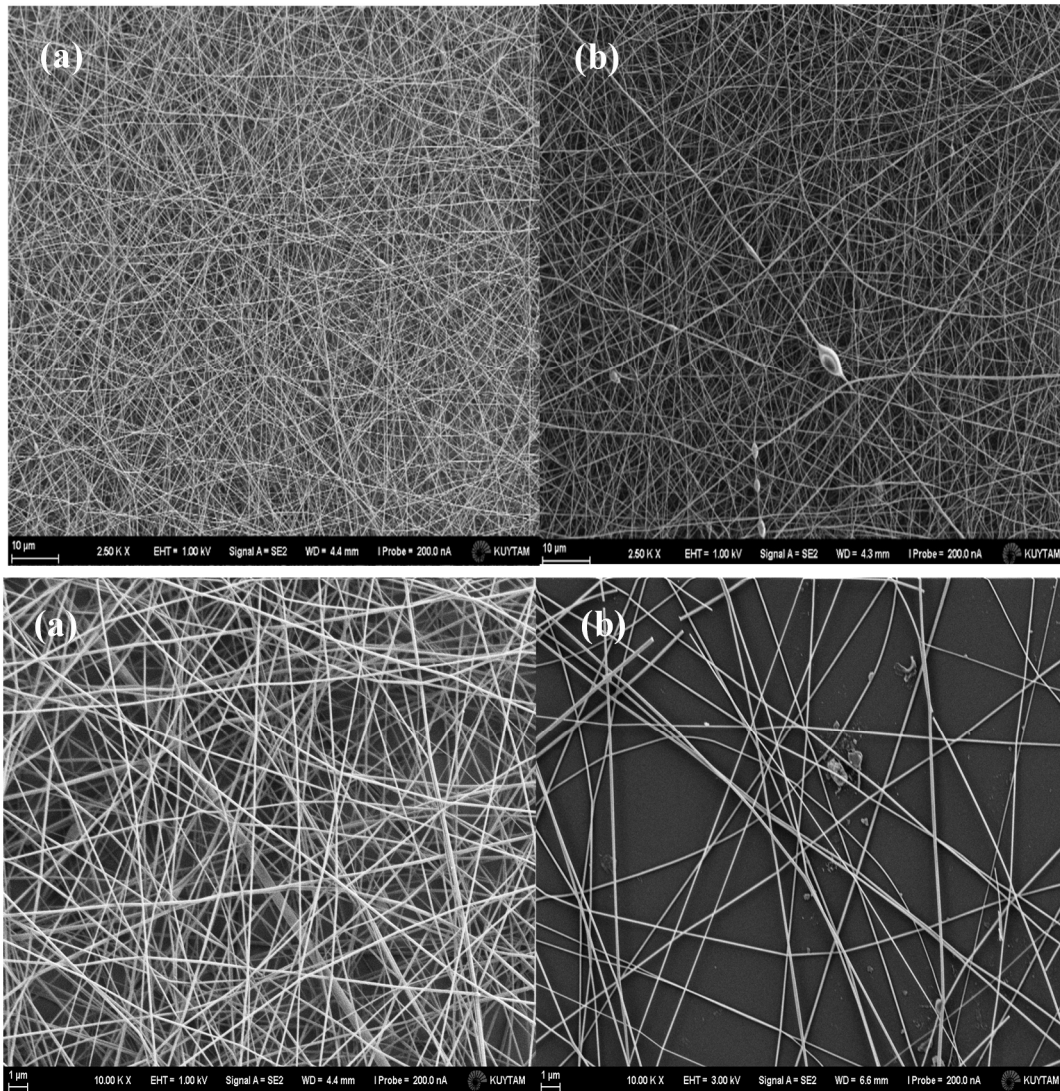


Figure 3.4 : SEM photographs of nanofiber from Solution 2 at different magnifications, a) before annealing b) after annealing.

Average diameter of nanofibers is 156 nm. Diameters of the nanofibers are in the range of 100 nm to 220 nm is given in Figure. Some nanofibers with diameters about 500 nm also observed. Nanofiber web contains a few beads. The number and diameter of nanofibers decreased after annealing because PVP was degraded and removed with the heating and only TiO_2 fibers remained on the sample.

SEM images of electrospun fibers obtained from Solution 2 with 18 kV voltage, 20 cm needle to collector distance and 1 ml/h feedrate are given in Figure 3.5. The dense, smooth and uniform morphology are also seen here. However, more bead formation is observed may be due to increase in voltage and distance between the needle tip and collector. Average diameter of nanofibers is calculated as 222 nm. Diameters of the nanofibers are in the range of 78 nm to 325 nm.

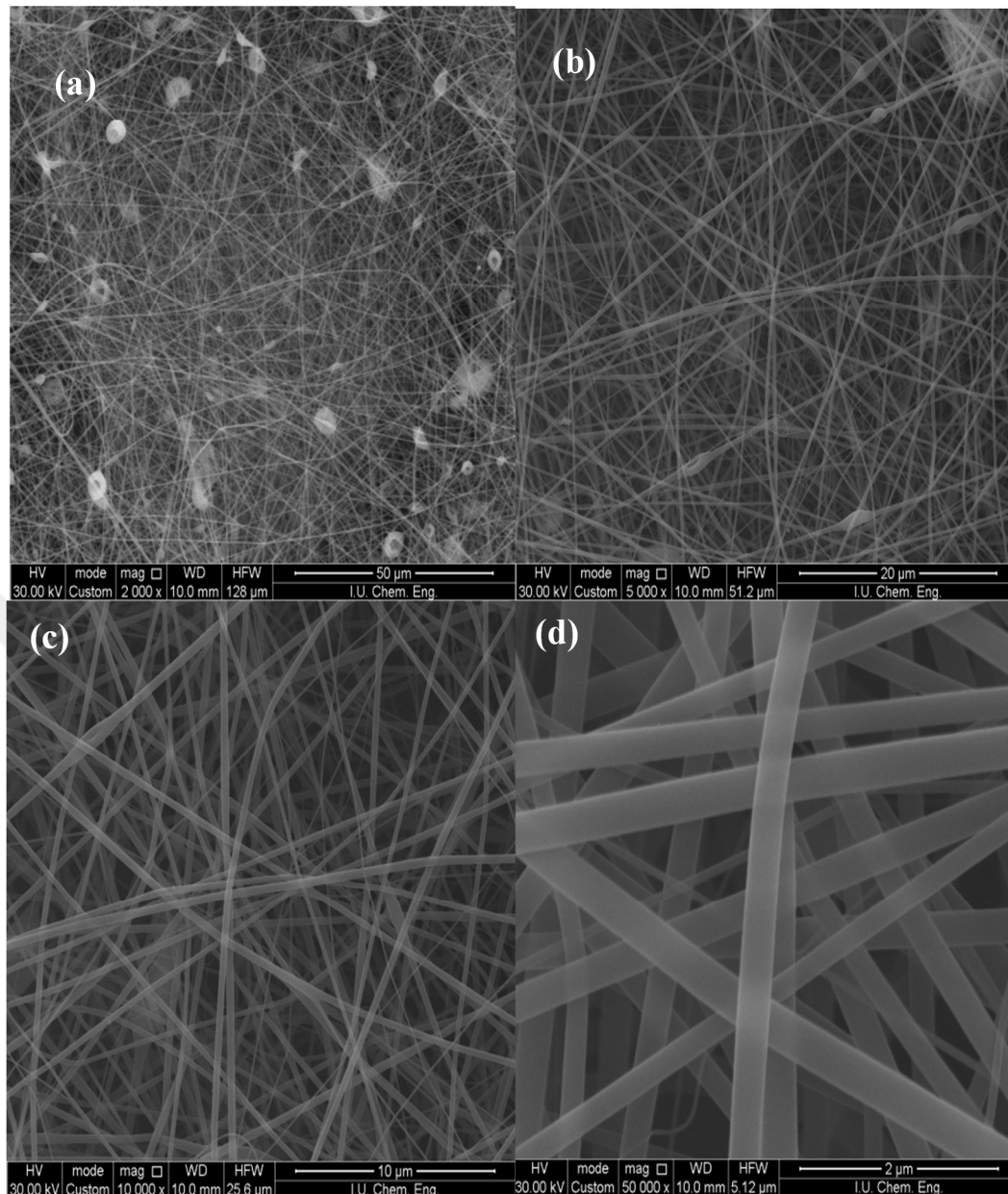


Figure 3.5 : SEM photographs of nanofiber from Solution 2 electrospun with higher voltage and distance at different magnifications, a) 2000x b) 5000x c)10000x d)50000x magnification.

SEM photographs of nanofibers obtained from Solution 2 with *Aloe vera* addition are given in Figure 3.6. Intense and high amount of bead formation is observed because of the gel structure of *Aloe vera*, but still the generation of nanofibers is found. Average diameter of nanofibers is calculated as 123 nm. Diameters of the nanofibers are in the range of 100 nm to 148 nm.

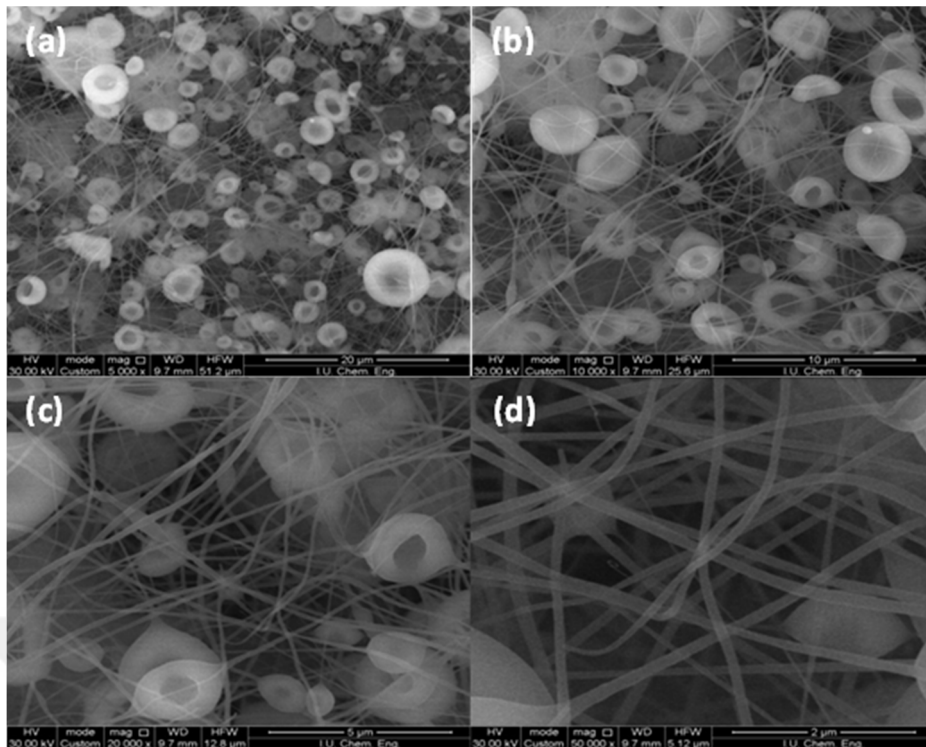


Figure 3.6 : SEM photographs of nanofiber from Solution 2 with *Aloe vera* at different magnifications, a) 5000x b) 10000x c)20000x d)50000x magnification.

3.1.3 XRD analysis

XRD spectra of heat treated Solution 2 fiber is shown in Figure 3.7. The phase development of TiO_2 with heat treatment was observed. TiO_2 samples that were heat-treated at around 500°C were found out to be mainly in the anatase phase without any rutile peaks observed as specified in the literature [68]. Peaks at 25° (101), 38° (004), 48° (200), 55° (105), 56° (211) are planes of the anatase [87].

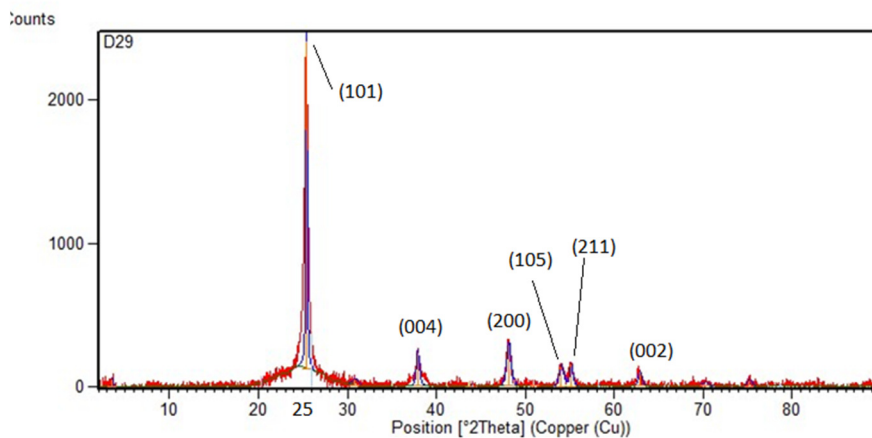


Figure 3.7 : X-ray diffraction pattern of electrospun TiO_2 fibers heat-treated at 500°C for 3 hours

3.1.4 Antibacterial activity of fibers

Staphylococcus aureus (Gram +) and *Escherichia coli* (Gram –) are the microorganisms used for the antimicrobial test. Test samples were sterilized under UV light. Two pieces of circular samples (diameter of 0.6 cm) was placed in each petri dish. CN10 (gentamycin), T30 (tetracycline), FOX 30 (cefoxitin) and AMP10 (ampicillin) impregnated disks were used as control group. The plates were incubated at 37°C for 48 h and the area of inhibition zone was measured. The inhibition zones are formed around the both samples but in different sizes. The inhibitory effects of samples are shown in Table 3.2.

Table 3.2 : Area of inhibitory zones of nanofibers

Sample	Area of inhibitory zone (cm ²)	
	<i>E. coli</i>	<i>S. aureus</i>
Solution 2 fibers	0.246	0.307
Solution 2 with aloe vera fibers	1.131	0.843
Antibiotic discs	1.815 (CN10)	2.977 (TE30)
	0.145 (FOX30)	1.455 (AMP10)

*CN10 (gentamycin), T30 (tetracycline), FOX 30 (cefoxitin) and AMP10 (ampicillin)

The control group and the experimental group were compared by measuring the inhibition zone diameters as shown in Figure 3.8 and Figure 3.9. Variations in zone diameters are observed due to the structural differences of the two different bacteria used in the experiments.

The antibacterial activities of TiO₂/PVP and TiO₂/PVP/*Aloe vera* gel fibers were investigated as their inhibitory effects toward Gram-positive bacteria, *Staphylococcus aureus*, and Gram-negative bacteria, *Escherichia coli*, using the agar disc diffusion method. Growth inhibition zones were measured for tested microorganisms with fiber mats and antibiotic discs, which were used as control. It is clear that the growth of *S. aureus* and *E. coli* bacteria inhibited in the field where fibers are applied and exhibited antibacterial activity. *Aloe vera* gel added nanofibers

represent admirable antibacterial affect that was almost five times more preventive of *E.coli* growth and three times more for *S.aureus* growth than the TiO₂/PVP fibers.

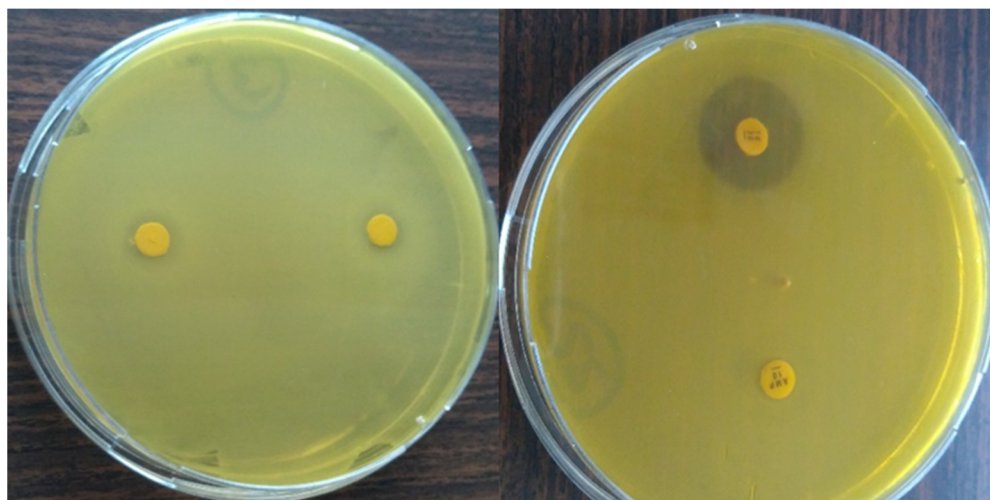


Figure 3.8 : Antimicrobial activities of PVP/TiO₂/*Aloe vera* fibers and antibiotic discs against *S. Aureus*.

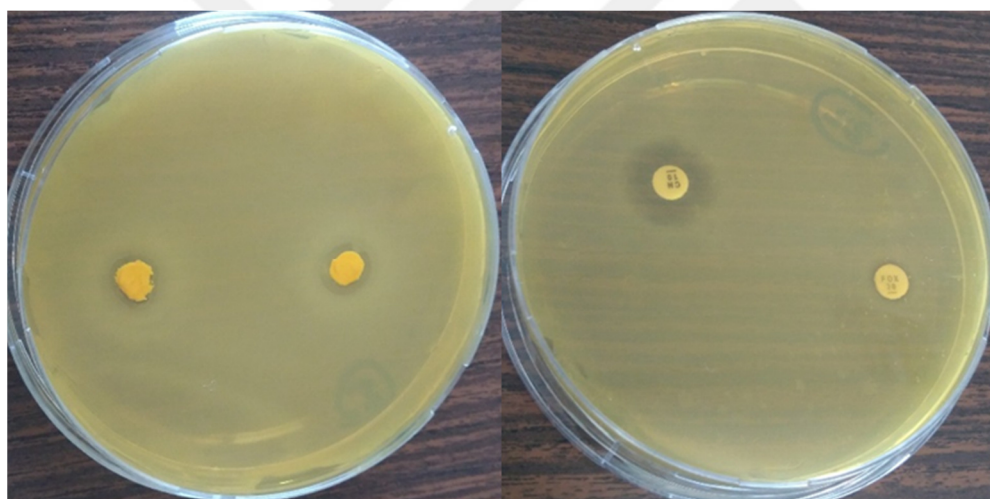


Figure 3.9 : Antimicrobial activities of PVP/TiO₂/*Aloe vera* fibers and antibiotic discs against *E. coli*.

3.2 Hydrogel Films Section

3.2.1 Surface morphology

Figure 3.10 shows SEM micrographs of the surface agar films with 20% *Aloe vera* content and without *Aloe vera* content in the film formulation. Both films have a homogeneous, almost smooth and continuous microstructure. This shows agar was well dissolved in water. Presence of *Aloe vera* in the films caused some irregularities in the film matrix. Some ridges and aggregation of particles were observed at the

surface of films. On the other hand, it is a successful result that there is no pore formation. Based on the observation, the addition of *Aloe vera* did not lead to significant defects in the structure.

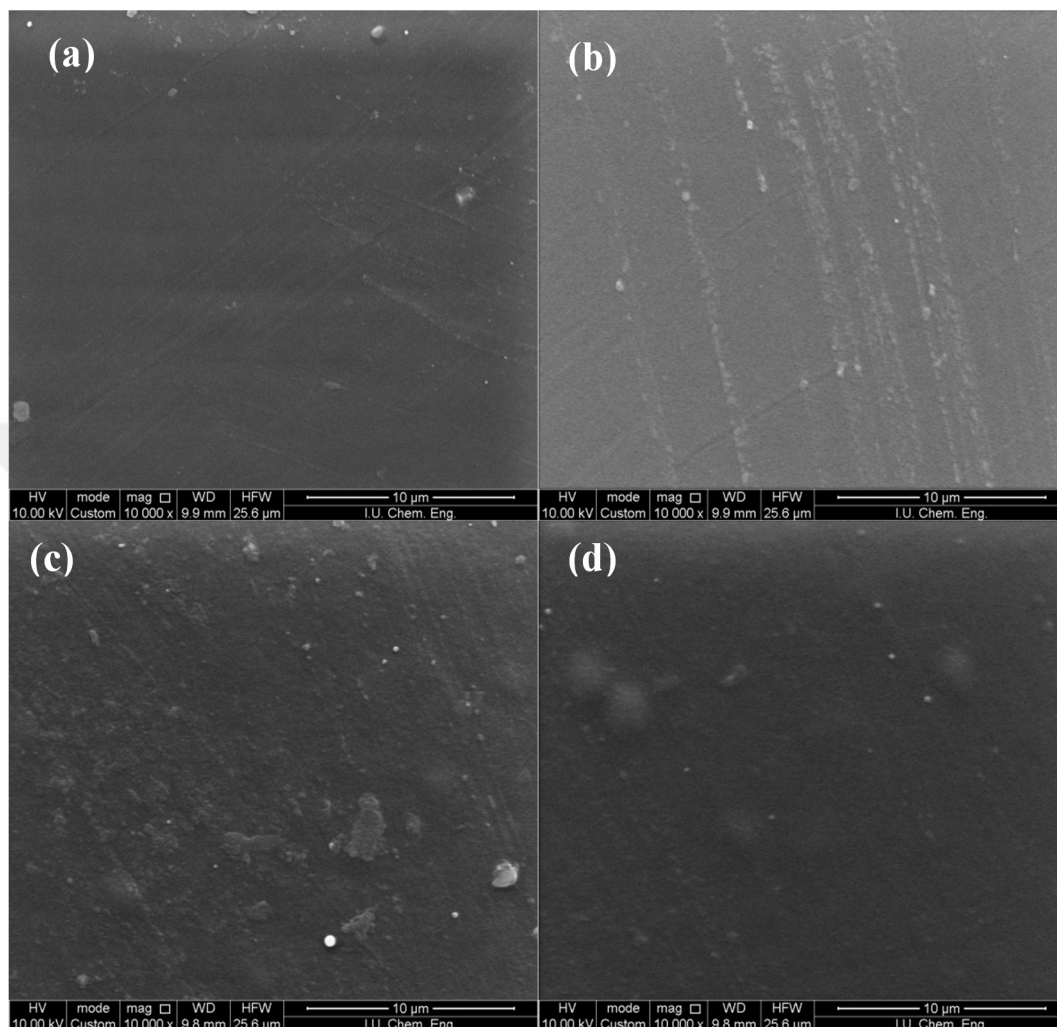


Figure 3.10 : SEM photographs of Agar films without *Aloe vera* (a-b) and with 20% *Aloe vera* (c-d)

3.2.2 FTIR characterization

Fourier transform infrared (FT-IR) spectra of the films were obtained using an attenuated total reflectance-Fourier transform infrared (ATR-FTIR) spectrophotometer (Thermo Nicolet Cary 630 FTIR) operated at a resolution of 4 cm^{-1} . The spectrum was recorded at wave number of $400\text{--}4000\text{ cm}^{-1}$. FT-IR results of agar films showed that all the film samples displayed similar peak patterns, suggesting that there might no chemical bond between agar polymer matrix and *Aloe vera*. Another factor can be argued that the concentration of *Aloe vera* is fairly low because 99% of *Aloe vera* is water, so there was no peak shifting. FTIR analysis of

agar/*Aloe vera* films is given in Figure 3.11. The agar film showed the broad absorption band at about 3330 cm^{-1} , which is assigned to O-H stretching of hydroxyl groups [88]. The peak around 2930 was observed because of C-H stretching of CH_2 [89]. The peak at 1637 cm^{-1} accounts to the H-O-H bending of the water [88]. The peak at 1372 cm^{-1} was due to an ester sulfate group [89]. The characteristic peaks at 1040 and 930 cm^{-1} indicated C-O stretching group of 3,6-anhydrogalactose [91]. Also peak at around 1150 cm^{-1} attributed to the vibration of ester-sulfate link. The peak at 886 cm^{-1} was due to an C-H stretching vibration of β -galactose [88].

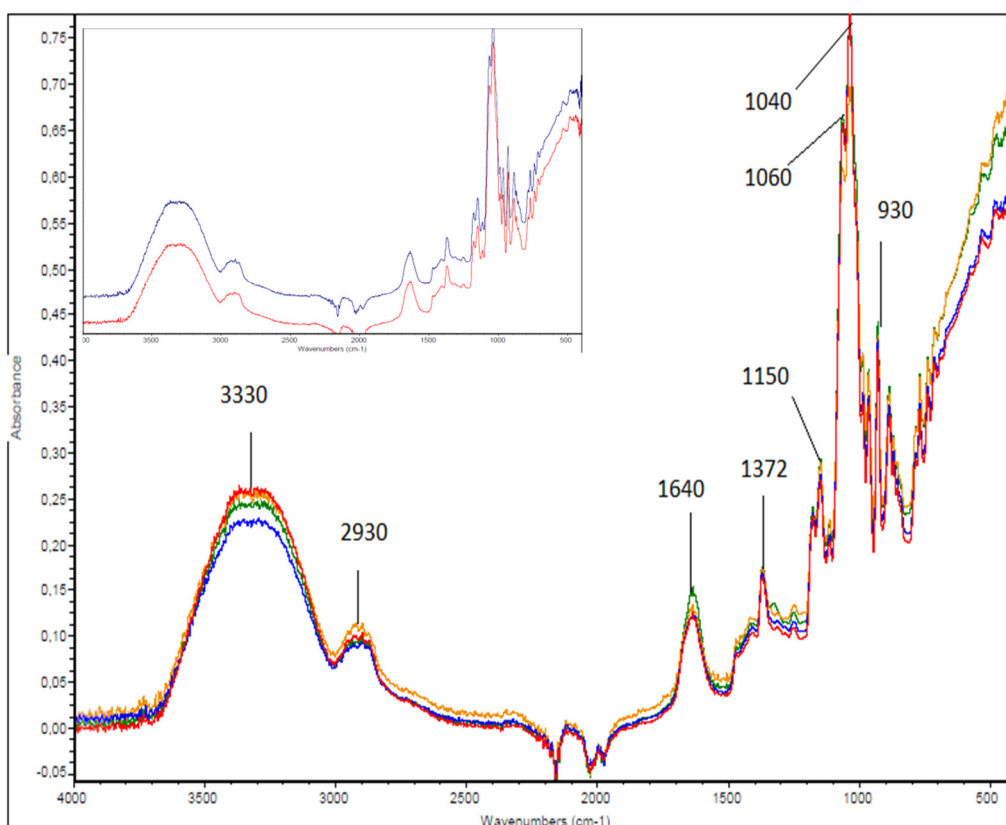


Figure 3.11: The FTIR spectra of A0(red), A10(green), A20(yellow) and A30(blue)

3.2.3 Antibacterial activity of films

Staphylococcus aureus (Gram +) and *Escherichia coli* (Gram -) are the microorganisms used for the antimicrobial test as mentioned in 3.1.3 Antibacterial activity of fibers section. The plates were incubated at 37°C for 48 h and the area of inhibition zone was measured. The areas of inhibitory zone of samples are shown in Table 3.3.

Table 3.3 : Area of inhibitory zones of films.

Sample	Area of inhibitory zone (cm ²)	
	<i>E. coli</i>	<i>S. aureus</i>
A0	0.136	0.134
A10	-	0.087
A20	0.307	0.589
A30	0.146	0.754
P0	0.136	0.307
P10	0.189	0.440
P20	0.246	0.167
P30	0.087	0.068
Antibiotic discs	1.815 (CN10) 0.145 (FOX30)	2.977 (TE30) 1.455 (AMP10)

*CN10 (gentamycin), T30 (tetracycline), FOX 30 (cefoxitin) and AMP10 (ampicillin)

The control group and the experimental group were compared by measuring the inhibition zone diameters as shown in Figure 3.12. Variations in zone diameters were observed due to the structural differences of the two different bacteria used in the experiments.

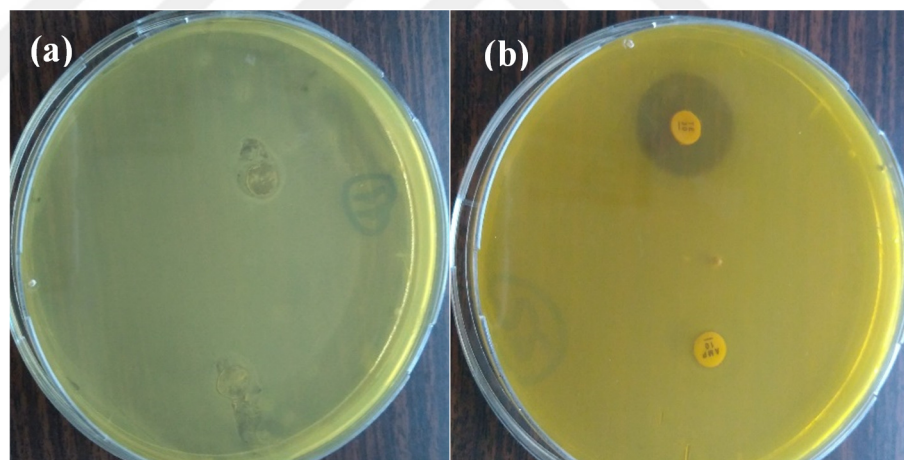


Figure 3.12: Antimicrobial activities of A30 film (a) and antibiotic discs (b) against *S. Aureus*

The highest antimicrobial activity was observed with A30 film against *S. aureus* and with A20 film for *E. coli*. The minimum activity was observed with A10 for both microorganisms. When the diameters of the areas are compared among the PVA films, P20 shows the highest activity against *E. Coli* while P10 shows for *S. Aureus*. The addition of *Aloe vera* content resulted the increase in the antimicrobial activity.

In addition, TiO₂ solution added agar films had an antibacterial effect against *E. Coli* and *S. Aureus* bacteria as inhibitory zones of 0.189 cm² and 0.558 cm² respectively.

2% and 4% ZnO nanoparticles-added A20 agar film showed a limited activity against the organisms as observed in Figure 3.13.

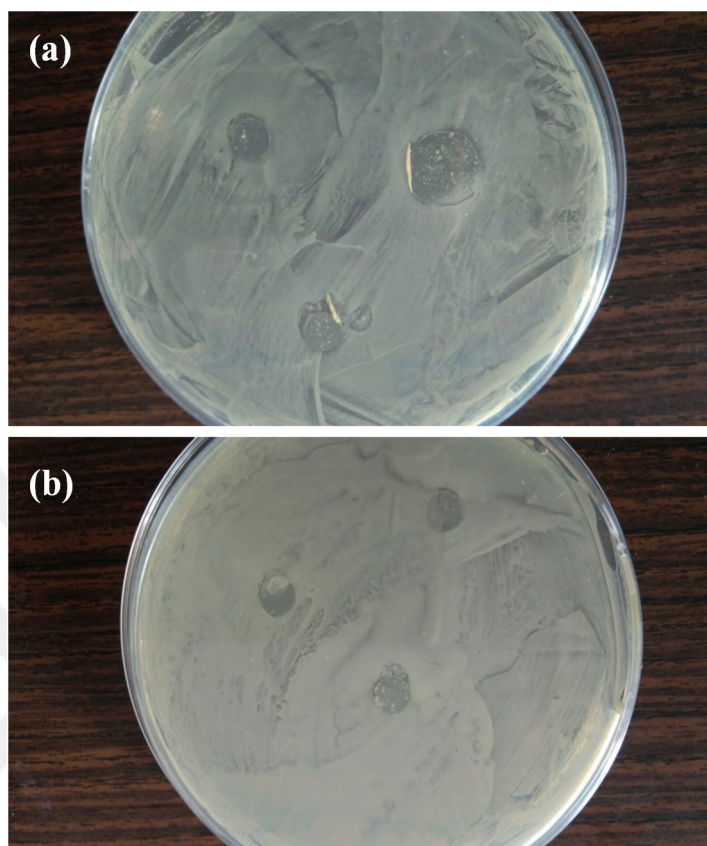


Figure 3.13: Antimicrobial activities of A20 film with 4% ZnO nanoparticle (a) against *E. coli* and (b) against *S. Aureus*

3.2.4 Mechanical properties

In order to determine the mechanical properties Shimadzu Autograph AGS-10kNJ with TRAPEZIUM2 data processing software was used with the cross-head speed of 15 mm/min according to the standard test method of ASTM D 882-88. The length, width and thickness of the films were measured to calculate elongation ratio, tensile strength and the exposed area. The tensile strength (TS) was calculated by dividing the maximum load (N) by the initial cross-sectional area (mm^2) of the films and expressed in MPa. The elongation (ϵ)(%) was determined by dividing the extension at the rupture of the film (Figure 3.14) by the initial length of the film multiplied by 100. The elastic modulus (E) was determined from the slope of the linear portion of the stress–strain curves. The mechanical analysis of the films were shown in Table 3.4. They were calculated by making three measurements.



Figure 3.14 : The torn film on the mechanical stress process.

Table 3.4 : Mechanical analysis of tensile strength (MPa) , elongation at break (e %), max. force at break (N) and Young's modulus (MPa) of the films

Sample Code	Tensile Strength (MPa)	Elongation at break (%)	Maximum Force (N)	Young's modulus (MPa)
A0	95.63±9.6	15.87±4.9	97.62±11.6	40.56±4.2
A10	94.53±21.8	14.31±5.7	88.03±8.5	39.48±17.9
A20	111.38±18.2	15.71±1.6	80.8±10.3	44.64±15.1
A30	58.45±14.3	6.44±1.1	50.46±7.7	28.42±3.4
P0	82.36±16.0	11.71±4.6	74.39±9.5	28.25±14.1
P10	60.29±10.9	12.99±5.5	53.40±12.2	16.31±5.5
P20	70.68±6.3	9.65±4.2	56.38±3.6	30.61±17.6
P30	86.25±21.8	10.98±5.3	46.64±7.7	25.40±14.0

*A is abbreviation of Agar and P is abbreviation of PVA, 0-10-20 and 30 represents the percentage of *Aloe vera*

Mechanical analysis of the films showed that, the agar films had tensile strength between 58.45 ± 14.3 MPa and 111.38 ± 18.2 MPa (Figure 3.15). Increasing the *Aloe vera* content up to 10% leads to no significant change and up to 20% resulted in an improvement in the mechanical properties of the agar film while further increase in *Aloe vera* proportion caused a dramatic decrease in the mechanical properties. Young modulus of the films nearly equal up to 30% elongation at break also nearly equal up to 30%. But at 30% Young modulus and elongation at break decreased nearly by half. The maximum force required to tear the films was decreased with the increasing percentage of *Aloe vera* as seen in Table 3.4.

When the Table 3.4 and graph in Figure 3.15 and Figure 3.16 are examined, as the amount of *Aloe vera* additive in the films increases, fluctuations are observed in the tensile strength of the samples in the range of 60.29-86.25 MPa and in the elongation rate of the samples in the range of 9.65-12.99% for PVA films. While the addition of 30% *Aloe vera* to agar film dramatically decreases its tensile strength and elongation rate, it has not same impact on the PVA film. Also, there is no meaningful correlation between the Young's modules of PVA films in terms of *Aloe vera* content.

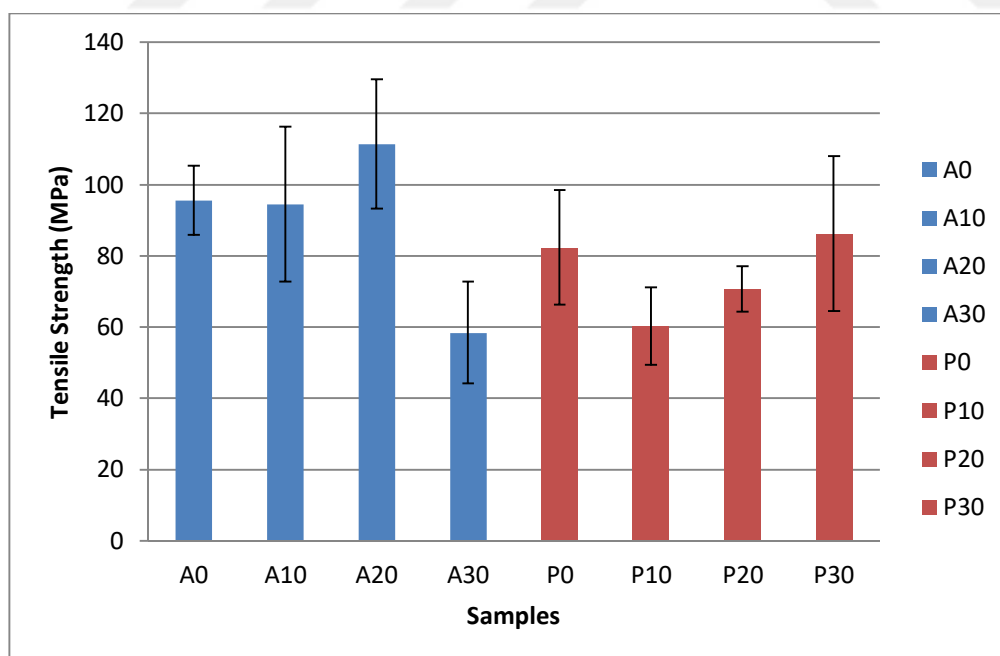


Figure 3.15 : Tensile strength of the *Aloe vera*-added films.

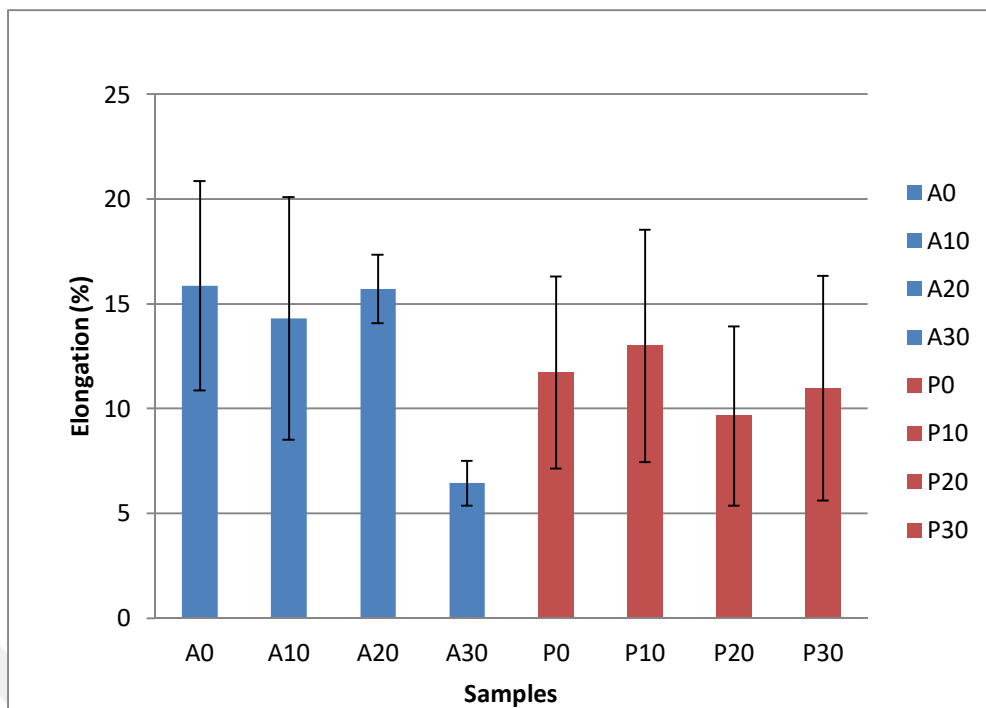


Figure 3.16 : Elongation ratios of the *Aloe vera*-added films.

Figure 3.17 presents the $\tan \delta$ curves of the A0 and A20 films and the values of T_g were identified from the peak of the curves. The neat agar film (A0) had one peak at 105.3 °C, while 20% *Aloe vera* added agar film had two peaks at 60.5 and 113.8 °C.

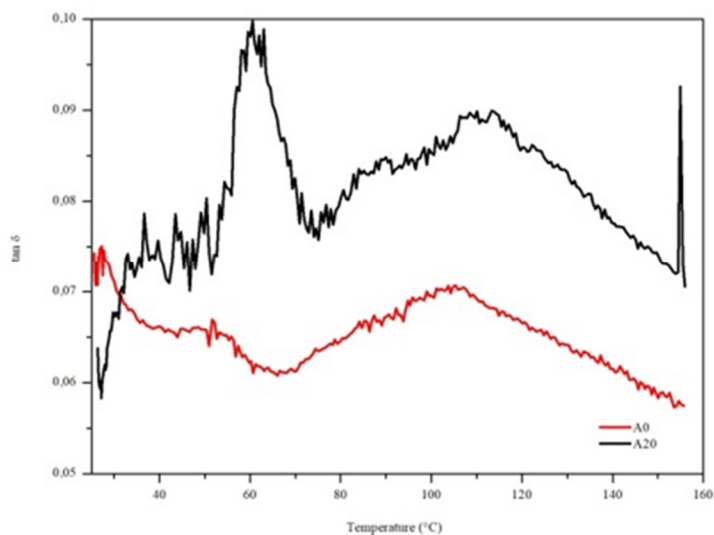


Figure 3.17: $\tan \delta$ curves of A0 (red line) and A20 (black line) films.

Definition of T_g is a way to analyze phase separation of polymer blends. An accepted rule for blending systems is as follows [92]: (1) If there are two T_g for the polymer

blend and they are the same as the two original T_g of the polymers, the polymers are fully incompatible, there are no molecular relation between the two polymers. Either, if they are different from the two original T_g , the two polymers are partially compatible as there are interactions between the chains of the two polymers. On the other hand, if just one T_g is existed, there are tough interactions between the chains of the polymers [32].

As observed in Figure, neat agar film had one peak and the film with *Aloe vera* had two peaks. These findings suggest that there is no molecular interaction between the agar and *Aloe vera*, or may be slight interaction because the peak was shifted from 105.3 °C to 113.8 °C. The storage and loss modules given to the $\tan \delta$ curves were shown in Figure 3.18.

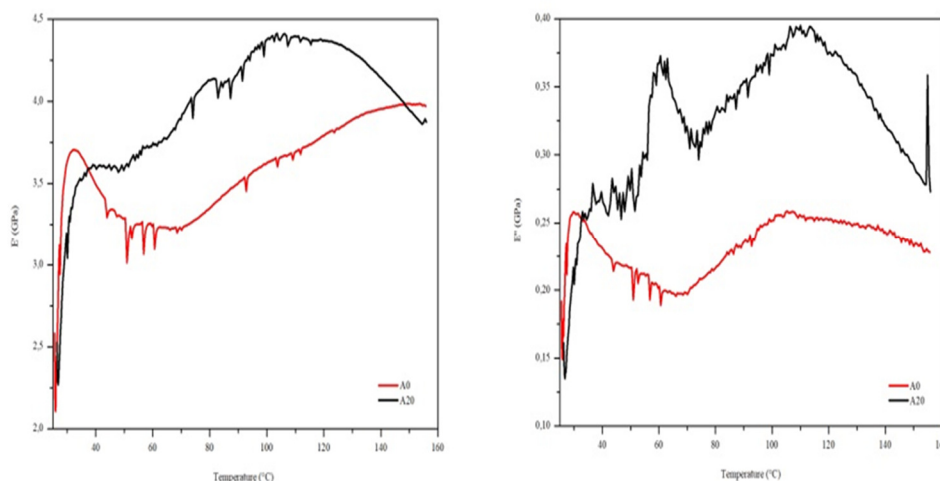


Figure 3.18 : Viscoelastic properties of A0 (red line) and A20 (black line) films, storage modules (on the left) and loss modules (on the right).

3.2.5 Contact angle measurements

KSV Instruments CAM200 contact angle meter was used to measure contact angles of films with high resolution cameras. 3 μ L water was dropped onto the film surfaces from syringe which can be observed in Figure 3.19. 10 images for each sample were taken with 1 second frame interval. Final contact angle were calculated by taking the average on left and right side contact angles of water droplet.

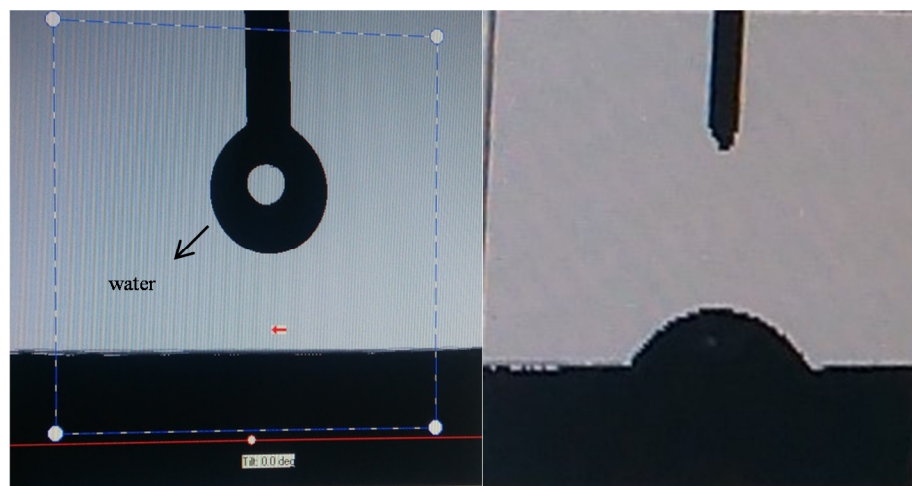


Figure 3.19 : Before water was dropped and after water was dropped onto the film surface.

Table 3.5 : Contact Angle degrees of the films.

Sample Code	Mean Contact Angle(degrees)	Sample Code	Mean Contact Angle(degrees)
A0	61.32±2.41	P0	22.37±7.83
A10	53.98±3.21	P10	21.80±4.49
A20	60.48±4.76	P20	38.67±9.82
A30	58.04±3.90	P30	28.53±2.88

Contact angle tests were made to examine the effect of *A. vera* on the hydrophilic properties of the surfaces of hydrogel film. The neat agar films (A0) and PVA films (P0) presented a hydrophilic surface with a water contact angle of 61.32±2.41 and 22.37±7.83 respectively as shown in Table 3.5. The addition of 10% *Aloe vera* decreased the contact angle of the surface to 53.98±3.21 and 21.80±4.49. It can be due to hydrophilic feature of *Aloe vera* gel [93]. However, increasing the content of *Aloe vera* caused an increase in contact angles to 60.48±4.76° for A20 (20% *A.Vera* film), to 58.04±3.90° for A30 (30% *A.Vera* film) and 38.67±9.82 for P20 and 28.53±2.88 for P30. It can be concluded that agar, PVA and *Aloe vera* are hydrophilic with different degrees, and increase in *Aloe vera* amount resulted in a

decrease in agar and PVA content which may cause the disruption of the hydrophilicity.

3.2.6 Transparency of films

Transparency is important for visual investigation of the wound without separation of the film from application area [61]. Likewise, transparency of edible films designed for packaging is a proper quality in most of the cases, because it has an effect of changing the appearance of the coated material [94]. Film light transmission was determined by spectrophotometry at between 200 nm - 800 nm according to the method used by Norajit et al [95].

It seems obvious that all the films display low light transmission in the ultraviolet (UV) light range, while in the visible range the light transmission remarkably increases in Figure 3.20. For the neat film (A0), the film light transmission increased until a maximum of $56.78 \pm 0.57\%$. The addition of Aloe vera within the agar films resulted in an increase in the light transmission. Transmission reached $69.78 \pm 0.49\%$ (Film A10), 78.96 ± 10.86 (Film A20) and 95.65 ± 3.79 (Film A30).

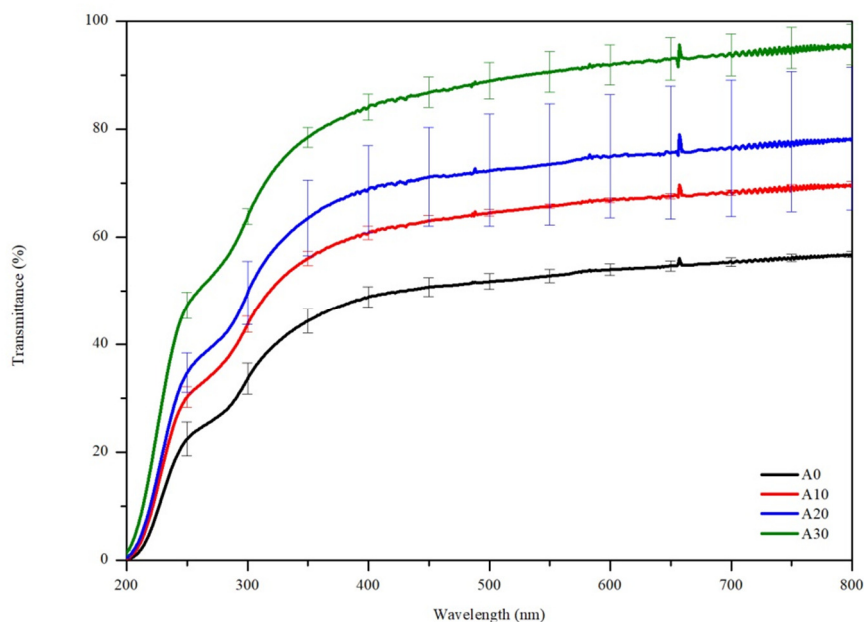


Figure 3.20: Transmittance of Agar/*A.vera* films

As shown in Figure 3.21, light transmission of P0, P10 and P20 films were very close to each other. P30 films exhibited the most transparency among the PVA films. For the neat film (P0), the film light transmission increased until a maximum of $80.48 \pm 2.11\%$. The addition of *Aloe vera* content up to 10% leads to no increase in transparency, P10 has a maximum of $78.68 \pm 2.41\%$ transmittance. P20 film has $81.35 \pm 0.68\%$ transmittance. Increasing the *Aloe vera* content to 30% resulted in increase in the transmittance as P30 has $89.40 \pm 0.84\%$ transmittance value.

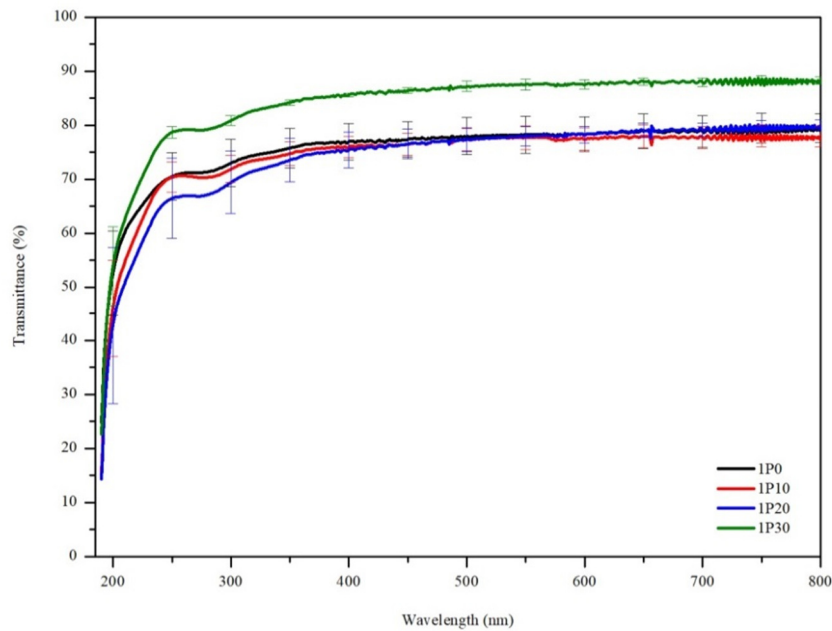


Figure 3.21 : Transmittance of PVA/*A. vera* films

3.2.7 Gas permeability

The primary problem of polymers in food packaging, is that they are all permeable to gases and low molecular weight molecules, which being an undesirable feature for packing items that are sensitive to atmospheric gases [31]. Figure 3.22 represents oxygen permeability of some biopolymer films [96].

The neat agar film (A0) and 20% *Aloe vera* added agar film (A20) was examined in terms of oxygen permeability. Oxygen permeability of A0 and A20 films were measured $43 \text{ cc} \cdot \mu\text{m}/\text{m}^2 \cdot \text{day} \cdot \text{bar}$ and $18.2 \text{ cc} \cdot \mu\text{m}/\text{m}^2 \cdot \text{day} \cdot \text{bar}$ respectively. The barrier properties of agar films were significantly higher compared to other biopolymer films.

Film/coating	Conditions	OP (cc × μm ² /day)
Pectin ^a	0% RH, 23°C	1000
Pectin ^a	50% RH, 23°C	2400
Pectin ^a	80% RH, 23°C	32,000
Pectin ^a + 10% nanoclay	0% RH, 23°C	600
Pectin ^a + 10% nanoclay	50% RH, 23°C	1200
Pectin ^a + 10% nanoclay	80% RH, 23°C	18,300
Pectin ^a + 20% nanoclay	0% RH, 23°C	400
Pectin ^a + 20% nanoclay	50% RH, 23°C	700
Pectin ^a + 20% nanoclay	80% RH, 23°C	11,300
Pectin ^a + 30% nanoclay	0% RH, 23°C	1400
Pectin ^a + 30% nanoclay	50% RH, 23°C	2600
Pectin ^a + 30% nanoclay	80% RH, 23°C	6400
Chitosan	80% RH, 23°C	9800
Chitosan + 17% nanoclay	80% RH, 23°C	4600
Chitosan + 50% nanoclay	80% RH, 23°C	1900
Chitosan + 67% nanoclay	80% RH, 23°C	1200
Chitosan crosslinked	80% RH, 23°C	980
Chitosan crosslinked + 50% nanoclay	80% RH, 23°C	280
CNF ^b bleached softwood	80% RH, 23°C	5200
CNF ^b bleached hardwood	80% RH, 23°C	2900
PVA-CNF	0% RH, 23°C	0.5
PVA-CNF	90% RH, 23°C	6790
PVA-CNF + 50% nanoclay	0% RH, 23°C	0.5
PVA-CNF + 50% nanoclay	90% RH, 23°C	190
CNF bleach birch pulp	0% RH, 23°C	<1
CNF bleach birch pulp	50% RH, 23°C	30
CNF bleach birch pulp	80% RH, 23°C	800
CNF ^a bleach birch pulp	0% RH, 23°C	3
CNF ^a bleach birch pulp	50% RH, 23°C	1700
CNF ^a bleach birch pulp	80% RH, 23°C	15,500
CNF bleach birch pulp (heat treated)	0% RH, 23°C	<1
CNF bleach birch pulp (heat treated)	50% RH, 23°C	2
CNF bleach birch pulp (heat treated)	80% RH, 23°C	300
PVA	90% RH, 23°C	45,000
CNF-PVA	90% RH, 23°C	50,000
Epoxy-CNF-PVA	90% RH, 23°C	48,000

^aPlasticized with glycerol. ^bPlasticized with sorbitol.

Figure 3.22 : Oxygen permeability of some biopolymer films [96].

As mentioned before, the crystallinity, degree of cross-linking and polymer chain motion is important parameters in permeability of polymers. A crosslinked network model has described the microstructural, mechanical and rheological properties of agar gels. Agar molecules connect to each other forming a three-dimensional network in the gel state. In the commonly accepted double-helix model, the basic structural unit is the double helix. Each chain forms a left-handed, 3-fold helix and the interior spacing of the helices contain water molecules. The hydroxyl groups from the 3,6 –anhydrogalactose are involved in hydrogen bonding with the water molecules or neighboring helices. These hydrogen-bonding interactions allow for the aggregation of double helices into higher order assemblies called suprafibers. They may contain up to 10^4 double helices and promote significantly to the elastic properties of the three-dimensional network. As the stiffness of the double helix increases, its conformational entropy that supports dissolution in the solvent is reduced [97]. The stiffness of the agar morphology may cause the low permeability of oxygen molecules through film.

3.2.8 Water vapor permeability

Weight loss over time was plotted to obtain the slope ($r^2 \geq 0.99$). WVTR was the measured water vapor transmission rate ($\text{g}/\text{m}^2 \text{ h}$), L was the mean thickness of the film (mm), and ΔP was partial water vapor pressure difference (kPa) across the film. The beaker containing distilled water has 100% RH; 2.41×10^3 Pa vapor pressure at 20.5°C and the room which the test was performed has 50% RH; 1.21×10^3 Pa at 20.5°C . The pressure difference across the film was measured as 1.2 kPa.

WVP was calculated according to equation 1.14 and the graph of datas was showed in Figure 3.23.

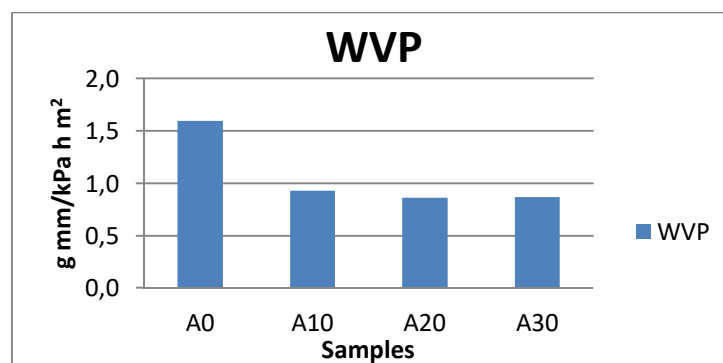


Figure 3.23: WVP values of agar/*Aloe vera* films

Comparing the samples with the *Aloe vera*-free agar film showed that WVP was affected by adding *Aloe vera*. The decrease of WVP could prevent fast water evaporation; hence the wound may remain in a humid environment which is necessary for wound healing.

3.2.9 Swelling behavior

The swelling behavior of the films was detected through the immersion of pre-weighted samples into 20 mL of phosphate buffered saline (PBS) solution pH 7.4 simulating the body fluid. The samples were collected from solution at determined periods of time, the excess of water was dried by a filter paper and its wet weight measured. The equation 1.15 gives the swelling ratio of the films. Figure 3.24 shows the influence of the *A. vera* content on the swelling behavior of the agar films.

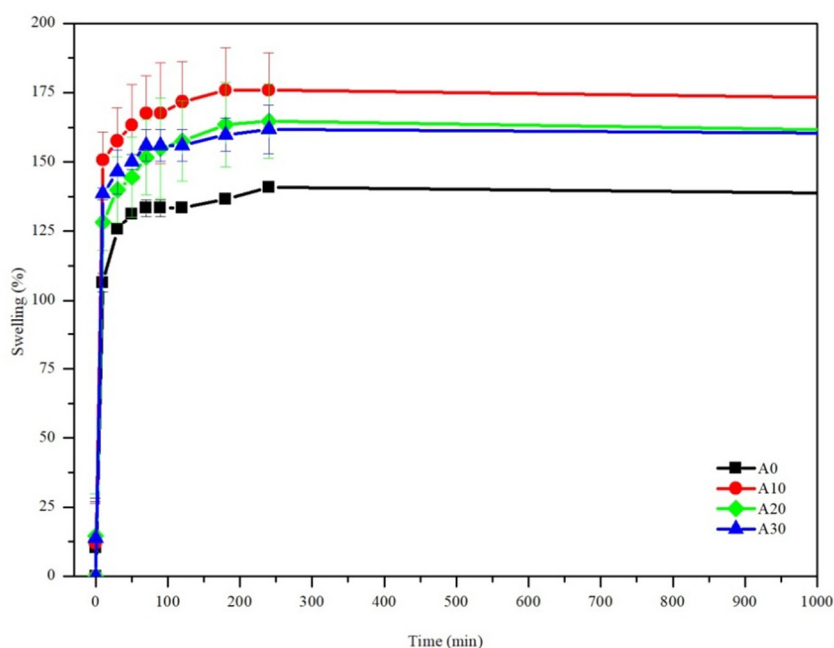


Figure 3.24: Swelling behavior of agar/*A. vera* films immersed in PBS buffer pH 7.4.

Regarding the water absorption representation of all samples, the films fastly absorbed water during 30 minutes when placed in PBS solution and they reached to equilibrium in about 240 minutes (Figure 3.24). A10, A20, and A30 displayed slightly higher water uptakes compared to the agar film. A10 (10% *A. Vera*) film absorbed the most amount of water as consistent with contact angle test results.

3.2.10 In vitro degradation studies

The in vitro degradation behavior of the films was figured via measuring the weight loss after keeping in PBS during 14 days. A piece of films were immersed in PBS and on days 1,2,3,7 and 14 the samples were taken from the solution, remaining water on the samples were dried with filter paper. Then, the samples were placed in an oven and dried at 37 °C until the masses were constant. The degradation ratio was calculated based on weight losses with the equation 1.16. Figure 3.25 presents weight loss ratios of the films.

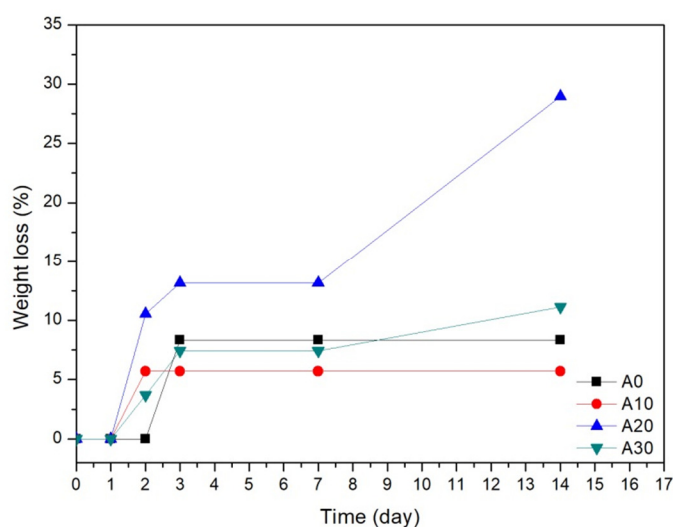


Figure 3.25 : Weight loss ratio of agar/*A.vera* films.

The agar film with 20% of *A. vera* displays the fastest degradation rate, the film with 10% of *A.vera* shows the lowest degradation rate. *A. Vera* mixed films started to degrade after one day, but *A.vera*-free agar film started after two days. The films exhibit a weight loss in a range from 5.7% and 28.9% as showed in Fig. 3.25.



4. CONCLUSION

In this work, we describe a procedure for producing biopolymer based fibers via electrospinning from different precursors that are titanium(IV) isopropoxide and titanium(IV) butoxide and enhanced them with PVP and *Aloe vera*. The parameters that influence the electrospinning process were investigated and by changing the conditions such as precursors, viscosity and so on and the properties of the electrospinning process, the size, continuity and functioning of fibers can be modified. Furthermore, we have prepared polymer films of the organic/synthetic polymers by addition of different amounts of *Aloe vera*. SEM characterization combined with image visualization showed that TiO₂/PVP fibers were produced nano-size, smooth, continuous and uniformly distributed via electrospinning method. Diameter size and the formed mat thickness of these obtained nanofibers were successfully controlled as desired by the convenience of this method. Fibers which are produced from titanium(IV) butoxide/PVP blend showed anatase TiO₂ crystalline structure. Antimicrobial activity of TiO₂/PVP and TiO₂/PVP /*Aloe vera* gel fibers was tested against Gram-positive and Gram-negative bacteria using agar diffusion method. The results showed that *Aloe vera* gel-added nanofibers showed 5 times more inhibition for growth of *E. coli* and 3 times more inhibition for growth of *S. Aureus* than neat fibers. *Aloe vera* gel-added TiO₂/PVP nanofibers are likely to perform well as antibiotics. These antibacterial findings raised important issues that have a bearing on the bio-applications, they can be used as an alternative in antibacterial applications by making more improvements.. The parameters that affect electrospinning process can be studied more deeply in the further studies.

Agar or PVA/*Aloe vera* blend hydrogel biopolymer films were prepared and the interaction of the biopolymers with that natural material as well as the film potential for application as wound dressings or edible films as packaging material was assessed. The prepared biopolymer films were characterized concerning their chemical structure, morphology, antimicrobial activity, transparency, oxygen and water vapor permeability, swelling and degradation properties. *Aloe vera* gel addition

into polymer films managed to inhibit the growth of *S. aureus* and *E. coli*. Hydrophilic property of the films was analyzed with contact angle measurement and it was found that low *Aloe vera* addition enhanced hydrophilicity but more *Aloe vera* addition gave opposite effect. Both oxygen and water vapor barrier properties increased with the addition of *Aloe vera* gel. The result of mechanical analysis demonstrated that the introduction of *Aloe vera* up to 20% improved the mechanical behavior of the agar films whereas incorporation of higher content adversely affected the mechanical properties. However, PVA based films did not show any correlated changes. Swelling behavior tests showed the films contained *Aloe vera* absorb more water than the unaltered films. Upon exploring the potential use of films containing the natural materials which are promising alternative to synthetic materials, it was evident that the incorporation of *Aloe vera* to agar was effective packaging or wound dressing material with suitable mechanical, physical and microbiological properties. In further analysis different concentrations of polymers and other natural additives might be studied.

REFERENCES

- [1] Ramakrishna, S., Fujihara, K., Teo, W.E., Lim, T.C. and Ma, Z. (2005). An Introduction to Electrospinning and Nanofibers, *World Scientific Publishing*, Singapur.
- [2] Asmatulu, R., Khan, W., Wamocha, H., and Adeniji, A. (2007). Improving the nanotechnology education for future engineers, *ASEE Midwest Section 2007 Annual Conference*, Wichita, KS, September 19–21.
- [3] Zufan, R. (2005). Electrospinning of Nanofibers, UIC-LPPD-080405. Retrieved April 11, 2017, from <http://vienna.bioengr.uic.edu/RET/Reports/Final%20Reports/ZufanRETFinal>.
- [4] Fang, J., Niu, H., Lin, T., Wang, X. (2008). Applications of electrospun nanofibers, *Chin. Sci. Bull.* 53: 2265.
- [5] Ramakrishna, S., Fujihara, K., Teo, W.E., Yong, T., Ma, Z.W. and Ramaseshan, R. (2006). Electrospun nanofibers: solving global issues, *Materials Today*, 9(3), 40-50.
- [6] Wendorff, J. H., Agarwal, S., & Greiner, A. (2012). *Electrospinning: materials, in: processing, and applications*. Germany: Wiley-VCH.
- [7] El-Aassar, MR., El Fawal, GF., El-Deeb, NM., Hassan, HS., Mo, X. (2016). Electrospun Polyvinyl Alcohol/ Pluronic F127 Blended Nanofibers Containing Titanium Dioxide for Antibacterial Wound Dressing, *Appl Biochem Biotechnol.*, 178(8):1488-502.
- [8] Rayleigh, L. (1882). On the Equilibrium of Liquid Conducting Masses charged with Electricity, *Philosophical Magazine*, 14: 184–186.
- [9] Formhals, A. (1934). Process and apparatus for preparing artificial threads. *US Patent. No 1,975,504*.
- [10] Cavaliere, S., Subianto, S., Savych, I., Jones, D.J., and Roziere, J. (2011). Electrospinning, designed architectures for energy conversion and storage devices, *Energy & Environmental Science, Royal Society of Chemistry*, 4, 4761-4785.
- [11] Haider, A., Haider, S., Kang, I.K. (2015). A comprehensive review summarizing the effect of electrospinning parameters and potential applications of nanofibers in biomedical and biotechnology, *Arabian Journal of Chemistry*
- [12] Norris, I.D., Shaker, M.M., Ko, F.K., MacDiarmid, A.G. (2000). Electrostatic fabrication of ultrafine conducting fibers, polyaniline/polyethylene oxide blends, *Synthetic Metals*, 11, 110-114.

- [13] Sukigara, S., Gandhi, M., Ayutsede, J., Micklus, M., Ko, F. (2003). Regeneration of Bombyx mori silk by electrospinning—part 1: processing parameters and geometric properties, *Polymer* 44, 5721-7.
- [14] Coles, S.R., Wooldridge, A. (2015). Optimising Solutions for Electrospinning. *Electrospinning: Principles, Practice and Possibilities*.
- [15] Heikkila, P. and Harlin, A. (2008). Parameter study of electrospinning of polyamide-6, *European Polymer Journal*, 44(10), 3067-3079.
- [16] Doshi, J., Reneker, D.H. (1995). Electrospinning process and applications of electrospun fibers. *J Electrostat*, 35:151–6.
- [17] Mit-uppatham, C., Nithitanakul, M. and Supaphol, P. (2004). Ultrathin electrospun polyamide-6 fibers: Effect of solution conditions on morphology and average fiber diameter, *Macromolecular Chemistry and Physics*, 205(17), 2327-2338.
- [18] Fong, H., Chun, I. and Reneker, D.H. (1999). Beaded nanofibers formed during electrospinning, *Polymer*, 40(16), 4585-4592.
- [19] Hohman, M.M., Shin, M., Rutledge, G., Brenner, M.P. (2001). Electrospinning and electrically forced jets. II. Applications, *Phys Fluids*, 13:2221–36.
- [20] Laudenslager, M.J., Sigmund, W.M. (2012). “Electrospinning” Encyclopedia of Nanotechnology. *Springer Publishers*, pp. 769–775.
- [21] Andrady, A. L. (2008). “Science and Technology of Polymer Nanofibers”, John Wiley & Sons, Inc.
- [22] Enoch, S., John Leaper, D. (2005). Basic science of wound healing, *Surgery (Oxford)*, 23:37–42.
- [23] Siddiqui, A.R., Bernstein, J.M. (2010). Chronic wound infection: facts and controversies, *Clin. Dermatol*, 28, 519.
- [24] Nagarajan, P., Rajagopalan, V. (2008). Enhanced bioactivity of ZnO nanoparticles—An antimicrobial study, *Science and Technology of Advanced Materials*, 9, 035004, 7 pp.
- [25] Abrigo, M., McArthur, S.L., Kingshott, P. (2014). Electrospun Nanofibers as Dressings for Chronic Wound Care: Advances, Challenges, and Future Prospects, *Macromol. Biosci*, 14, 772–792.
- [26] Gao, Y., Bach Truong, Y., Zhu, Y., Louis Kyratzis, I. (2014). Electrospun antibacterial nanofibers: production, activity, and in vivo applications, *J. Appl. Polym. Sci.* 131 (18).
- [27] Mahmoudi, N., Ostadhossein, F., Simchi, A. (2016). Physicochemical and antibacterial properties of chitosan-polyvinylpyrrolidone films containing self-organized graphene oxide nanolayers. *J. Appl. Polym. Sci.*, 133, 43194.
- [28] Ebara, M., Kotsuchibashi, Y., Narain, R., Idota, N., Kim, Y.-J., Hoffman, J.M., Uto, K., Aoyagi, T., (2014). Smart Hydrogels, *Smart Biomaterials* (Ed.1, pp.9-65) . Springer Japan.

- [29] **Barros, S.C., da Silva, A.A., Costa, D.B. et al.**, (2014). Thermo-sensitive chitosan–cellulose derivative hydrogels: swelling behaviour and morphologic studies, *Cellulose*, 21: 4531.
- [30] **Zhang, H., Zhang, F., Wu, J.** (2013). Physically crosslinked hydrogels from polysaccharides prepared by freeze–thaw technique, *React Funct Polym* 73:923–928.
- [31] **Galdi, M.R.** *Design and production of active films for food packaging application* (Doctoral Dissertation). UNIVERSITÀ DEGLI STUDI DI SALERNO
- [32] **Shi, X.** (1998). *Self-Supporting Edible and Biodegradable Packaging Films From Polysaccharides* (Doctoral Dissertation). Available from ProQuest Dissertations and Theses database (UMI No. 3138281)
- [33] **Goldstein, I.J., Newbury, D.E., Echlin, P., Joy, D.C., Romig, A.D., Lyman, C.E., Fiori C., Lifshin, E.** (1992). Scanning Electron Microscopy And X-Ray Microanalysis, *Plenum Press, New York*, ISBN 0-306-44175-6.
- [34] **Young, R. A. and Kalin, R.V.** (1986). Microelectronics processing: inorganic materials characterization, ACS Symp. Series, Plymouth, USA.
- [35] **Teo, B.K.** (1986). X-Rays and Electrons. In: EXAFS: Basic Principles and Data Analysis. *Inorganic Chemistry Concepts*, 9., Springer, Berlin, Heidelberg.
- [36] **Sharma, R. et al.** (2012). X-ray diffraction: a powerful method of characterizing nanomaterials. *India : Recent Research in Science and Technology*.
- [37] **Zschornack, G.** (2006). Handbook of X-Ray Data, *Springer*, Dresden.
- [38] **Amand, L.E., Tullin, C.J.** (n.d) *The Theory Behind FTIR Analysis*, Chalmers University of Technology.
- [39] **Berthomieu, C., Hienerwadel, R.** (2009). Fourier transform infrared (FTIR) spectroscopy, *Photosynthesis Research*, 101, Issue 2–3, pp 157–170.
- [40] **Desbois, A.P., Smith, V.J.** (2015). Disk Diffusion Assay to Assess the Antimicrobial Activity of Marine Algal Extracts. In: Stengel D., Connan S. (eds) *Natural Products From Marine Algae. Methods in Molecular Biology*, vol 1308.
- [41] **Brandon, L.** Simple and Differential Staining of bacteria, General Microbiology Lab, Retrieved December 01, 2017 from <http://www2.muw.edu/~lbrandon/bsm131L.html>
- [42] **Creech, C. B., Al-Zubeidi, D. N., Fritz, S. A.** (2015). Prevention of Recurrent Staphylococcal Skin Infections, *Infectious Disease Clinics of North America*, 29(3), 429–464.
- [43] "*Escherichia coli*". CDC National Center for Emerging and Zoonotic Infectious Diseases. Retrieved December 01, 2017 from <https://www.cdc.gov/ecoli/index.html>.
- [44] **Yang, L., Paulson, A. T.** (2000). Effects of lipids on mechanical and moisture barrier properties of edible gellan film. *Food Research International*, 33, 571–578.

- [45] **Anseth, K.S., Bowman, C.N., Brannon-Peppas, L.** (1996). Mechanical properties of hydrogels and their experimental determination. *Biomaterials*, 17, 1647–1657.
- [46] Dynamic Mechanical Analysis (DMA). A Beginner's Guide. *PerkinElmer, Inc.*, 2008-2013, available at www.perkinelmer.com.
- [47] Contact Angle, Retrieved March 08, 2018 from <https://www.biolinscientific.com/measurements/contact-angle>.
- [48] Surface energy of solids. (2013). Cambridge Polymer Group, Retrieved March 08, 2018 from http://www.campoly.com/files/7414/0293/8070/023_Surface_energy_of_solids_ADMIN-0171_v1.1.pdf
- [49] **Baba, E.M.** (2015). *Investigation of Optical And Wettability Properties of Polymer Coatings* (Master's Thesis). Istanbul Technical University, Graduate School of Science Engineering and Technology.
- [50] **Owen, T.** (2000). Fundamentals of modern UV-visible spectroscopy, *Agilent Technologie*.
- [51] **Barnes, H.A., Hutton, J.F., Walters, K.** (1989). An introduction to rheology (5. impr. ed.). Amsterdam: Elsevier.
- [52] **Macosko, C.W.** (1994). Rheology: Principles, Measurements, and Applications. Wiley-VCH.
- [53] Radiometer Analytical. (2004). *Conductivity Theory and Practice*. Radiometer Analytical SAS, Retrieved March 02, 2018 from http://www.analytical-chemistry.uoc.gr/files/items/6/618/agwgimometria_2.pdf.
- [54] **Gray, J.R.** (2004). *Conductivity Analyzers and Their Application*. In Down, R.D; Lehr, J.H. Environmental Instrumentation and Analysis Handbook. Wiley. pp. 491–510.
- [55] Surface and Interfacial Tension. Langmuir-Blodgett Instruments. Retrieved March 02, 2018 from https://web.archive.org/web/20071012031017/http://www.ksvinc.com/surface_tension1.htm on 2007-10-12.
- [56] DCAT product series, *Tensiometry – an introduction*. DataPhysics Instruments GmbH, Retrieved March 02, 2018 from http://www.dataphysics.de/fileadmin/user_upload/pdf/Datasheet/DCA_T/DCAT_EN.pdf.
- [57] **Galić, J., Galić, K., Kurtanjek, M., Ciković, N.** (2000). Gas permeability and DSC characteristics of polymers used in food packaging. *Polymer Testing*, vol. 20, no. 1, pp. 49–57.
- [58] **Siracusa, V.** (2012). Food Packaging Permeability Behaviour: A Report, vol. 2012.
- [59] Gas Permeability Testing Manual, Brugger Feinmechaik GmbH.

- [60] ASTM, 2005. Standard test method for water vapor transmission of materials (E 96-05). In: In Annual Book of ASTM Standards. American Society for Testing Materials, Philadelphia, PA.
- [61] Pereira, R., Carvalho, A., Vaz, D.C., Gil, M.H., Mendes, A., Bártolo, P. (2013). Development of novel alginate based hydrogel films for wound healing applications, *International Journal of Biological Macromolecules*, 52, 221–230.
- [62] Muscat, J., Swamy, V.; Harrison, N.M. (2002). First-principles calculations of the phase stability of TiO₂. *Physical Review B*, 65, (22).
- [63] Gökgöz, E.E. (2010). *Renklendirilmiş Organik TiO₂ ile Kaplanmış Camların Yapısal, Optik ve Elektriksel Özelliklerinin İncelenmesi*, (Master's Thesis). Süleyman Demirel Üniversitesi Fen Bilimleri Enstitüsü, Isparta
- [64] Rino, J.P., Studart, N. (1999). Structural correlations in titanium dioxide. *Physical Review*, 59(2): p.6643.
- [65] Winkler, J. (2003). Titanium Dioxide, Vincentz Network, *European Coatings Literature*, Hannover.
- [66] Ahmad, R., Sardar, M. (2013). TiO₂ nanoparticles as an antibacterial agents against *E. Coli*, *International Journal of Innovative Research in Science, Engineering and Technology*, 2 (8).
- [67] Karkare, M.M. (2014). Choice of precursor not affecting the size of anatase TiO₂ nanoparticles but affecting morphology under broader view, *Int Nano Lett*, 4:111.
- [68] Park, H. (2010). *Electrospinning of nanofibers for filtration media* (Doctoral Dissertation). Available from ProQuest Dissertations and Theses database (UMI No. 3416716).
- [69] Foltmann, H., Quadir, A., (2008). Polyvinylpyrrolidone (PVP) – One of the Most Widely Used Excipients in Pharmaceuticals: An Overview, *Drug Delivery Technology*, 8(6), 22-27.
- [70] Zhang, L., Hu, J., Voevodin, A.A., Fong, H. (2010). Synthesis of continuous TiC nanofibers and/or nanoribbons through electrospinning followed by carbothermal reduction, *Nanoscale*, 9(8).
- [71] New Jersey Institute of Technology. *Green Chemistry in Teaching Laboratory*. [Online] [Accessed at: 12 October 2017] https://web.njit.edu/~mitra/green_chemistry/EXP_2.htm.
- [72] Aytimur, A., Uslu, I. (2014). Promising materials for wound dressing: PVA/PAA/PVP electrospun nanofibers, *Polym. Plast. Technol. Eng.*, 53, 655–660.
- [73] Gajra, B., Pandya, S.S., Vidyasagar, G., Rabari, H., Dedania, R R., Rao, S. (2012). Poly vinyl alcohol hydrogel and its pharmaceutical and biomedical applications: A review., *Int. J. Pharm. Res.* 4, 20–26.
- [74] Matsushashi, T. (1990). Agar. In P. Harris (Ed.), *Food Gels* (pp. 1-51). New York: Elsevier Science Publishers.

- [75] **Armisen, R., Galatas, F.** (2009). Agar, Handbook of Hydrocolloids: Second Edition, , pp. 82-107.
- [76] **Medin, A.** (1995). 'Studies of Structure and Properties of Agarose'. PhD Thesis, Acta Universitatis Upsaliensis, 126, 74.
- [77] **Bao, X., Hayashi, K., Li, Y., Teramoto, A., and Abe, K.** (2010). Novel agarose and agar fibers: fabrication and characterization. *Mater. Lett.*, 64, 2435-2437.
- [78] **Ni, Y.; Turner, D.; Yates, K.M.; Tizard, I.** (2004). Isolation and characterisation of structural components of Aloe vera L. leaf pulp. *Int. Immunopharmacol.*, 4, 1745-1755.
- [79] **Liu, P., Chen, D., Shi, J.** (2013). Chemical constituents, biological activity and agricultural cultivation of Aloe vera. *Asian Journal of Chemistry*, 25(12), 6477-6485.
- [80] **Hamman, J.H.** (2008).Composition and Applications of Aloe vera Leaf Gel, *Molecules*, 13, 1599-1616.
- [81] **Reynolds, T.; Dweck, A.C.**(1999). Aloe vera leaf gel: a review update. *J. Ethnopharmacol.*,68, 3-37.
- [82] **Takzare, N., Hosseini, M.J., Hasanzadeh, G., Mortazavi, H., Takzare, A., Habibi, P.** (2009). Influence of aloe vera gel on dermal wound healing process in rat. *Toxicol Mech Methods*, 19:73-77.
- [83] **Adzick, N.S.** (1996). Wound healing: Biologic and clinical features. In Sebastian DC (ed): Textbook of Surgery: The Biological Basis of Modern Surgical Practice, 15th ed. WB Saunders Company, Philadelphia, pp. 207-220.
- [84] **Habeeb, F., Shakir, E., Bradbury, F., Cameron, P., Taravati, M.R., Drummond, A.J., Gray, A.I., Ferro, V.A.** (2007). Screening methods used to determine the anti-microbial properties of Aloe vera inner gel. *Methods*, 42, 315-320.
- [85] **Alves, D.S.; Pérez-Fons, L.; Estepa, A.; Micol, V.** (2004). Membrane-related effects underlying the biological activity of the anthraquinones emodin and barbaloin. *Biochem. Pharmacol.* 2004, 68, 549-561.
- [86] **Chrissafis, K., Paraskevopoulos, K. M., Papageorgiou, G. Z., Bikiaris, D. N.** (2008). Thermal and dynamic mechanical behavior of bionanocomposites: Fumed silica nanoparticles dispersed in poly(vinyl pyrrolidone), chitosan, and poly(vinyl alcohol), *Journal of Applied Polymer Science*, 110 (3), 1739-1749.
- [87] **Ramos, R.A., Boratto, M.H., Li, M.S., Scalvi, L.V.A.** (2017). Emission Properties Related to Distinct Phases of Sol-Gel Dip-Coating Titanium Dioxide, and Carrier Photo-Excitation in Different Energy Ranges. *Materials Research*, 20(4), 866-873.
- [88] **Kanmani, P., Rhim, J. W.** (2014). Antimicrobial and physical-mechanical properties of agar-based films incorporated with grapefruit seed extract. *Carbohydrate Polymers*, 102, 708-716.

- [89] Volery, P., Besson, R., Schaffer-lequart, C. (2004). Characterization of commercial carrageenans by Fourier transform infrared spectroscopy using single-reflection attenuated total reflection. *Journal of Agricultural and Food Chemistry*, 52, 7457–7463.
- [90] Nur Hanani, Z.A., Roos, Y.H., Kerry, J.P. (2011). Fourier transform infrared (FTIR) spectroscopic analysis of biodegradable gelatin films immersed in water. International Congress on Engineering and Food, Proceedings.
- [91] Shankar, S., Rhim, J. W. (2015). Amino acid mediated synthesis of silver nanoparticles and preparation of antimicrobial agar/silver nanoparticles composite films. *Carbohydrate Polymers*, 130, 353–363.
- [92] MacKnight, W.J., Karasz, F.E., Fried, J.R. (1978). Solid state transition behavior of blends. In “*Polymer blends*,” ed. D.R. Paul, and S. Newman. Vol. I. pp. 186-238. Academic Press, Inc., New York.
- [93] Saibuatong, O.A., Phisalaphong, M. (2010). Novo Aloe vera–bacterial cellulose composite film from biosynthesis. *Carbohydrate Polymers*, 79, 455–46.
- [94] Ma, W., Tang, C.H., Yin, S.W., Yang, X.Q., Wang, Q., Liu, F. (2012). Characterization of gelatin-based edible films incorporated with olive oil. *Food Res. Int.* 49, 572–579.
- [95] Norajit, K., Kim, K.M., Ryu, G.H. (2010). Comparative studies on the characterization and antioxidant properties of biodegradable alginate films containing ginseng extract. *J. Food Eng.*, 98, 377–384.
- [96] Vartiainen, J., Vähä-Nissi, M., Harlin, A. (2014). Biopolymer Films and Coatings in Packaging Applications—A Review of Recent Developments. *Materials Sciences and Applications*, 5, 708-718.
- [97] Labropoulos, K.C. (2001). *Modeling of the Theological behavior of agar gels* (Doctoral Dissertation). Available from ProQuest Dissertations and Theses database (UMI No. 3038377).



CURRICULUM VITAE



Name Surname : Tuğçe Köroğlu
Place and Date of Birth : Fatih/İstanbul 02.02.1991
E-Mail : koroglu.tugce@gmail.com

EDUCATION :

- **B.Sc.** : 2015, Istanbul Technical University, Molecular Biology and Genetics

PROFESSIONAL EXPERIENCE:

- 2016 – Laboratory application specialist at Done Genetik ve Biyoinformatik A.Ş